Studies in Nonperturbative Quantum Gravity

by

Muhammad Muzammil

Bachelor of Science, Lahore University of Management Sciences, 2020

A Dissertation Submitted in Partial Fulfilment of
the Requirements for the Degree of

Doctor of Philosophy

In the Graduate Academic Unit of Mathematics and Statistics

Supervisor:	Viqar Husain, Ph.D., Dept. of Mathematics and Statistics
Examining Board:	Edward Wilson-Ewing, Ph.D., Dept. of Mathematics and Statistics Sanjeev Seahra, Ph.D., Dept. of Mathematics and Statistics, Abdelhaq Hamza, Ph.D., Dept. of Physics
External Examiner:	Hari Kunduri, Ph.D., Dept. of Mathematics and Statistics, McMaster University

This dissertation is accepted by the
Dean of Graduate Studies

THE UNIVERSITY OF NEW BRUNSWICK

December, 2025

© Muhammad Muzammil, 2025

Abstract

This thesis investigates how quantum effects modify the evolution of cosmological space-times and what those modifications teach us about the viability of candidate quantum-gravity frameworks. Two complementary approaches are pursued.

First, we develop a semiclassical geometrodynamics in which a fully dynamical classical metric is coupled to quantized matter with self-consistent back-reaction. For isotropic Friedmann–Robertson–Walker (FRW) universes and for the anisotropic Bianchi IX (mixmaster) model we derive Hamiltonian "classical–quantum" (CQ) equations and solve them numerically. Quantum excitations of the scalar field affect the Kasner exponents, leave a late-time energy-density remnant that can mimic dark energy, and admit exact static solutions in the isotropic case. When spacetime-discreteness corrections are included, the mixmaster dynamics changes: a sequence of bounces replaces the classical singularity, anisotropies grow and decay through each bounce, and Lyapunov exponent and fractal dimension analyses show a marked suppression of chaos compared with the purely classical system.

Second, we test the functional renormalization group programme in a symmetry-reduced setting. We recast an FRW minisuperspace with a massless scalar field and dust into harmonic-oscillator variables and track its RG flow using the exact, non-perturbative Wetterich equation. In contrast to Reuter's four-dimensional Einstein–Hilbert truncation, we find no ultraviolet fixed points – instead, we find that at

low energies, the cosmological constant flows to small values, and the gravitational constant flows to zero as energies grow high.

Taken together, the two lines of inquiry demonstrate (i) how quantum matter back-reaction can leave durable imprints on large-scale, late-stage cosmology, (ii) how effective discreteness mitigates classical mixmaster chaos, curbs the initial singularity, and (iii) how the absence of fixed points in symmtery-reduced models constrains the scope of asymptotic safety. The work therefore sharpens our understanding of the accuracy and validity of minisuperspace reductions, and what obstacles remain on the path to a complete quantum theory of gravity.

Dedication

This thesis is dedicated to the children whose lives have been irreversibly marked by the violence of war – those in Palestine, in Gaza and the West Bank; in Ukraine, Sudan, and the Congo – where childhood has been stolen by siege, exile, and grief. It is for those whose laughter was quieted too soon, whose classrooms became shelters, and whose futures were rewritten by forces beyond their choosing. May their stories not be forgotten in the silence of statistics.

It is dedicated to all victims of colonialism and all the systemic injustice and violence it sowed, and continues to sow, the venom of which poisoned, and continues to poison, generations of memory, identity, and possibility – erasing languages, uprooting communities, and distorting the very mirror through which peoples see themselves. May this work stand, however humbly, as a refusal to forget.

And to Dr. Aimen Mukhtar, who we lost on February 4, 2022. You continue to inspire me everyday.

For Ammi and Baba.

Acknowledgements

Committing, and staying committed, to a Ph.D program is not something that is a unilateral effort. It takes a village to complete a Ph.D, even if at the end, there's only one who is awarded the degree. This perhaps is going to be one of the longer 'acknowledgements' section that one has read. My journey during the Ph.D was anything but regular or usual. It was marked with significant developments in my personal life, all of which contributed to shape me as a scholar, teacher, and student of Science.

I would first and foremost like to thank my supervisor, Professor Dr. Viqar Husain. I found him to be extremely smart and quick-witted. In addition to his remarkable acumen in physics, I found his knowledge on almost all facets of life: politics, poetry, linguistics, and society to be the most impressive. He inspires me to be a life-long learner like himself. He pushed me enough to bring out a better researcher out of me. He taught me to embrace the discomfort of learning extremely unfamiliar new things, and question, question everything. He taught me the importance of teaching simply as a way to learn.

The gravity group at UNB gathered from all over the world the loveliest people. Fruitful discussions turned to lifelong friendships here. Who knew that it would be in Fredericton where Italian and Pakistani cuisine would come together in the most wonderful unbeknownst ways. The time I spent with Luca & Marta, Francesco &

Giulia, Nomaan, Mustafa, Doyeon, Irfan, Hassan, Karthik, and Lisa, who visited us just for a summer but became an essential part of the group, was beautiful. I want to especially thank Mustafa, Irfan and Hassan for all their help and discussions on Physics and Math throughout my Ph.D, and for helpful comments on this thesis. A special thank you to Robert Santacruz for leaving behind the best sound system – the entire Ph.D. was done with songs on. I would also like to acknowledge Arad and Augusto for making my last semester at UNB particularly enjoyable, especially the discussions over lunch at the SUB.

I'm deeply grateful to Steph Gibson, whose warmth and expertise made every official business not just smooth, but genuinely pleasant. Brandon deserves heartfelt thanks for creating such a welcoming atmosphere in our offices and ensuring our boards were always ready for our next discussions. And also, to the amazing team at the UNB Tim Horton's, especially Chelsea, Tracy, and Tanya, who not only knew my order better than I did, but whose friendly faces and cheerful greetings became a cherished part of my daily routine. These wonderful people made my academic journey feel less like work and more like being part of a caring community on campus.

My first friends at UNB played a key role helping me settle in. Their love and camaraderie is something that I prize to this day and will continue to do so beyond. Thank you Ben for randomly inviting me to your birthday. Thank you Matt for being who you are – original, kind, informed, and smart. Thank you for introducing me to Evan & Jordyn. I would especially like to acknowledge and thank Tim Blackmore. Lunches at the Cellar and discussions on QFT and life with him were precious. Also, Lyndia & Kamal, thank you for introducing me to your families, and to your homes. Christmas at the Belczewski's will never be forgotten. And lastly, Maryam & Amer who showed me the most generous hospitality and introduced me to the Levantine culture.

During these past five years, times did grow tough at more than a few instances. I started this Ph.D. during the pandemic. I would not have lasted the first year in the cold new city of Fredericton had it not been for my friends who were always a call away. I shared my cherished undergraduate life with them, but their presence and availability during the first two years of my Ph.D was supremely precious to me. Thank you Waleed, Suha, Maaz, Haider, Usman & Anoosha, Maryam & Qasim for all those wonderful video calls and support.

My friends back home mean the world to me. Their unwavering support for me forms the foundation of my belief in myself. I am supremely fortunate to have found the friendship of these lovely, kind souls with whom I not only shared a better part of the last decade but also am excited to share the rest of my life. Thank you Adil, Afnan, Izza, Qasim, Tehrema & Saeed, Waleed & Nazish, Saad & Maha, Usman Sohail & Iman, Momina & Rafae, Haniya, Suha & Maaz, Anoosha & Usman Khalid, Haider, Manum, Mohsin Jamil, Mustafa Ghani, Muneeb Faridi, Dr. Sameer, Dr. Nadia, and Dr. Umer Ali.

My love and passion for physics did not ignite in vacuum. It was kindled, and rekindled, by teachers whom I was fortunate enough to learn from. Had Sir Yawar Abbas in 2013 not agreed to take me under his wings, I would not have made the leap to do an undergraduate, let alone a doctorate, in physics. He took my questions with kindness, spent extra time with me. I was terrible at Math and Physics, and he made me not only fall in love with the subject, but also to choose a career in it. Teachers like him are a gift from God Himself. It would be amiss to not mention Miss Ambreen Shah and Miss Shehla Shamim who taught me that Economics and Biology are subjects you just have to know, and know well, to be a holistic human being. They instilled in me a curiosity of what was happening around us, inside us, and why.

My friend Owais Jawaid, taught me the subtleties of the Harmonic Oscillator. He was perhaps, in a very different way, the one who made me appreciate Sydney Coleman's quote, "The career of a young theoretical physicist consists of treating the harmonic oscillator in ever-increasing levels of abstraction." Though he may not know it, his passion for physics was infectious, and I was the first victim. For that, I will forever be grateful.

I was fortunate enough to be able to teach seven courses during my Ph.D. I was able to meet the most wonderful bunch of students from all over the world. Knowing their names, and learning their stories gave me a reason to show up excited everyday, I thank all of them for making me appreciate Math more. Making them fall in love with Math (or rather, making them hate it a little less) is one of my proudest achievements. I thank Dr. Sanjeev Seahra and Dr. Tariq Hasan for trusting me with this immense responsibility.

Of all my incredible students, I would like to acknowledge Edie Russell, who later became a friend. Although, Edie graduated and left Fredericton in the Summer of 2023, she introduced me to a group which became my family in Fredericton, people who made Fredericton home away from home – the Fredericton Trail Runners. My life in Fredericton was changed completely when I met the loveliest of folks at FTR. They made me fall in love with the beautiful city of Fredericton, the trails, and the wonderful sport of trail running. I will never forget the kindness the FTR showed me, and the space they gave me to improve. Much of this thesis was thought about on these trails. I would especially like to thank my closest friends from the FTR for listening to my ramblings in life and the graduate school: Ryan Murphy, Maxime & Véro, Kurt Goddard, Philip Lowery, Jason Fleming, Mark Tennant, Emily Prystupa, James McMahon, Kaylee Hopkins, Benoît LeBlanc, Bob Dumouchel, and Josh Waite (*our fearless leader*).

Another key moment came in late 2023, when we met Aniqa and Farrukh. Together with my wife, Aamina, and Hassan, I have found a group of friends whom I can completely trust with almost anything. *Tatreez* has since become our weekend escape. Every hangout including hikes, trips, runs, dinners, with them has since become infinitely more beautiful.

I would like to thank my family back home. Without their support, love, and most importantly, prayers, I would not have accomplished anything. I want to thank Ammi, Baba, and Maaz, and Mama and Apa. Calls with all of them kept me sane. They instilled in me values to seek knowledge and stay curious no matter what. No amount of lines or words would ever yield the matter of how much they all mean to me.

Lastly, I would like to thank my wife, Aamina, the smartest, most kind, most beautiful human I know, who makes everything all the more worth it. Her unwavering support means everything to me. She pulled me through the toughest of times, through anxiety, restlessness, and panic. I would have quit a long time ago had it not been for her. Thank you for keeping up with my antics; you make me want to become a better human being. *I love you, completely.*

To my son, Mustafa, who arrived just in time when I was making the final edits on this thesis. You are my whole life.

Thank you Lord, it's only you and I who know that I was not capable of any of this. Thank you for bestowing me with the privilege of being able to do something meaningful for people around me.

Table of Contents

Abstract **ii**

Dedication **iv**

Acknowledgments **vi**

Table of Contents **xii**

List of Tables **xv**

List of Figures **xvi**

1 Invitation **1**

1.1 Hamiltonian Semiclassical Gravity 6

1.2 Exact Renormalization Group 11

2 Isotropic Cosmology **16**

2.1 Classical-Quantum isotropic cosmology 18

2.1.1 Classical-Quantum equations: FRW 22

2.1.2 Static classical-quantum solutions 24

2.1.3 Linear stability analysis 26

2.1.4 Comparison of exact classical-quantum and classical dynamics 28

2.2 Classical-Quantum anisotropic cosmology 32

2.2.1 CQ Kasner 34

2.2.2 Numerical solution 36

2.2.3 CQ Bianchi Universes 40
2.3 Summary and Discussion 43

3 Anisotropic Cosmology **47**
3.1 Mixmaster Cosmology 49
3.1.1 Effective equations 51
3.1.1.1 Effective cosmology with classical scalar field 53
3.1.1.2 Effective cosmology with quantum scalar field 54
3.2 Numerical Results 55
3.2.1 Volume, anisotropy and Kasner sum evolution 59
3.2.2 Scalar field excitation and density 61
3.2.3 Chaos 63
3.2.3.1 Lyapunov exponents 64
3.2.3.2 Fractal dimension 66
3.3 Summary and Discussion 67

4 Exact RG for minisuperspace cosmology **70**
4.1 Exact Renormalization Group 73
4.1.1 Wetterich Equation 75
4.2 Matter Time in General Relativity 80
4.2.1 The Dust time gauge 82
4.3 Universe as an oscillator 84
4.4 FRG for Cosmology with a Scalar Field 87
4.4.1 RG Flow Equations 89
4.5 Results 90
4.6 Summary and Discussion 93

5 Conclusion **96**

Bibliography **112**

A Wetterich Equation in Quantum Mechanics **113**

A.1 Quantum Effective Action 116

A.2 Scale dependence 119

A.3 Flow Equation 123

A.4 Anharmonic Oscillator 126

Vita

List of Tables

3.1 Maximal Lyapunov Exponents for the six models 65

List of Figures

1.1 Full quantum gravity is where energies are highest, and length scales are smallest. Conversely, classical General Relativity lies on the opposite end with large lengths and low energies. 7

2.1 A typical comparative evolution of the classical-quantum (CQ) and classical (C) evolution with scalar field of mass 10^{-3} (Planck units) initially in its ground state $|0\rangle$. Initial data is a perturbation of a static semiclassical solution; the first four frames show the scale factor, Hubble parameter, acceleration, and density, relative to their initial values; the fifth frame shows the occupation probabilities $|c_i|^2$ of higher scalar field states (with $c_n = c_{40}$); the last frame confirms conservation of probability and of the effective Hamiltonian constraint. 29

2.2 A typical comparative evolution of the classical-quantum (CQ) and classical (C) evolution for the same data as in Fig. 2.1 but with scalar field initial state $(\sqrt{3}/2)|0\rangle + (1/2)|1\rangle$. 30

2.3 Numerical solution of the Kasner classical-quantum equations with the scalar field starting in the vacuum $|0\rangle$: the first frame shows the (dynamical) Kasner exponents, followed by comparison graphs of volume and scalar field density; the forth frame shows conservation of the effective constraint and probability; the last two frame show the excitation of the higher scalar states, and the difference between the classical and classical-quantum Kasner exponents. 35

2.4 Numerical solution of the Kasner classical-quantum equations with the scalar field starting in the state $(\sqrt{3}/2)|0\rangle + (1/2)|1\rangle$: the first frame shows the (dynamical) Kasner exponents for the CQ case, followed by comparison graphs of volume and scalar field density; the last two frames show the excitation of the higher scalar states; $c_n = c_{50}$ is the truncation level of the scalar field basis. 37

2.5 The difference between the CQ and C dynamical Kasner exponents for the data used for Fig. 2.4. 38

3.1 A typical evolution for the classical and effective Mixmaster universe in vacuum, and with classical and quantum scalar field. The dashed blue line is for the classical Bianchi IX Hamiltonian; the solid line represents the effective Bianchi IX Hamiltonian. The first row shows multiple bounces in the volume for the effective universe. The second row shows the evolution of the anisotropies $\beta_\pm$, and the third, the log of the Kasner squared sum rule overlayed with log of the volume. . . 56

3.2 Anisotropy variables $\beta_\pm$ near the first bounce point for each of the models studied. 57

3.3 Scalar field state excitations for the Hamiltonians H_Q (classical gravity) top row, and H_Q^{eff} (effective gravity) bottom row, starting from the initial ground state. Both show excitations from the ground state as the singularity/bounce is approached, de-excitation as the universe expands after the bounce, and probability conservation. 57

3.4 The first few and and the last few even-state excitations of the scalar field (with Hilbert space truncation $n = 30$) through the first bounce of the effective universe; the volume is overlaid (in red). 58

3.5 Scalar field densities in a classical and effective universe. In the former case (dashed blue line) the density diverges at the singularity; in the latter cases (orange line) the density spikes at a maximum at each bounce shown in Fig. 3.1 63

3.6 Numerical conservation of the Hamiltonian constraint for the evolutions shown in Figs. 3.1, 3.3, and 3.5. 64

3.7 Zoomed-in phase plots of the anisotropies $\beta_{\pm}$ for each of the six models studied. Self-similarity and fractal-like structure is evident in each case; all are qualitatively similar, but with notable differences for the quantum scalar field. 65

3.8 We see here the results of the box-counting analysis to compute the dimensions of the plots in Figure 3.7. For each plot in the figure, we use the polymerized and unpolymerized counterparts for each species (vacuum, classical scalar field, and quantum scalar field). We see that in each case, polymerization reduces the fractal dimension of the image, rendering the system to be less chaotic. 66

4.1 Renormalization group flows of the dimensionless cosmological constant Λ_k (top panel) and the dimensionless Newton coupling g_k (bottom panel) as functions of the RG scale k. Arrows indicate the direction of decreasing k (i.e. the UV flow). Although both couplings start from finite values in the infrared ($k \simeq 2$), their UV behavior is radically different: as $k \to 0$, the Newton coupling vanishes, signaling the effective disappearance of gravitational interactions, whereas the cosmological constant grows without bound, indicating a divergent vacuum energy in the deep UV. 91

4.2 Renormalization group flow trajectories in the dimensionless coupling plane (Λ_k, g_k) for a variety of infrared initial conditions. Arrows mark the direction of decreasing RG scale k (toward the UV). Although all flows emanate from the vicinity of the Gaussian point $(\Lambda, g) = (0, 0)$ at high k, they do not settle at any non-trivial fixed point as $k \to 0$. Instead, g_k universally tends toward zero while Λ_k diverges positively or negatively depending on the chosen trajectory. The lack of any vanishing arrow vectors in the plotted region confirms the absence of additional fixed points. 92

Chapter 1

Invitation

At the time of writing of this thesis in 2025, the search for a complete quantum description of gravity remains one of the central and most vigorous pursuits in theoretical physics. There are several approaches, tackling the problem from various sides, angles, and methodologies, with various starting assumptions [1]. Before delving into the main body of the thesis, it is useful to foreground the key challenges that any complete theory of quantum gravity must confront, and to indicate how the work presented here engages with those challenges.

One of the major motivations for a quantum theory of gravity is the mismatch among the quantum description of the four fundamental forces of nature. While three (electromagnetism, weak, and the strong force) have successful quantum field theoretic descriptions that reduce smoothly to their classical limits at large scales and low energies, gravity does not. A consistent quantum description of gravity would allow a description of gravity at high energies in the language of quantum mechanics (or quantum field theory) as we can for all other interactions in the universe. Thus, any candidate for a theory of quantum gravity must grapple with this enigma: how does classical General Relativity (GR) emerge from the respective quantum proposal?

Moreover, GR provides an exceptionally accurate account of physics on cosmic scales, whereas Quantum Mechanics (QM) and Quantum Field Theory (QFT) are incredibly successful at describing phenomena at the tiniest distances. Yet these descriptions of physics do not fit together smoothly as scales at which phenomena is probed changes: the theories that excel at describing physics at the smallest of scales, for example sub-nuclear distances – between a nucleus and its electrons, or among the nucleons themselves, are inherently different from those that describe cosmic phenomena at the grandest of length scales, and the reverse is equally true. While these theories that describe physics at these disparate length scales remain incompatible at several levels, some of which we describe below, there is reason to believe that a fully quantum theory of gravity may be able to bridge this gap, for more details consult [2].

One issue that is cause for this incompatibility between existing frameworks in quantum theory and GR is the fact that fundamental interactions like electromagnetism and the weak and strong interactions are described by 'renormalizable' quantum field theories: the couplings in their Lagrangians change with energy but stay finite in the ultraviolet, and a finite set of parameters suffices to calculate every S-matrix element. The same Lagrangians reduce smoothly to classical Maxwell–Yang–Mills equations at low energies.

Gravity behaves differently. When one tries to quantize the Einstein–Hilbert action perturbatively, each loop order produces new curvature terms – R^2, $R_{\mu\nu}R^{\mu\nu}$, $R\Box R$, and so on – with their own independent couplings. This "tower" is infinite because Newton's constant has negative mass dimension[1], so ever-higher derivatives are needed to absorb the ultraviolet divergences. Since the powers of mass keep increasing from one loop order to the next, this list of required terms – and the corresponding coupling constants that would have to be measured in a lab – never

[1]In D spacetime dimensions, $[G] = M_{pl}^{2-D}$, here M_{pl} is the Planck mass.

ends. Put simply, one would need an infinite number of experiments to pin down all those couplings, so straightforward perturbative quantization of Einstein's theory cannot be predictive. This failure to be renormalizable is one motivation for seeking a quantum theory of gravity that tames, or avoids the endless counter-term problem altogether and seeks a non-perturbative approach to the problem.

Yet, the technical issue of non-renormalizability is only part of the story. General Relativity is background-independent: the metric that measures distances is itself a dynamical field. Due to this, the standard machinery of quantum field theory which is defined around a fixed spacetime geometry, with well-defined mode expansions, is rendered invalid. Furthermore, since the background is not fixed, the roles of time and space are intertwined, and there remains no fixed external time coordinate as in QM and QFT [3, 4]. When one tries to use conventional quantization techniques [5], this lack of a time coordinate and a fixed background in general, presents tremendous conceptual hurdles – one cannot straightforwardly define Hamiltonians, propagators, or vacuum states, etc. Thus, the problem of time is of fundamental importance in a theory of quantum gravity. Due to this absence of external time in quantum gravity, any notion of physical clocks would have to be internal to the system: these can be geometric in nature, for example: spatial volume, the mean curvature, or logarithmic scale factors [6, 7, 8, 9], or in a gravity-matter system, one can use the matter degrees-of-freedom as the relational marker against which change can be measured, for example a scalar field, dust, or some other perfect fluid, etc [10, 11, 12, 13].

Numerous approaches have been developed to tackle these, and other, obstacles on the road to a complete quantum theory of gravity. Broadly, the proposals can be grouped into three main families [14, 15]:

- The first class of candidate theories attempts to quantize gravity starting with

writing gravity as a constrained[2] Hamiltonian theory, and then proceeding to promote phase space variables to operators [16, 17]. Combinations or functions of these phase space variables can be used to make the resultant quantum theory simpler. The Wheeler-DeWitt (WDW) program, Loop Quantum Gravity (LQG), Causal Dynamical Triangulations (CDT), and Spin Foams are examples of this approach. Some challenges that befall this approach is the question of solving the quantum constraint algebra consistently, identifying physical observables, and resolving the problem of time.

- The second strategy draws inspiration from the standard model of particle physics, aiming to treat gravity within the same quantum-field-theoretic framework that successfully describes the other forces. Gravity's perturbative non-renormalizability long stymied this effort, but Weinberg's conjecture about gravity's ultraviolet behaviour rekindled the hope that its couplings could remain finite all the way up to the highest energy scales [18]. If true, this would entail that only a few parameters need to be measured, after which the theory yields definite, calculable predictions from laboratory scales up to the Planck regime. That turns quantum-gravity effects – such as tiny deviations from Newton's law or specific imprints in cosmological and gravitational-wave data – into concrete, testable targets for experiments. This idea of couplings remaining finite at higher energies (the UV) is called 'asymptotic safety'. This has also driven two main research programmes: the Exact Renormalization Group (ERG) (also called the Functional Renormalization Group (FRG)) approach, which tracks how gravitational couplings change with energy, and string theory, where gravity emerges from the vibrations of tiny strings rather than point-like particles. Furthemore, the holographic (AdS/CFT) approach has provided a fully non-perturbative definition of quantum gravity in spacetimes with nega-

[2] A constraint is a fixed relationship between the phase space variables of a theory.

tive cosmological constant by mapping it exactly to a conformal field theory on the boundary, yielding sharp results on black-hole entropy, information recovery, and the emergence of spacetime from quantum entanglement [19, 20].

- A third line of research adopts a more radical, bottom-up strategy. Instead of quantizing Einstein's equations or embedding gravity in a conventional quantum field theory, these approaches attempt to construct spacetime from underlying quantum constituents and then show that classical geometry emerges as a large-scale limit. In Group Field Theory, for example, "atoms of space" are created and annihilated by field operators on a Fock space; a many-body phase of this system is expected to approximate General Relativity after coarse-graining. Causal-Set theory posits a fundamentally discrete, partially ordered set of spacetime elements whose continuum approximation should satisfy Einstein's equations. Related programmes, including Causal Dynamical Triangulations and tensor models, follow the same principle: formulate the microscopic quantum rules first, and demonstrate that classical spacetime, and ideally General Relativity, arise in the appropriate macroscopic limit.

Although none of these candidate theories has achieved empirical confirmation, each demonstrates a concrete mechanism by which the conceptual obstacles of non-renormalizability and background dependence may be overcome, lending confidence that a consistent quantum description of spacetime is within reach. Despite these, and other concerted efforts, several of these approaches aim to quantize gravity in vacuum, usually only introducing matter only when it serves as an internal clock.

This thesis aims to further efforts and establish frameworks to facilitate future research in quantum gravity – especially on the problems of background-independence and adding matter to the quantization process. For the majority of this work, we will adhere to the first approach: using a canonical quantization of a symmetry-

reduced gravitational system (homogeneous cosmology[3]) with matter. Towards the end, we also employ techniques from the second approach – in particular, the exact renormalization group to study the UV behaviour of cosmological systems with matter.

Two broad questions we address are:

1. How would we add quantized matter over a fully dynamical background, with full backreaction in a self-consistent manner? This would be a step beyond quantum field theory on curved spacetimes (QFTCS).

2. Can a non-perturbative functional renormalization group analysis be conducted for a symmetry-reduced (cosmological) gravitational setting with matter to study the UV behaviour of the system?

We shall now describe the two problems outlined above in more detail as important facets in the journey towards quantum gravity. The next section will motivate Hamiltonian semiclassical gravity – which is the framework upon which chapters 2 and 3 are based. After that we will describe the use of functional RG methods to study the behaviour of gravity-matter systems as probing energy scales change from low (classical) to high (quantum).

1.1 Hamiltonian Semiclassical Gravity

On the road to full quantum gravity (QG) – where both matter and the background are treated quantum mechanically, lies the crucial juncture that is called 'Semiclassical Gravity' (SCG), [14, 21]. This stop is best illustrated via an energy scale

[3]These are gravitational systems in which each point on a three-dimensional spatial slice is identical.

diagram[4]. In the figure below, the all-successful, classical General Relativity (GR)

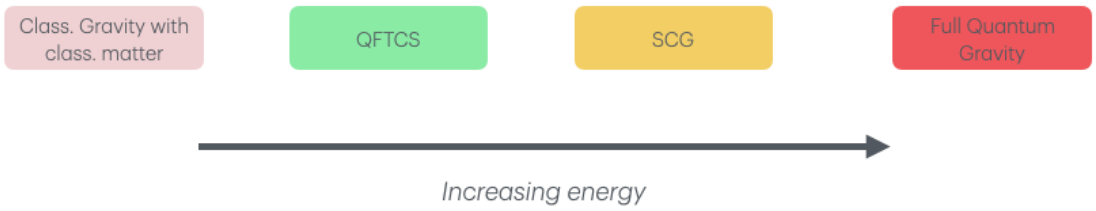


Figure 1.1: Full quantum gravity is where energies are highest, and length scales are smallest. Conversely, classical General Relativity lies on the opposite end with large lengths and low energies.

finds itself on the left-end of the energy scale diagram – this part represents the regime where length scales are large, and densities and energies are low. As we move along towards the right, we find the regime where we describe quantum matter fields on curved spacetimes. Here, the background is fixed and quantum fields merely propagate on it. Any phenomenological attributes come from the evolution and behaviour of quantum fields on these curved backgrounds, i.e. the quantum fields, in turn, do not affect the curved backgrounds they live on, but rather behave in special ways (for example, particle creation, et cetera) due to them being on these curved, but fixed, backgrounds.

It is only natural that the next stop would be a framework where the quantum matter affects the classical background. In this, the background (the classical metric $g_{\mu\nu}(x)$) would have its dynamics 'informed' by the 'backreaction' (feedback) of the quantum fields. This is the semiclassical gravity regime which is identified by the yellow box in the energy diagram above.

In principle, to incorporate quantum matter backreaction on a classical metric, one would replace the classical stress-energy tensor on the right-hand side of the Einstein's field equations with an expectation value of a stress-energy tensor in a quantum state. This expectation value would then in turn affect the metric that one is

[4]the energy here represents the gravity-matter interaction energy in each case.

solving for. This set up is also called the semiclassical Einstein equation.

$$G_{\mu\nu} + \Lambda g_{\mu\nu} = 8\pi G \, \langle \Psi | \hat{T}_{\mu\nu}(\hat{\phi}, \, g_{\mu\nu}) | \Psi \rangle. \tag{1.1}$$

The semiclassical Einstein equation is fully specified after the following inputs are fixed: (i) the matter content, and – crucially – (ii) the quantum state $|\Psi\rangle$ from which the stress tensor $\langle T_{\mu\nu} \rangle$ is computed. With those choices in place one must solve the coupled, nonlinear field equations for the metric itself. Consequently, the resulting semiclassical metric $g_{\mu\nu}$ is not a universal object; its form depends sensitively on the selected quantum state. Consider, for example, the situation in which $g_{\mu\nu}$ and $\gamma_{\mu\nu}$ are two solutions to (1.1) arising from two distinct states $|\Psi\rangle_1$ and $|\Psi\rangle_2$; there does not seem to be a connection between $\gamma_{\mu\nu}$ and $g_{\mu\nu}$, and also solutions arising from linear combinations of $|\Psi\rangle_1$ and $|\Psi\rangle_2$. This introduces nonlinearities into the quantum regime of the theory – this is now a problem if the full quantum theory of gravity is believed to be like the usual familiar quantum mechanics [14].

This semiclassical scheme also depends on the careful definition of $\langle T_{\mu\nu} \rangle$. In general, the right-hand side of (1.1) is ultraviolet divergent. Regularization methods only yield sensible results if the background is static or stationary – this is clearly not ideal in a semiclassical theory that is approaching a complete quantum gravity framework where the spacetime would be allowed to be dynamical as its classical counterpart.

What we present is a canonical picture of semiclassical gravity. Here, quantum matter backreacts on the fixed curved background [22]. In addition, the analysis we present is completely non-perturbative. The general starting point is the Hamiltonian of the full theory, i.e. a classical part and a quantum part taken as an expectation

in some state of the quantum matter. We have

$$H_{SC} = H_{cl}(q,\, p) + \langle \Psi | \hat{H}_{qm}(\hat{Q},\, \hat{P},\, q,\, p) | \Psi \rangle, \tag{1.2}$$

Here, $(q,\, p)$ are classical phase space variables and $(\hat{Q},\, \hat{P})$ are quantum operators. An interesting feature is the presence of variables $(q,\, p)$ in the quantum Hamiltonian $\hat{H}_{qm}$ – this is the mathematical manifestation of (quantum) matter backreaction on the classical background. The appearance of q and p inside the quantum Hamiltonian $\hat{H}_{qm}$ is not a coincidence: the matter action has dot products of first-order derivatives of the matter fields. This dot product explicitly requires the metric for its definition. This is how the background informs the dynamics of the matter fields. When one performs the Legendre transform to obtain the Hamiltonian, factors of the metric (or its determinant $\sqrt{-g}$) survive as a function in $\hat{H}_{qm}$.

Due to the matter Hamiltonian depending on (q, p), the expectation value computed from $\hat{H}_{qm}$ feeds back into the classical gravity equations that determine those very variables. This mutual dependence is the back-reaction loop: geometry shapes quantum evolution, and quantum energy–momentum in turn curves geometry. Similar couplings appear in other hybrid systems: electrons moving in the classical potentials induced by nuclei, or photons interacting with a vibrating mirror – but in gravity the coupling is universal and encoded in the metric itself, making the interplay unavoidable and central to semiclassical dynamics.

For a gravity–matter system, the semiclassical Hamiltonian (1.2) naturally separates into two pieces:

1. **A classical gravitational sector:** This is represented by phase-space variables (q, p) – in the context of GR these can be the scale factor a and its conjugate momentum p_a, or the volume of the universe ν and its canonically

conjugate momentum p_ν. For the general variables q and p the dynamics are given by Hamilton's equations

$$\begin{aligned} \dot{q} &= \{q, H_{SC}\}, \\ \dot{p} &= \{p, H_{SC}\}. \end{aligned} \tag{1.3}$$

2. **A quantum-matter sector:** Here the Hamiltonian depends parametrically on the classical variables. The dynamics of the quantum state are given by the time-dependent Schrodinger equation

$$i|\dot{\Psi}\rangle = \hat{H}_{qm}|\Psi\rangle. \tag{1.4}$$

General Relativity's four-dimensional diffeomorphism invariance translates, in its $(3+1)$ (canonical) formulation, into gauge freedom under arbitrary spatial coordinate relabelings and time reparameterizations. In the language of constrained Hamiltonian systems [16] these gauge transformations are generated by first-class constraints: the three momentum constraints enforce spatial diffeomorphism invariance, and the Hamiltonian constraint enforces invariance under time translations. Because the total Hamiltonian in GR is just a linear combination of these constraints, it must vanish identically. Since our semiclassical Hamiltonian is derived from the total gravity and matter system, it too is constrained to vanish for all times

$$\frac{d}{dt} H_{SC} = 0. \tag{1.5}$$

The equations of motion preserving the constraint (1.5), and the norm of quantum state remaining unity throughout the evolution ensures that our analysis is self-consistent.

Having developed a consistent semiclassical framework, we shall now apply this to homogeneous spacetimes in the following chapters.

1.2 Exact Renormalization Group

Another key thing to study is how gravitational interactions behave as we decrease lengths or increase energies approaching the Planck scales. This allows us to probe the ultraviolet structure of gravity, or in other words helps us answer the question, 'how does gravity (or a gravity-matter system) behave as we go to length scales where quantum effects cannot be ignored?'

Answering this question would entail having a quantum description of gravity as for the other fundamental interactions in the standard model. However, with gravity such an analysis is not straightforward. This is due to gravity's inherent nonrenormalizability: any attempt to perturbatively quantize the Einstein-Hilbert action, leads to curvature counter-terms and introduces divergences as we probe the theory at high energies.

The renormalization group (RG) is a field theoretic toolkit that allows us to study the physics that a theory describes (via an action principle) at different energy, or length scales. In usual QFT, for instance quantum electrodynamics, one calculates scattering amplitudes at a chosen momentum scale, absorbs the ultraviolet divergences into a finite set of renormalized couplings and masses, and then finds that these parameters vary, or "run," as the energy scale is changed [23].

Kenneth Wilson showed that one can think of a quantum field theory as a succession of 'coarse-grained' effective actions S_k: we start with a bare action at a very high (but finite) cut-off energy, then lower a sliding scale k and systematically integrate out fluctuations with momenta above k [24, 25]. The entire family S_k traces a path

through an abstract "theory space," and that path is governed by an exact functional differential equation – this trajectory is called the RG flow of a theory, and any functional differential equation dictating this flow is termed the 'flow equation'.

For different flow equations, the starting points and inputs are different. For example, Wilsonian RG implements the RG process on the generating functional, $Z[J]$, of correlation functions in the presence of a source $J(x)$. The idea here is to successively integrate out thin shells of high energy modes, and see how the couplings in the action change as k is lowered. This evolution of the couplings reveals the RG flow of the theory.

Polchinski's equation chooses, for its starting point, the Schwinger functional $W[J]$ [26]. This is simply the logarithm of the generating functional – the advantage of using this is economy: functional derivatives of $W[J]$ generate connected n-point functions only, sparing one the proliferation of disconnected Feynman diagrams that appear when differentiating $Z[J]$ itself. The resulting integro-differential equation describes how $W[J]$ changes as successively higher-momentum modes are eliminated.

Christoph Wetterich pushed the idea one step further by working with the effective average action $\Gamma_k[\phi]$ – a Legendre transform of $W[J]$ that includes an infrared regulator R_k [27]. This regulator acts like a mass term, suppressing the effect of 'heavier' (low energy) modes in the effective average action Γ_k. This effective average action is somewhere between the bare action (at large k) and the full quantum effective action (as $k \to 0$). He chose this as his starting point because its functional derivatives yield one-particle-irreducible ($1PI$) vertices at scale k – these carry information most succinctly as opposed to the generating or Schwinger functionals. This can be seen from the fact that their respective Feynman diagrams cannot be split into two disconnected pieces by cutting a single internal line. These 1PI vertices can then be used as building blocks for constructing truncated, manageable approximations

of the full theory. Moreover, Γ_k evolves via a single, exact equation – the Wetterich equation – that is completely non-perturbative.

To summarize, Wilson blocks the generating functional shell-by-shell, Polchinski flows the connected generating functional, and Wetterich flows the scale-dependent effective action (also, termed the Quantum Effective Average Action). Each successive choice packages the relevant physical information more compactly.

The resulting flows from these RG equations in the theory space tell us a lot about the quantum field theory in question. For instance, if this flow settles to one point, and any change thereafter in the probing scale k, leaves the couplings in the action unaltered – we say that theory has a fixed point. At this point the theory becomes scale invariant – any change in the coarse-graining probing scale (length or energy) does not change the physics. If, for example, this fixed point occurs at high energies (or, in the UV), the theory is said to remain predictive in the UV – none of the couplings diverge.

Examples of these fixed points include the Gaussian or free-field fixed point, reached by an ordinary scalar field (and, famously, by QCD) as one probes ever higher energies: all dimensionless couplings slide toward zero, so the theory stays well behaved and calculations remain under control. In other situations the flow can be drawn to a Non-Gaussian (interacting) fixed point instead – most famously the Wilson–Fisher fixed point that governs critical phenomena in three-dimensional magnets. Whether the fixed point is free or interacting[5], its key virtue is the same: only a handful of "relevant" directions in theory space need to be experimentally input, while every other coupling is pinned down by the flow itself.

This analysis for gravity's Einstein-Hilbert action is not as straightforward. The cou-

[5]In one line: at a non-interacting (Gaussian) fixed point all dimensionless couplings vanish, whereas at an interacting (non-Gaussian) fixed point at least one coupling settles to a finite, non-zero value.

pling that appears in front of this action, Newton's constant G, has negative mass dimension, so at each loop order you generate new counter-terms with ever more curvature factors. Perturbative renormalization fails. To remedy these bleak prospects, Steven Weinberg's asymptotic-safety conjecture offered a way out: perhaps gravity still had a fixed point, but a decidedly a non-Gaussian (interacting) one, so that the infinite tower of couplings collapses onto a finite "critical surface" after all [18].

The first concrete hint that this might work came from Reuter in 1998 [28]. Using the Wetterich equation for RG as outlined above, he truncated the gravitational action to just two running couplings (the cosmological constant and Newton's constant) and found a non-Gaussian fixed point in four Euclidean dimensions. Since then, many groups have extended the truncation and generally seen the same qualitative behaviour [29, 30, 31, 32, 33].

More details about the derivation of this functional differential equation follow in chapter 4, alongside its application to a cosmological action. Here, we shall study the behaviour of gravity as scales are changed in a symmetry-reduced setting. In this controlled setting, we ask whether the asymptotic safety scenario – evident in Reuter's full-theory treatment survives in symmetry-reduced models.

The structure of this thesis is as follows: in chapters 2 and 3, we shall apply the framework outlined in section 1.1 to minisuperspace settings. In the former, we will study the application of the SCG framework to the FRW universe and the homogeneous, but anisotropic, Kasner universe. In chapter 3, we shall extend the idea to include the Mixmaster spacetime,(Bianchi-IX) with LQG inspired effective corrections to the background. These chapters are based on the papers [34, 35].

In chapter 4, we apply the Exact Renormalization Group Technique (ERG) to the FRW cosmology minimally coupled to a massless scalar field and dust. The dust here

serving as a matter-time gauge. We then compute the flow equations for couplings in the Euclideanized bare action and search for any fixed points.

Chapter 5 summarizes the key findings from the preceding chapters and outlines avenues for future investigation, all aimed at advancing the quest for a complete quantum theory of gravity.

Chapter 2

Isotropic Cosmology

The road to quantum gravity (QG), albeit long and full of challenges, has provided some initial stepping stones. The well-studied area of quantum fields propagating on curved spacetime (QFCS) [36, 37, 38] may be considered a first step; it applies where gravity is not dynamical. The next step is a theory where the important issue of backreaction of quantum matter on classical gravity is taken into account. This requires an idea for classical-quantum coupling. An attempt towards incorporating backreaction is the semiclassical Einstein equation

$$G_{ab} + \Lambda g_{ab} = 8\pi G \, \langle \Psi | \hat{T}_{ab}(\hat{\phi}, \, g_{ab}) | \Psi \rangle. \tag{2.1}$$

This is an equation for a semiclassical metric given a (Heisenberg) state $|\Psi\rangle$ of matter. It requires for its formulation a construction of the stress-energy tensor on an apriori undetermined metric. It is also (manifestly) non-linear in the state, unlike QFCS and QG—if it is presumed to be like usual quantum theory. Other issues with this proposal have been pointed out in the literature [14]. Despite these shortcomings, there have been many investigations of this equation (see e.g. [39, 40, 41, 42] and references therein). In addition, its applications to cosmology have been studied

where the expectation value on the stress-energy tensor includes higher derivative corrections [43]. There is also recent work on this equation, again with higher derivative corrections where the metric is chosen to be static [44]. The standard approach used for studying (2.1) comes from noting that its right hand side, suitably renormalized, is in general a symmetric divergence free tensor $F_{ab}(g)$; this tensor inevitably has higher derivative curvature terms [42] computed to some order, with the accompanying issues that come with higher time derivatives.

In contrast, the work we report here uses a canonical approach starting from the Arnowitt-Deser-Misner (ADM) hamiltonian formulation for general relativity. The idea is to formulate a "semiclassical geometrodynamics" with effective constraints where the matter field is quantized and the gravitational phase space variables remain classical; the matter state evolves via a (functional) time dependent Schrodinger equation, and the gravitational phase space variables evolve via the effective constraints. As we show below, this system is self-consistent and provides a method to compute state and geometry evolution with full backreaction. The approach is similar to that used recently in the so-called Friedmann-Schrödinger equation [45], where a quantum state and scale factor evolve self-consistently from initial data via the Friedmann equation and the time-dependent Schrödinger equation.

To illustrate the approach and demonstrate its potential usefulness, we consider the case of scalar field coupled to homogeneous cosmology, both the isotropic and anisotropic cases. The general case of the latter with three scale factors moving in a potential has been the subject of much classical study beginning with the pioneering work of Belinskii, Lifshitz and Khalatnikov (BKL) [46]; further classical work on these models appears in [47, 48]; a survey of Hamiltonian cosmology, mainly in vacuum with a view to quantization appears in [49]. To date there is no comprehensive study of the corresponding semiclassical system, at least along the lines we present here.

While our main interest in this chapter is semiclassical cosmological dynamics with full backreaction, we also point out that there are static solutions of the classical-quantum equations. These are of interest in their own right and also due to past work, both in general relativity and in modified theories of gravity [50, 51, 52, 53, 54, 55]; our approach may be viewed as a "modified gravity theory," but not one with higher derivative terms.

We begin in Sec. II with a numerical study of the isotropic case where we show the self-consistency of the classical-quantum (CQ) system, including preservation of the effective constraint under both state and geometric evolution, and conservation of probability; we give dynamical solutions numerically, and static semiclassical solutions that resemble, but are different from the classical Einstein Static Universe; lastly, we compare classical and semiclassical evolution from comparable initial data. In Sec. III we generalize to the case of anisotropic cosmology; we solve the semiclassical equations numerically to find quantum matter-induced corrections to the Kasner exponents and their classical sum rules; we also show that the Bianchi IX case admits static CQ solutions. We conclude in Sec. IV with a summary and discussion of further applications of this approach to semiclassical geometrodynamics.

2.1 Classical-Quantum isotropic cosmology

The system we consider arises as a symmetry reduction of the Arnowitt-Deser-Misner (ADM) canonical action

$$S = \int dt d^3x \left\{ \pi^{ab} \dot{q_{ab}} + p_\phi \dot{\phi} - N \left(\mathcal{H}_G + \mathcal{H}_\phi \right) - N^a \left(C_a^G + C_a^\phi \right) \right\}. \qquad (2.2)$$

$(q_{ab},\, \pi^{ab})$ and $(\phi,\, p_\phi)$ are phase space variables for gravity and the scalar field respectively; N is the shift, N^a is the lapse; C_a^G and C_a^ϕ are the diffeomorphism constraint

functions; $\mathcal{H}_G$ and $\mathcal{H}_\phi$ are the components of the Hamiltonian constraint:

$$\begin{aligned}
\mathcal{H}_G &= \frac{1}{\sqrt{q}}\left(\pi^{ab}\pi_{ab} - \frac{1}{2}\pi^2\right) + \sqrt{q}\left(\Lambda - R^{(3)}\right) \\
\mathcal{H}_\phi &= \frac{1}{2}\left(\frac{p_\phi^2}{\sqrt{q}} + \sqrt{q}q^{ab}\partial_a\phi\partial_b\phi\right) + \sqrt{q}V(\phi) \\
C_a^G &= -2D_b\pi_a^b \\
C_a^\phi &= p_\phi\partial_a\phi;
\end{aligned} \tag{2.3}$$

(∂_a and D_a are the spatial partial and covariant derivatives and we have set $8\pi G = 1$ (to be reintroduced later)).

The reduced canonical action for the 3-sphere FLRW model is given by the parametrization [49] $q_{ab} = a^2(t)\Sigma_{ab}$ and $\pi^{ab} = (p(t)/6a(t))\ \Sigma^{ab}\sqrt{\det\,\Sigma}$, where

$$\Sigma_{ab}dx^a dx^b = R^2\left(\sigma_1^2 + \sigma_2^2 + \sigma_3^2\right) \tag{2.4}$$

is the 3-sphere metric of curvature $\kappa = 1/R^2$ defined by the frame fields $\sigma_1 = \sin\psi\sin\theta d\phi + \cos\psi d\theta$, $\sigma_2 = \cos\psi\sin\theta d\phi - \sin\psi d\theta$, $\sigma_3 = \cos\theta d\phi + d\psi$, with $\theta \in [0,\pi]$, $\phi \in [0,2\pi]$, $\psi \in [0,4\pi]$. The ADM action becomes

$$S = V_0\int dt\left(p\dot{a} + p_\phi\dot{\phi} - N\left(\mathcal{H}_G + \mathcal{H}_\phi\right)\right) \tag{2.5}$$

$$\mathcal{H}_G = -\frac{p^2}{24a} + \Lambda a^3 - \kappa a, \tag{2.6}$$

$$\mathcal{H}_\phi = \frac{p_\phi^2}{2a^3} + a^3V(\phi) \tag{2.7}$$

where $V_0 = \int\sqrt{\det\,\Sigma} = R^3\int\sigma_1\wedge\sigma_2\wedge\sigma_3$.

Under the rescaling $R \to lR$, we have $\kappa \to \kappa/l^2$, $V_0 \to l^3V_0$, and the phase space variables scale as

$$a \to a/l,\ p \to p/l^2,\ \phi \to \phi,\ p_\phi \to p_\phi/l^3, \tag{2.8}$$

(the latter because p_ϕ is a density of weight one). Therefore, it is useful to define the scale invariant variables

$$\begin{aligned} a \to a(V_0)^{1/3},\ \kappa \to \kappa(V_0)^{2/3}, \\ p \to p(V_0)^{2/3},\ p_\phi \to V_0 p_\phi, \end{aligned} \tag{2.9}$$

and the invariant volume $V \equiv V_0 a^3$; the rescaled a has dimension length and the rescaled κ is dimensionless. The fundamental Poisson bracket becomes $\{a, p\} = 1$. We use these variables in the following.

Exploring static solutions in cosmology is of great interest. These solutions to Einstein's field Equations, like Einstein's static universe discussed below, are crucial as they initiated modern relativistic cosmology by solving Friedmann equations for a homogeneous, finite, closed universe with a cosmological constant to balance matter density and achieve stasis. They act as fixed points in dynamical systems, helping analyze phase space, stability under perturbations, and transitions to expanding models–unstable in general relativity but potentially stable in modified gravities [51, 56]. These solutions test gravity theories, matter equations of state, and early-universe scenarios, such as emergent models avoiding singularities, while providing backgrounds for perturbation studies that inform structure formation [57, 58]. Let us first see if there are classical static solutions in our analysis.

The equations of motion (with $8\pi G$ reintroduced) are

$$\begin{aligned}
\mathcal{H} &\equiv \mathcal{H}_G + 8\pi G\, \mathcal{H}_\phi = 0, && (2.10)\\
\dot{a} &= \{a, \mathcal{H}\} = -\frac{p}{12a}, && (2.11)\\
\dot{p} &= \{p, \mathcal{H}\} = -\frac{p^2}{24a^2} - 3\Lambda a^2 + \kappa + 24\pi G \left(\frac{p_\phi^2}{2a^4} - a^2 V(\phi)\right) && (2.12)\\
\dot{\phi} &= \{\phi, \mathcal{H}\} = \frac{p_\phi}{a^3}, && (2.13)\\
\dot{p}_\phi &= \{p_\phi, \mathcal{H}\} = -a^3 V'(\phi). && (2.14)
\end{aligned}$$

Let us consider the static ansatz

$$\begin{aligned}
a &= R = \text{constant} > 0;\\
\phi &= \phi_0 = \text{constant}; \quad p = p_\phi = 0. && (2.15)
\end{aligned}$$

Then eqn. (2.14) requires $V'(\phi_0) = 0$, i.e. ϕ_0 must be an extremum of the potential, or the potential is a constant in a domain around ϕ_0. With $v_0 \equiv V(\phi_0)$ eqns. (2.10) and (2.12) become

$$\begin{aligned}
\Lambda R^2 - \kappa + 8\pi G R^2 v_0 &= 0,\\
-3\Lambda R^2 + \kappa - 24\pi G R^2 v_0 &= 0, && (2.16)
\end{aligned}$$

These have the solution

$$\Lambda = -8\pi G v_0, \quad \kappa = 0, \tag{2.17}$$

that is, the cosmological constant is fixed by the potential at an extremum value $\phi = \phi_0$; this is of course flat space interpreted as an exact cancellation of the cosmological constant with $V(\phi_0)$. However, if the potential is quadratic, $V(\phi) = m^2\phi^2/2$, eqn. (2.14) requires $\phi_0 = 0$ due to the static ansatz (2.15), and eqns. (2.16) have no

non-trivial solutions.

To summarize the classical situation, we have seen that there are flat static solutions for non-quadratic potentials, but no solutions for the quadratic potential. We will see that the latter is not the case for the classical-quantum equations we propose.

2.1.1 Classical-Quantum equations: FRW

We now describe the coupling of classical gravity with a quantized scalar field with quadratic potential. A canonical version for the model may be defined in the Schrödinger picture by starting with an effective Hamiltonian constraint where the scalar field is quantized, and deriving dynamics from such a constraint [45]; the scalar field Hamiltonian operator is

$$\hat{\mathcal{H}}_\phi = \frac{\hat{p}_\phi^2}{2a^3} + \frac{1}{2}a^3 m^2 \hat{\phi}^2. \tag{2.18}$$

The proposed equations for the classical-quantum theory are

$$\begin{aligned}
\mathcal{H}_{\rm eff} &\equiv -\frac{p^2}{24a} + \Lambda a^3 - \kappa a + 8\pi G\, \langle\psi|\hat{\mathcal{H}}_\phi|\psi\rangle = 0, && (2.19)\\
i|\dot{\psi}\rangle &= \hat{\mathcal{H}}_\phi|\psi\rangle, && (2.20)\\
\dot{a} &= \{a, \mathcal{H}_{\rm eff}\} = -\frac{p}{12a}, && (2.21)\\
\dot{p} &= \{p, \mathcal{H}_{\rm eff}\} = -\frac{p^2}{24a^2} - 3\Lambda a^2 + \kappa - 8\pi G \frac{\partial}{\partial a}\langle\psi|\hat{\mathcal{H}}_\phi|\psi\rangle. && (2.22)
\end{aligned}$$

The last term of (2.22) may be expanded to give

$$\begin{aligned}
\frac{\partial}{\partial a}\langle\psi|\hat{\mathcal{H}}_\phi|\psi\rangle &= \frac{1}{\dot{a}}\left(\langle\dot{\psi}|\hat{\mathcal{H}}_\phi|\psi\rangle + \langle\psi|\hat{\mathcal{H}}_\phi|\dot{\psi}\rangle\right) + \langle\psi|\frac{\partial}{\partial a}\hat{\mathcal{H}}_\phi|\psi\rangle\\
&= -\frac{3}{2}\left(\frac{\langle\hat{p}_\phi^2\rangle_\psi}{a^4} - a^2 m^2 \langle\hat{\phi}^2\rangle_\psi\right); && (2.23)
\end{aligned}$$

the first term is zero by (2.20) and the last expression is a direct calculation from the scale factor dependence of $\hat{\mathcal{H}}_\phi$ in (2.18). We use variables (2.9) for the above, this allows the equations (2.19-2.22) to remain invariant under rescalings (2.8). It is readily checked that the equations of motion ensure conservation of the effective Hamiltonian constraint $\mathcal{H}_{\text{eff}}$ (2.19):

$$\begin{aligned}
\frac{d}{dt}\mathcal{H}_{\text{eff}} &= \frac{\partial \mathcal{H}_{\text{eff}}}{\partial a}\dot{a} + \frac{\partial \mathcal{H}_{\text{eff}}}{\partial p}\dot{p} + 8\pi G\left(\langle\dot{\psi}|\hat{\mathcal{H}}_\phi|\psi\rangle + \langle\psi|\hat{\mathcal{H}}_\phi|\dot{\psi}\rangle\right) \\
&= -\left(-\frac{p^2}{24a^2} - 3\Lambda a^2 + \kappa - 8\pi G\frac{\partial}{\partial a}\langle\psi|\hat{\mathcal{H}}_\phi|\psi\rangle\right)\left(-\frac{p}{12a}\right) \\
&+ \left(-\frac{p}{12a}\right)\left(-\frac{p^2}{24a^2} - 3\Lambda a^2 + \kappa - 8\pi G\frac{\partial}{\partial a}\langle\psi|\hat{\mathcal{H}}_\phi|\psi\rangle\right) \\
&+ 8\pi G\left(i\langle\psi|\hat{\mathcal{H}}_\phi^2|\psi\rangle - i\langle\psi|\hat{\mathcal{H}}_\phi^2|\psi\rangle\right) \\
&= 0.
\end{aligned} \tag{2.24}$$

It is also readily shown that probability is conserved. This ensures that the proposed system of equations is self-consistent.

Initial data for this classical-quantum system at some $t = t_0$ is the set $\{a(t_0), p(t_0), |\psi\rangle(t_0)\}$ subject to the constraint $\mathcal{H}_{\text{eff}} = 0$; such data may be constructed by choosing $a(t_0)$ and $|\psi\rangle(t_0)$, and solving $\mathcal{H}_{\text{eff}} = 0$ for $p(t_0)$. In this way the $p(t_0)$ is state dependent, and the free data is $\{a(t_0), |\psi\rangle(t_0)\}$. In contrast, the constraint-free data for the classical system is $\{a(t_0), \phi(t_0), p_\phi(t_0)\}$, with p determined by solving the Hamiltonian constraint. Conservation of the semiclassical constraint (shown above) ensures, as in classical theory, that the evolved data continues to satisfy the constraint; we verify this explicitly in the numerical solutions presented below.

2.1.2 Static classical-quantum solutions

Existence of static solutions of the classical-quantum equations may be checked by setting $a = R =$ constant > 0 and $p = 0$, and $|\psi\rangle = |n\rangle$, an energy eigenstate of $\hat{\mathcal{H}}_\phi$ (2.18). For fixed $a = R$, scalar field mass m, and integer n,

$$\hat{\mathcal{H}}_\phi|n\rangle = E_n|n\rangle = m(n + 1/2)|n\rangle. \tag{2.25}$$

This reduces the evolution equations (2.19-2.22) to

$$\begin{aligned} \Lambda R^3 - R\kappa + 8\pi G m\,(n + 1/2) &= 0, & (2.26)\\ -3R^2\Lambda + \kappa &= 0 & (2.27)\\ |\psi\rangle(t) = e^{-iE_n(t-t_0)}|n\rangle, & & (2.28) \end{aligned}$$

where the first equation comes from (2.19), the second from (2.22), and the third is the stationary state solution of the TDSE; eqn. (2.21) holds identically. Viewing the first two equations as conditions on Λ and κ gives the solutions

$$\begin{aligned} \kappa_n &= 12\pi\,\frac{Gm}{R}\left(n + \frac{1}{2}\right) = 12\pi G R^2\langle n|\hat{\rho}_\phi|n\rangle, & (2.29)\\ \Lambda_n &= 4\pi\,\frac{Gm}{R^3}\left(n + \frac{1}{2}\right) = 4\pi G\langle n|\hat{\rho}_\phi|n\rangle, & (2.30) \end{aligned}$$

where $\hat{\rho} = \hat{\mathcal{H}}_\phi/R^3$; (recall that κ is dimensionless in the scale invariant variables (2.9)).

Thus, unlike the classical case with quadratic potential, static semiclassical solutions arise with set values of both the cosmological constant and curvature; there are no static solutions with either κ or Λ being zero. The reason there is a semiclassical static solution and no classical one is that the expectation value $\langle n|\hat{\mathcal{H}}_\phi|n\rangle$ is independent of the scale factor (unlike the classical $\mathcal{H}_\phi$), therefore the Poisson bracket

$\{p, \langle n|\hat{\mathcal{H}}_\phi|n\rangle\} = 0$; this simplifies the $\dot{p} = 0$ condition and permits a solution. Intuitively, an apparent reason is that there is a state of the massive scalar field in a 3−sphere universe which does not spread due to the values of the cosmological constant and curvature. This may not hold for states $|\psi\rangle$ that are not eigenstates of $\hat{\mathcal{H}}_\phi$ (or linear combinations of such eigenstates), precisely because $\langle\psi|\hat{\mathcal{H}}_\phi|\psi\rangle$ would be a function of the scale factor, and hence be time-dependent.

If the effective Hamiltonian constraint (2.19) is calculated in a coherent state $|\alpha\rangle$ of the scalar field, then $\langle\alpha|\hat{\mathcal{H}}_\phi|\alpha\rangle = m|\alpha|^2 + 1/2$, and again $\{p, \langle\alpha|\hat{\mathcal{H}}_\phi|\alpha\rangle\} = 0$; thus, the static semiclassical solution still arises, but now with (2.26-2.28) replaced by

$$\Lambda R^3 - R\kappa + 8\pi G m\left(|\alpha|^2 + 1/2\right) = 0, \tag{2.31}$$

$$-3R^2\Lambda + \kappa = 0 \tag{2.32}$$

$$|\alpha\rangle(t) = e^{-|\alpha|^2/2}\sum_{n=0}^{\infty} e^{-iE_n(t-t_0)}\frac{\alpha^n}{\sqrt{n!}}|n\rangle. \tag{2.33}$$

The solution is the same as (2.29-2.30) with n replaced by $|\alpha|^2$, and unlike the eigenstate case it allows any real values of κ and Λ, but with both dependent on $|\alpha|$.

In summary, we see that there are no static solutions for coupling to a classical massive scalar field, but there are for the classical-quantum case. For comparison, let us recall the static Friedmann equations ($a = R$) for perfect fluid equation of state $P = \sigma\rho$:

$$-\frac{4\pi G\rho}{3}(1 + 3\sigma) + \frac{\Lambda}{3} = 0 \tag{2.34}$$

$$\frac{8\pi G\rho}{3} + \frac{\Lambda}{3} - \frac{\kappa}{R^2} = 0, \tag{2.35}$$

which lead to

$$\Lambda = 4\pi G\rho(1+3\sigma); \tag{2.36}$$

$$\kappa = 4\pi G\rho R^2(1+\sigma). \tag{2.37}$$

It is therefore evident that classical static solutions arise for $\Lambda = 0$ and $\kappa > 0$ if $\sigma = -1/3$; and $\Lambda > 0$ and $\kappa = 0$ if $\sigma = -1$; the $\mathbb{R} \times S^3$ Einstein static Universe is the case $\Lambda > 0$, $\kappa > 0$ for any $\sigma \geq 0$.

In contrast, the classical-quantum static solutions require $\Lambda > 0$ and $\kappa > 0$ from eqns. (2.29-2.30); these exist for coherent states and any linear combination of energy eigenstates of the scalar field. Thus, these are like the Einstein static Universe but with Λ and κ determined by the scalar field state.

In summary, for the massive scalar field, there are no classical static solutions, but there are classical-quantum static solutions.

2.1.3 Linear stability analysis

To check linear stability of the static solution ($a = R$, $p_a = 0$, and $|\psi\rangle = |n\rangle$), let

$$\begin{aligned} a(t) &= R + \epsilon\, a_1(t) + \mathcal{O}(\epsilon^2), \\ p(t) &= 0 + \epsilon\, p_1(t) + \mathcal{O}(\epsilon^2), \\ |\psi\rangle(t) &= |n\rangle + \epsilon\, |\chi\rangle(t) + \mathcal{O}(\epsilon^2), \end{aligned} \tag{2.38}$$

with

$$|\chi\rangle(t) = \sum_k c_k(t)|k\rangle, \tag{2.39}$$

where $|k\rangle$ are eigenstates at the static point $a = R$; we insert these into the equations of motion (2.19-2.22). The effective constraint becomes

$$\begin{aligned}\mathcal{H}_{\text{eff}} &= \Lambda R^3 - \kappa R + 8\pi G m\,(n + 1/2) \\ &\quad + \epsilon\left[3\Lambda a_1 R^2 - \kappa a_1 + 8\pi G\left(\langle n|\hat{\mathcal{H}}_\phi^{(1)}|n\rangle\right.\right. \\ &\quad \left.\left. + \langle\chi|\hat{\mathcal{H}}_\phi|n\rangle + \langle n|\hat{\mathcal{H}}_\phi|\chi\rangle\right)\right], \end{aligned} \tag{2.40}$$

where

$$\hat{\mathcal{H}}_\phi^{(1)} = \frac{3}{2}\left(-\frac{a_1}{R^4}\,\hat{p}_\phi^2 + a_1 R^2 m^2 \hat{\phi}^2\right). \tag{2.41}$$

The first order constraint and evolution equations are

$$\mathcal{H}_{\text{eff}}^{(1)} \equiv m(2n+1)\text{Re}\{c_n\} = 0, \tag{2.42}$$

$$\dot{a}_1 = -\frac{p_1}{12R}, \tag{2.43}$$

$$\dot{p}_1 = -\left(6\Lambda R + \frac{9m}{R^2}\left(n + \frac{1}{2}\right)\right)a_1 - \frac{3m}{R}g(n), \tag{2.44}$$

$$i\dot{c}_k = E_k c_k + \frac{3ma_1}{2R}\left(\sqrt{n(n-1)}\;\delta_{k,n-2} + \sqrt{(n+1)(n+2)}\;\delta_{k,n+2}\right), \tag{2.45}$$

where in (2.44)

$$g(n) \;=\; \text{Re}\{c_{n+2}\}\sqrt{(n+1)(n+2)} + \text{Re}\{c_{n-2}\}\sqrt{n(n-1)}. \tag{2.46}$$

From (2.45) it is evident that only c_{n-2} and c_{n+2} evolve with a "source," and all other perturbed state components ($k \neq (n-2), (n+2)$) satisfy $c_k(t) = c_k(0)e^{-iE_k t}$, . Furthermore, the perturbed constraint $\mathcal{H}_{\text{eff}}^{(1)} = 0$ is solved for all time if $c_n(0) = 0$; i.e. the state perturbation excludes the static solution state $|n\rangle$, i.e. $|\chi\rangle(t) = \sum_{k\neq n} c_k(t)|k\rangle$. Interestingly, this also ensures that probability is conserved to first

order:

$$\begin{aligned}\langle\psi|\psi\rangle &= \langle n|n\rangle + \epsilon\left(\langle\chi|n\rangle + \langle n|\chi\rangle\right) + \mathcal{O}(\epsilon^2) \\ &= 1 + \mathcal{O}(\epsilon^2). \end{aligned} \tag{2.47}$$

For $n = 0$ the above equations for linear perturbations reduce to a coupled set for a_1, p_1 and c_2; the equations for c_1 and $c_k,\ k > 2$ have solutions $c_k = \exp\{-iE_k t\}c_k(0)$. The three eigenvalues for the former set depend on the values of the static solution parameters m, R and Λ; a numerical check for a range of these parameters reveals that two of these are growing modes, and one is a decaying mode.

2.1.4 Comparison of exact classical-quantum and classical dynamics

In the last section we showed that there are exact static solutions of the classical-quantum system and discussed their linear stability. We now present numerical solutions of the full classical-quantum equations (2.19-2.22) with initial data that is a small perturbation of the static classical-quantum universe; we compare these with the evolution of the classical-classical system (2.10-2.14) with the same initial data. Specifically, we track the evolution of energy density, Hubble parameter, and acceleration in the two systems, while checking the conservation of the respective Hamiltonian constraints and the probability for the classical-quantum case.

Suppose $\{a_s, |n\rangle; \Lambda_n, \kappa_n, m\}$ is a static solution of the classical-quantum equations. Then, the perturbed data we consider is the set

$$\{a_s + \Delta a, |n\rangle\} \tag{2.48}$$

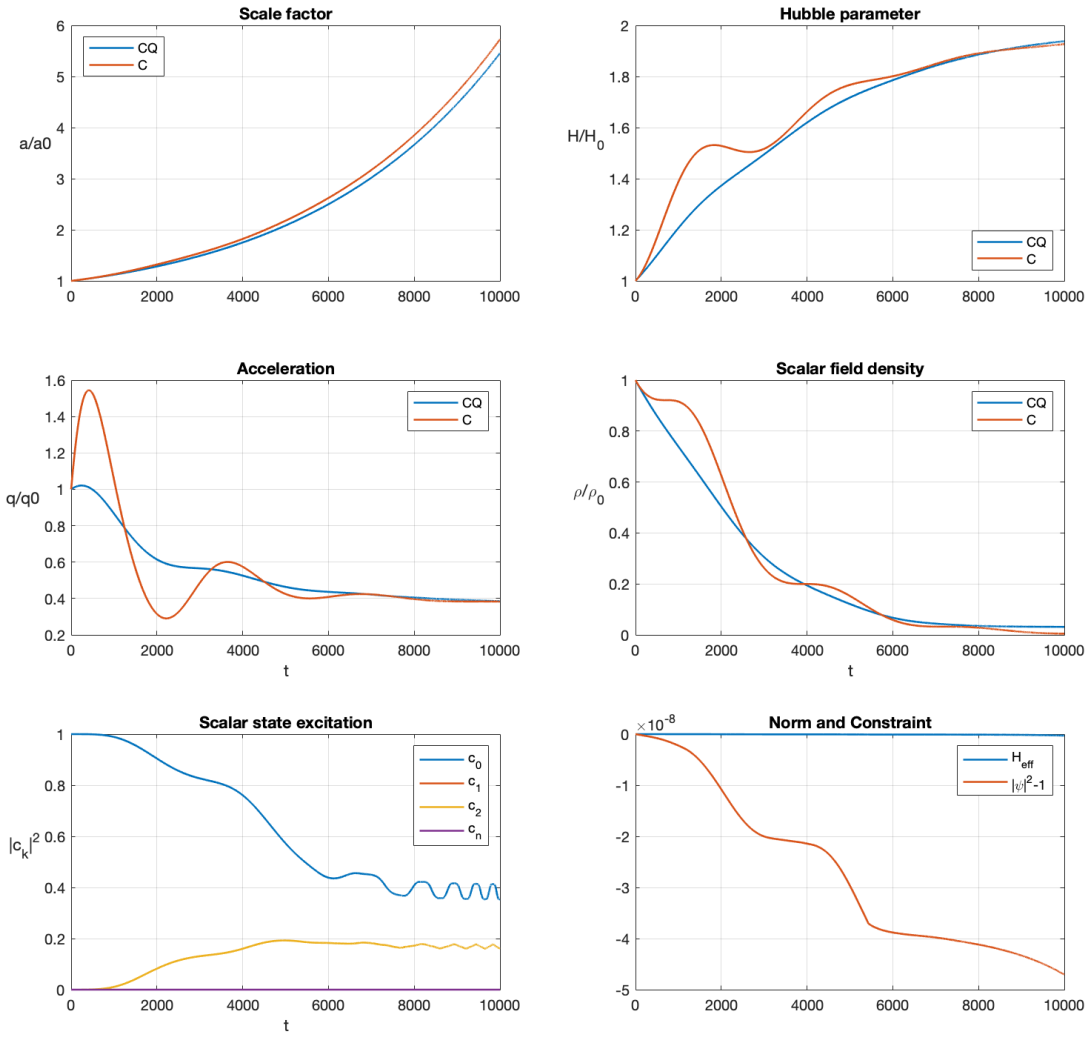


Figure 2.1: A typical comparative evolution of the classical-quantum (CQ) and classical (C) evolution with scalar field of mass 10^{-3} (Planck units) initially in its ground state $|0\rangle$. Initial data is a perturbation of a static semiclassical solution; the first four frames show the scale factor, Hubble parameter, acceleration, and density, relative to their initial values; the fifth frame shows the occupation probabilities $|c_i|^2$ of higher scalar field states (with $c_n = c_{40}$); the last frame confirms conservation of probability and of the effective Hamiltonian constraint.

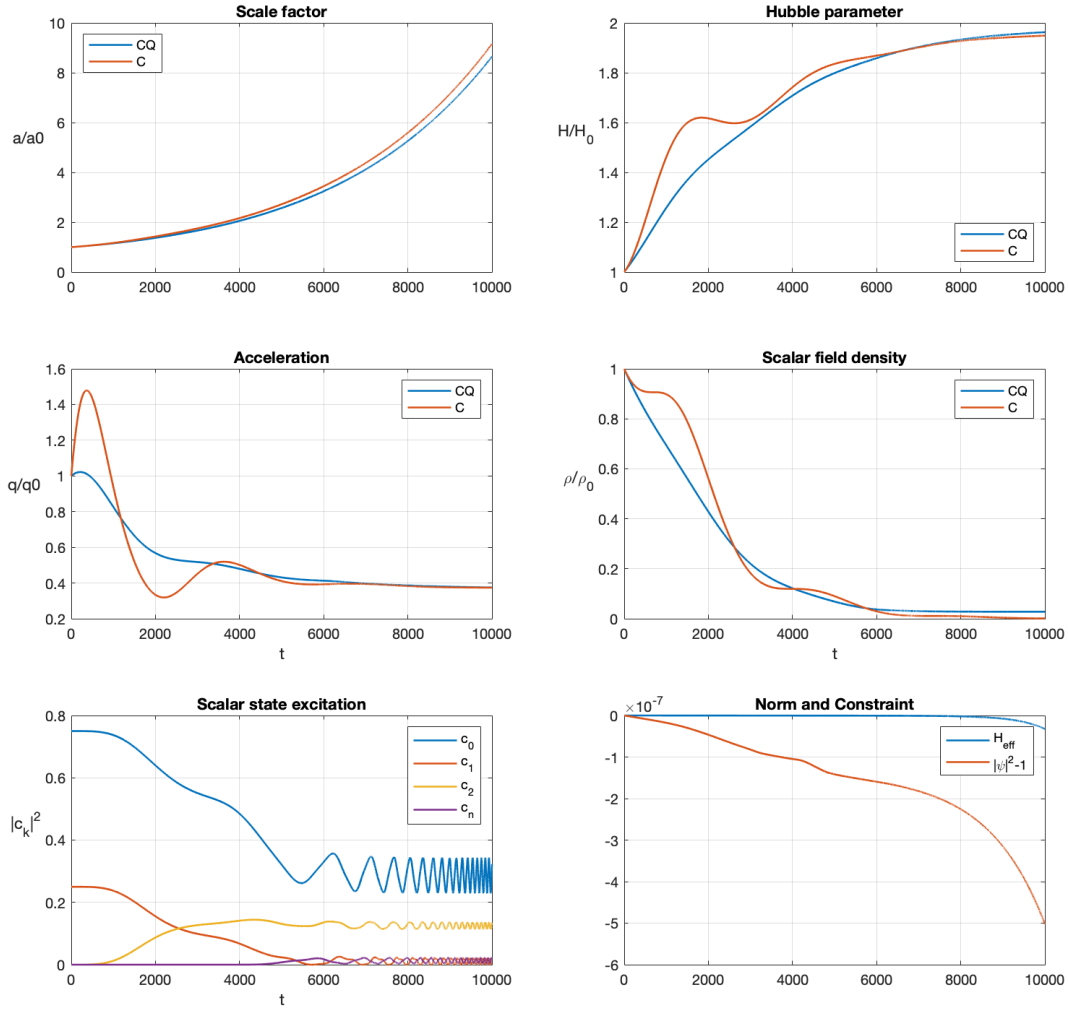


Figure 2.2: A typical comparative evolution of the classical-quantum (CQ) and classical (C) evolution for the same data as in Fig. 2.1 but with scalar field initial state $(\sqrt{3}/2)|0\rangle + (1/2)|1\rangle$.

for the same parameter values $\{\Lambda_n, \kappa_n, m\}$. Solving $\mathcal{H}_{\rm eff} = 0$ (2.19) with this perturbed data gives the initial value of p. From this we can compute initial values for the observables of interest, the Hubble and acceleration parameters $H = \dot{a}/a$ and $q = \ddot{a}/aH^2$, and energy density $\rho = \langle\hat{\mathcal{H}}_{\rm eff}\rangle_n/a^3$; the initial acceleration q is proportional to $\dot{p}$ and is determined by the r.h.s. of eqn. (2.22).

Initial data for the classical-classical equations is the set $\{a_s + \Delta a, \phi, p_\phi\}$, with p determined by solving the Hamiltonian constraint. Matching the classical-quantum data requires the initial values of $\{\phi, p_\phi\}$ from the state $|n\rangle$. This is accomplished by setting

$$\phi = \sqrt{\langle\hat{\phi}^2\rangle_n}; \quad p_\phi = \sqrt{\langle\hat{p}_\phi^2\rangle_n}, \tag{2.49}$$

a choice that matches the initial energy densities ρ and accelerations q for the CQ and C equations. The truncation of the scalar field Hilbert space used for numerical evolution is $n = 40$, a number that does not affect probability conservation provided maximum evolution time is not too large and the chosen initial state is close to the ground state.

Fig. 2.1 illustrates typical evolution for the classical-quantum and classical systems. Initial data is $a_0 = a_s + 5$ with $a_s = 10$ with the scalar field initially its ground state $|n = 0\rangle$; $m = 10^{-3}$, $\Lambda = 2.5 \times 10^{-10}$ and $\kappa = 7.5 \times 10^{-6}$ (in Planck units) are fixed by the static solution for $a_s = 10$. It is evident that the CQ and C evolutions differ, with the classical evolution of various quantities oscillating around the CQ one, and that at late times the CQ and C approach each other with small differences; the fifth frame shows the excitation of higher states of the scalar field as the universe expands (with $c_n = c_{40}$, the truncation level of the oscillator basis used; the last frame demonstrates numerical conservation of probability and the effective Hamiltonian constraint.

Fig. 2.2 shows a similar evolution to that in Fig. 2.1, the only difference being the

choice of initial state which is now $(\sqrt{3}/2)|0\rangle + (1/2)|1\rangle$. The comparative dynamics is nearly identical, except for the excitation probabilities of higher scalar field states. This occurs because the state evolution also connects all odd states in addition to even states as in Fig. 1. It is also evident that there is now also a small excitation of the last level in the truncation of the Hilbert space used for the numerical evolution.

A variety of initial data that are perturbations of the semiclassical static solution yield qualitatively similar evolution. The agreement of the classical and classical-quantum results at late times provides justification for the classical-quantum effective Hamiltonian constraint. Lastly, instead of eigenstates of the scalar Hamiltonian, we can also use coherent states, or arbitrary linear combinations thereof. The results are again qualitatively similar. The reason is that although the state evolves, $\langle\hat{\mathcal{H}}_\phi\rangle$ does not; the initial state only serves to fix the initial momentum p conjugate to the scale factor via the effective constraint.

2.2 Classical-Quantum anisotropic cosmology

In this section we extend the approach used above to the flat Kasner metrics

$$ds^2 = -N^2(t)dt^2 + \sum_{k=1}^{3}\left(a_k(t)dx^k\right)^2 \tag{2.50}$$

With a scalar field the reduced ADM canonical action for this metric is

$$\begin{aligned} S &= \int dt\left(\sum_{k=1}^{3}\pi_k\dot{a}_k + p_\phi\dot{\phi} - N\left(\mathcal{H}_K + \mathcal{H}_\phi\right)\right), \\ \mathcal{H}_K &= \frac{1}{4v}\left[\sum_k \lambda_k^2 - \frac{1}{2}\left(\sum_k \lambda_k\right)^2\right] + \Lambda v \\ \mathcal{H}_\phi &= \frac{p_\phi^2}{2v} + vV(\phi), \end{aligned} \tag{2.51}$$

where $v = \prod_k a_k$ and $\lambda_k = a_k \pi_k$.

For the vacuum case with $\Lambda = 0$ and $N = 1$, Hamilton's equations give

$$\dot{\lambda}_i = \{\lambda_i, \mathcal{H}_K\} = 0, \tag{2.52}$$

$$\dot{v} = \{v, \mathcal{H}_K\} = -\frac{1}{4} \sum_k \lambda_k \equiv \mu \tag{2.53}$$

$$h_k = \frac{\dot{a}_k}{a_k} = \frac{1}{2v} \left(\lambda_k + 2\mu\right). \tag{2.54}$$

Thus, λ_i are constants of the motion,

$$v(t) = \mu t + v_0 \tag{2.55}$$

and the solution for the scale factors is

$$a_k(t) = a_k(0) \left[v(t)\right]^{p_k}, \quad p_k = 1 + \frac{\lambda_k}{2\mu}. \tag{2.56}$$

It is readily verified from the definition of μ (3.11) that the Kasner exponents p_k satisfy

$$\sum_k p_k = 1, \quad \sum_k p_k^2 = 1, \tag{2.57}$$

where the latter follows from the Hamiltonian constraint $\mathcal{H}_K = 0$. These steps summarize the derivation of the well-known Kasner solution from the canonical equations. For non-zero scalar field and Λ, λ_k are no longer constants of the motion as $\{\lambda_k, v\} = -v$.

To see if there are classical static solutions with scalar field and non-zero Λ, we set $\phi = \phi_0 =$ constant, $p_\phi = 0 = \pi_k$, and $a_k = a_{k0} =$ constants; in addition the r.h.s. of $\dot{p}_\phi$ and $\dot{\pi}_k = \{\pi_k, \mathcal{H}_K + \mathcal{H}_\phi\}$ must be set to zero. These conditions and the

Hamiltonian constraint respectively give

$$\begin{aligned} V'(\phi)|_{\phi_0} &= 0, \\ \{\pi_k, v\}(\Lambda + V(\phi_0)) &= 0, \\ v_0(\Lambda + V(\phi_0)) &= 0. \end{aligned} \tag{2.58}$$

Hence, there are non-trivial static solutions provided the potential has extrema $\phi_0 \neq 0$ with tuned $\Lambda = -V(\phi_0)$. Such solutions would have at least one linearly stable mode at extrema that are local minima, the double well being an obvious example; there is no non-trivial static solution for the purely quadratic potential.

2.2.1 CQ Kasner

We now consider a quantum scalar field coupled to Kasner spacetime. As for the FRW case discussed above we define the dynamics through an effective Hamiltonian constraint

$$\mathcal{H}_{\text{eff}} \equiv \mathcal{H}_K + \langle\psi|\hat{\mathcal{H}}_\phi(v)|\psi\rangle. \tag{2.59}$$

The proposed semiclassical geometrodynamics equations in the Schrodinger picture for the Kasner model are

$$\mathcal{H}_{\text{eff}} = 0, \tag{2.60}$$

$$i|\dot{\psi}\rangle = \hat{\mathcal{H}}_\phi|\psi\rangle(v), \tag{2.61}$$

$$\dot{a}_k = \{a_k, \mathcal{H}_K\}, \tag{2.62}$$

$$\dot{\pi}_k = \left\{\pi_k, \mathcal{H}_K + \langle\psi|\hat{\mathcal{H}}_\phi(v)|\psi\rangle\right\}. \tag{2.63}$$

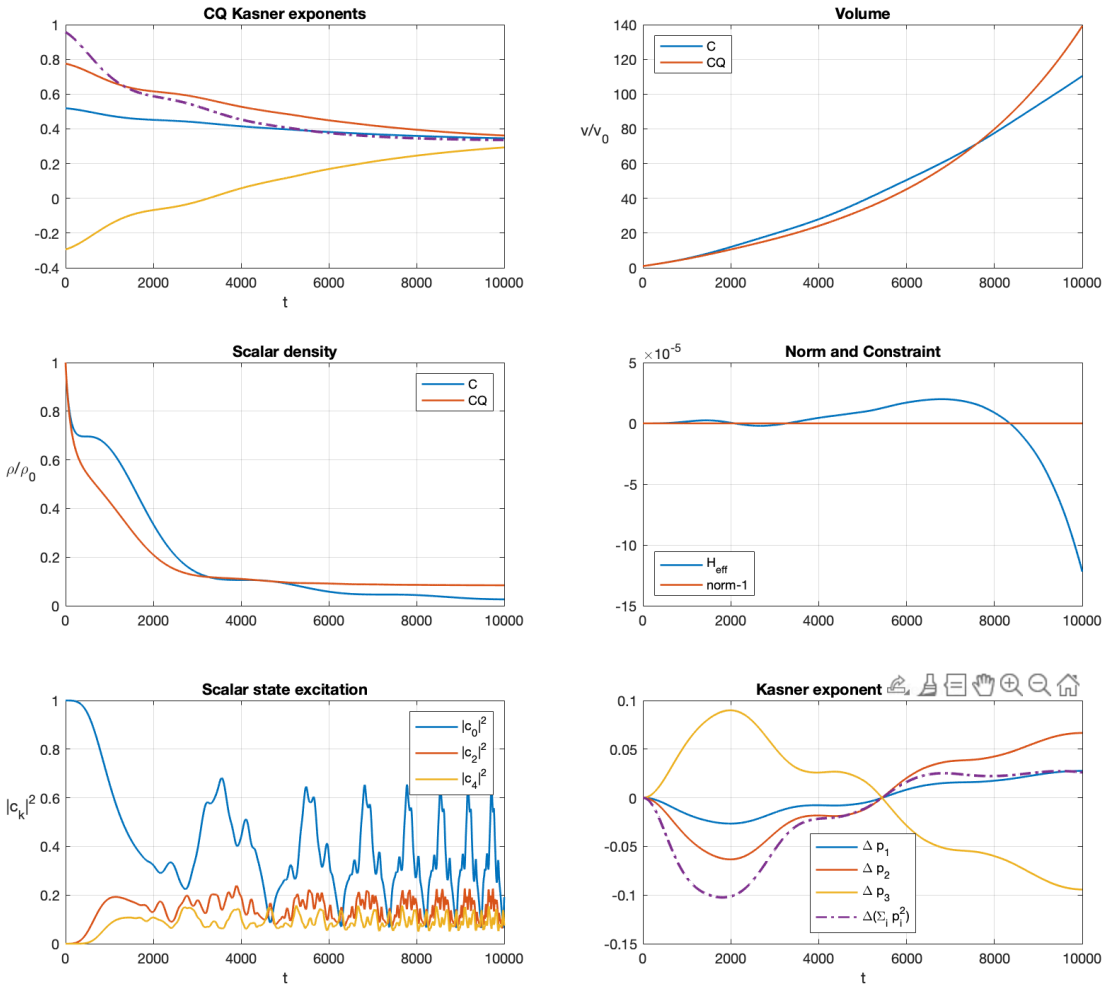


Figure 2.3: Numerical solution of the Kasner classical-quantum equations with the scalar field starting in the vacuum $|0\rangle$: the first frame shows the (dynamical) Kasner exponents, followed by comparison graphs of volume and scalar field density; the forth frame shows conservation of the effective constraint and probability; the last two frame show the excitation of the higher scalar states, and the difference between the classical and classical-quantum Kasner exponents.

The scalar field Hamiltonian operator is

$$\hat{\mathcal{H}}_\phi = \frac{\hat{p}_\phi}{2v} + vV(\hat{\phi}) \tag{2.64}$$

Evolution of π_k is explicitly state dependent through the factor v in $\hat{\mathcal{H}}_\phi$, and that of the scale scale factors a_k is implicitly through π_k. As for the FRW case above, state evolution is in the Schrodinger picture in a truncated fixed oscillator basis $|\psi\rangle = \sum_k^N c_k(t)|k\rangle$.

It is readily verified that $\mathcal{H}_{\rm eff}$ is conserved using the evolution equations:

$$\frac{d}{dt}\mathcal{H}_{\rm eff} = \sum_{k=1}^{3}\left[\frac{\partial \mathcal{H}_{\rm eff}}{\partial a_k}\dot{a}_k + \frac{\partial \mathcal{H}_{\rm eff}}{\partial \pi_k}\dot{\pi}_k\right] + \ \langle\dot{\psi}|\hat{\mathcal{H}}_\phi|\psi\rangle + \langle\psi|\hat{\mathcal{H}}_\phi|\dot{\psi}\rangle = 0.$$

2.2.2 Numerical solution

Let us first note that there are no static solutions of the above equations: setting the scale factors to constants and their conjugate momenta to zero, the effective Hamiltonian constraint in an eigenstate of $\mathcal{H}_\phi$ and the $\dot{\pi}_k$ equations are

$$\begin{aligned} \Lambda v_0 + m(n+1/2) &= 0, \\ \{\pi_k, \mathcal{H}_K\}|_{\pi_k=0} &= v_0\Lambda/a_k; \end{aligned} \tag{2.65}$$

the first gives $\Lambda = -m(n+1/2)/v_0 \neq 0$ while the second requires $\Lambda = 0$. This indicates that static solutions require non-zero curvature; this is shown below for the Bianchi IX case.

Of interest for a numerical study of eqns. (2.60-2.63) is the dynamics of Kasner exponents (3.14); these are constants of the motions for the vacuum equations with $\Lambda = 0$, but not otherwise. In particular, it is of interest to compare their dynamics

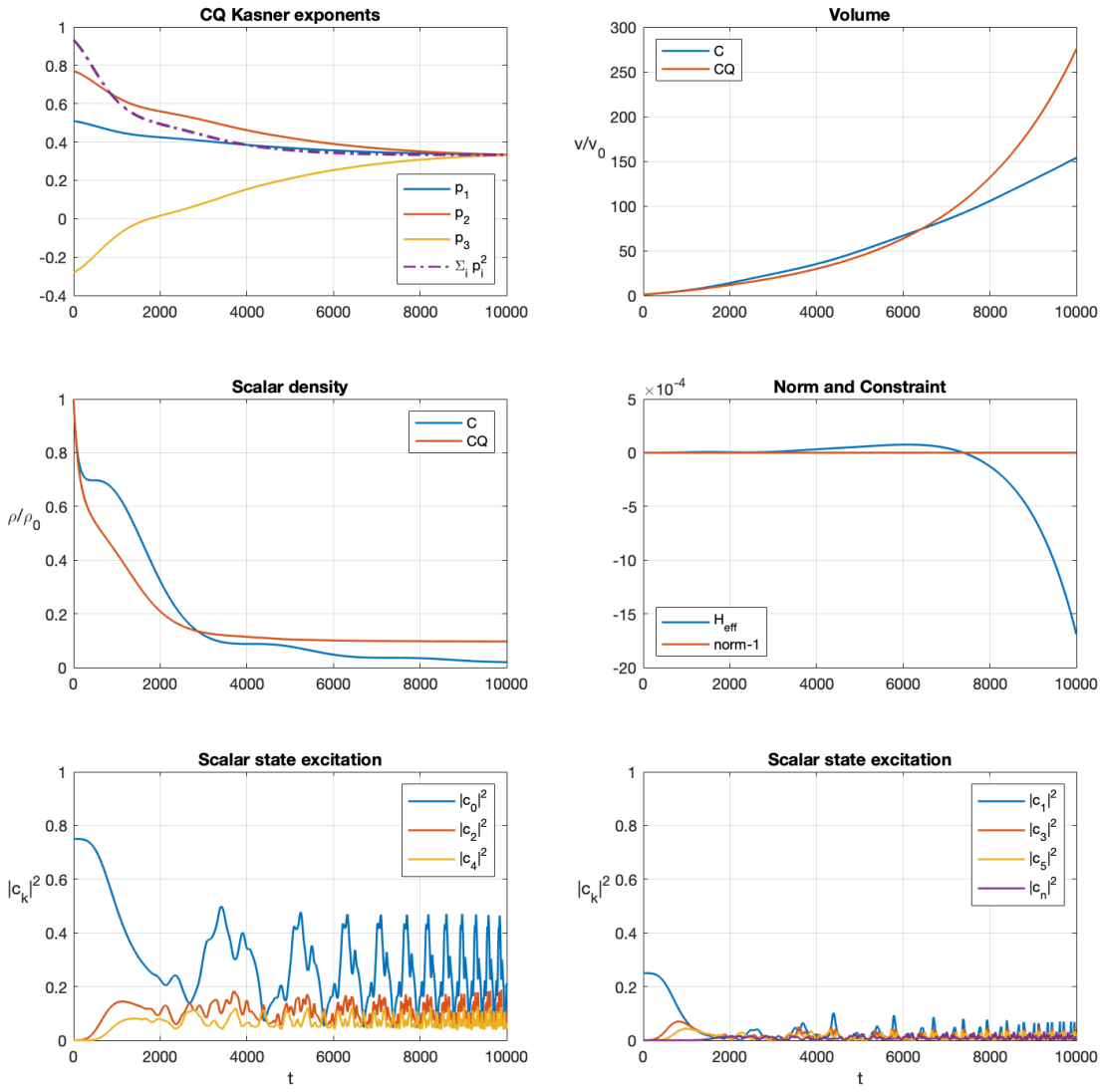


Figure 2.4: Numerical solution of the Kasner classical-quantum equations with the scalar field starting in the state $(\sqrt{3}/2)|0\rangle + (1/2)|1\rangle$: the first frame shows the (dynamical) Kasner exponents for the CQ case, followed by comparison graphs of volume and scalar field density; the last two frames show the excitation of the higher scalar states; $c_n = c_{50}$ is the truncation level of the scalar field basis.

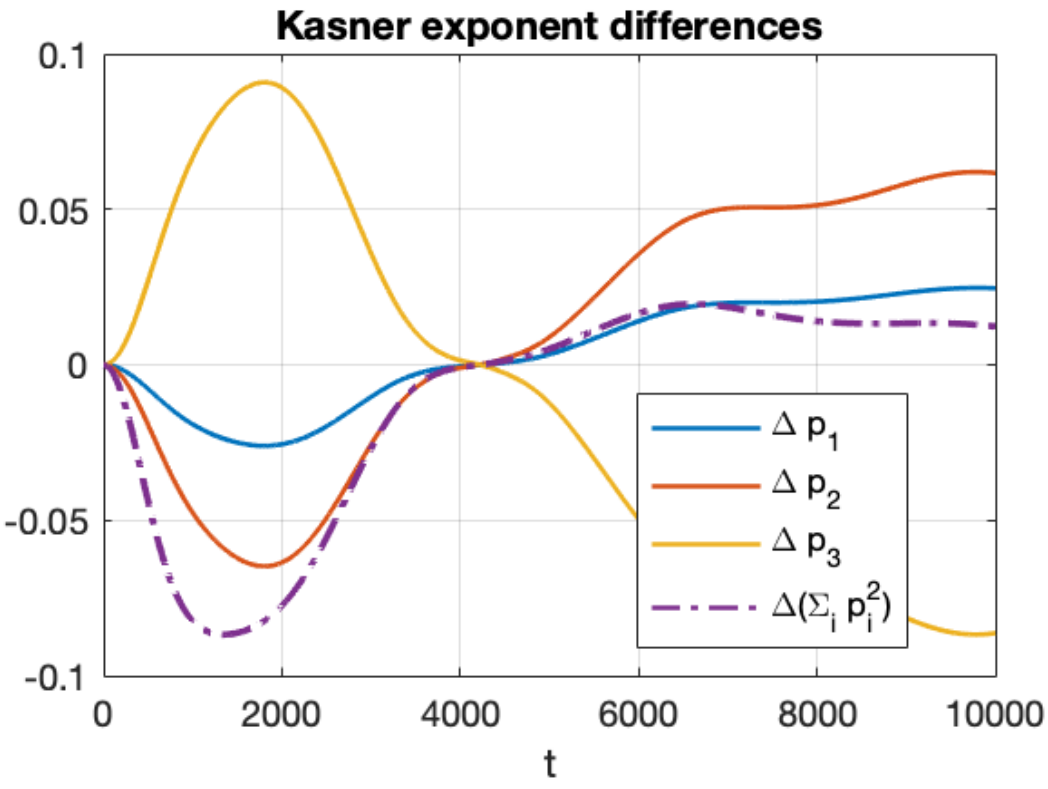


Figure 2.5: The difference between the CQ and C dynamical Kasner exponents for the data used for Fig. 2.4.

in the classical and classical-quantum cases as the singularity is approached and as the universe expands and approaches isotropy.

Numerical solutions of eqns. (2.60-2.63) are shown in Fig. 2.3 and 2.4 for the initial data $a_1 = 15.0$, $a_2 = 14.0$, $a_3 = 4.0$, $\pi_1 = -0.2$, $\pi_2 = -0.1$, with $m = 0.001$ and $\Lambda = 0$, and initial scalar states $|0\rangle$ and $(\sqrt{3}/2)|0\rangle + (1/2)|1\rangle$ respectively; π_3 is determined by solving $\mathcal{H}_{\text{eff}} = 0$, and the initial data for the classical scalar field case is again determined by eqn. (3.32). The first frame shows the evolving Kasner exponents for the CQ case, including one of the sum rules; isotropization occurs as the universe expands, as for the classical case, but there are differences in both the volume and density at large volume. The energy density ρ/ρ_0 for the CQ case approaches a constant at large volume whereas the energy density of the C case continues to decline. Both the volume and energy density are larger for the CQ case at late times.

Fig. 2.5 shows the difference in the evolution of the C and CQ exponents $p_k^C - p_k^{CQ}$, $k = 1, 2, 3$ and the difference between their sum of squares for the data used for Fig. 2.4; while these differences are small, their cumulative affect on volume and energy density is evident at late time in the volume and scalar energy density mentioned above.

The differences between Figs. 2.3 and 2.4 arise solely from the different initial states of the scalar field. In both cases the expectation value of the scalar density $\rho = \langle\hat{\mathcal{H}}_\phi\rangle/v$ differs from the classical ρ; the latter shows some oscillation and decays to zero, whereas the former does not and appears to decay at a much slower rate (up to the integration times shown). This is potentially significant in that it suggests the emergence of a "cosmological constant" or equivalent "dark energy" apparently caused by excitation of higher states of the scalar field at late times together with isotropization. The other main difference is in the volume, which at late times is

larger than for the classical equations for both initial scalar states.

Lastly, the other main difference between Figs. 2.3 and 2.4 is the excitation of higher energy levels of the scalar field as the universe expands. This is the homogeneous analog of particle creation; the initial state $|0\rangle$ shows excitation of only the even levels (since the Hamiltonian is quadratic in creation/annihilation operators) whereas the the initial state $\sqrt{3}/2)|0\rangle + (1/2)|1\rangle$ shows excitation of all levels. The Hilbert space truncation level used was $n = 50$ for both figures.

2.2.3 CQ Bianchi Universes

The difference between Kasner and the other Bianchi models is the addition of spatial curvature. This is best studied in Misner's parametrization [59] where the universe's volume is separated from its anisotropy variables; the curvature arises as a function of the latter through a gravitation potential term in the Hamiltonian constraint [49]. Misner's parametrization is a transformation of the metric variables (a_1, a_2, a_3) to $(\Omega, \beta_-, \beta_+)$:

$$\Omega = -\frac{1}{3}\ln(a_1 a_2 a_3) \tag{2.66}$$

$$\beta_+ = \frac{1}{3}\ln\left(\frac{a_1 a_2}{a_3^2}\right), \tag{2.67}$$

$$\beta_- = \frac{1}{\sqrt{3}}\ln\left(\frac{a_1}{a_2}\right). \tag{2.68}$$

The conjugate momenta are related by

$$p_\Omega = -(ap_a + bp_b + cp_c), \tag{2.69}$$

$$p_+ = ap_a + bp_b - 2cp_c, \tag{2.70}$$

$$p_- = \sqrt{3}(ap_a - bp_b). \tag{2.71}$$

In terms of these variables, the CQ effective Hamiltonian constraint is

$$\begin{aligned} H_{\rm eff} &= \frac{e^{3\Omega}}{24}\left(p_+^2+p_-^2-p_\Omega^2\right)+e^{-3\Omega}\Lambda+e^{-\Omega}V(\beta_+,\,\beta_-)+\langle\hat{H}_\phi\rangle_\psi \\ &= 0, \end{aligned} \tag{2.72}$$

where

$$\langle\hat{H}_\phi\rangle_\psi=\frac{e^{3\Omega}}{2}\langle\hat{p}_\phi^2\rangle_\psi+\frac{1}{2}m^2e^{-3\Omega}\langle\hat{\phi}^2\rangle_\psi. \tag{2.73}$$

The spatial curvature term is $e^{-\Omega}V(\beta_-,\beta_+)$ which is determined by the Bianchi type summarized in the table below. The canonical equations of motion are

$$\dot{\Omega} = \{\Omega,\,H\}=-\frac{e^{3\Omega}}{12}\,p_\Omega \tag{2.74}$$

$$\dot{\beta}_\pm = \{\beta_\pm,\,H\}=\frac{e^{3\Omega}}{12}\,p_\pm \tag{2.75}$$

$$\dot{p}_\pm = \{p_\pm,\,H\}=-e^{-\Omega}\frac{\partial}{\partial\beta_\pm}V(\beta_+,\,\beta_-) \tag{2.76}$$

$$\dot{p}_\Omega = \{p_\Omega,\,H\}=-3(H_K-e^{-3\Omega}\Lambda)+e^{-\Omega}V(\beta_+,\,\beta_-)-\frac{\partial}{\partial\Omega}\langle\psi|\hat{H}_\phi|\psi\rangle, \tag{2.77}$$

where the last term expands as

$$\begin{aligned} \frac{\partial}{\partial\Omega}\langle\hat{H}_\phi\rangle_\psi &= \frac{1}{\dot{\Omega}}\left(\langle\dot{\psi}|\hat{H}_\phi|\psi\rangle+\langle\psi|\hat{H}_\phi|\dot{\psi}\rangle\right)+\langle\frac{\partial\hat{H}_\phi}{\partial\Omega}\rangle_\psi \\ &= \frac{3}{2}\left(e^{3\Omega}\langle\hat{p}_\phi^2\rangle_\psi-m^2e^{-3\Omega}\langle\hat{\phi}^2\rangle_\psi\right). \end{aligned} \tag{2.78}$$

We now check if there are static solutions for any of the Bianchi universes by setting

Bianchi Type	$V(\beta_+,\, \beta_-)$
I	0
II	$e^{-8\beta_+}$
III	$4e^{-(2\beta_+ - 2\sqrt{3}\beta_-)}$
IV	$e^{4\beta_+}(12 + e^{4\sqrt{3}\beta_-})$
V	$12e^{4\beta_+}$
VIII	$e^{-8\beta_+} + 2e^{4\beta_+}\left[\cosh\left(4\sqrt{3}\beta_-\right) - 1\right]$ $+ 4e^{-2\beta_+}\cosh\left(2\sqrt{3}\beta_-\right)$
IX	$e^{-8\beta_+} + 2e^{4\beta_+}\left[\cosh\left(4\sqrt{3}\beta_-\right) - 1\right]$ $- 4e^{-2\beta_+}\cosh\left(2\sqrt{3}\beta_-\right)$

metric functions constant and all momenta zero:

$$\begin{aligned} \Omega &= \Omega_0, \quad \beta_+ = \bar{\beta}_+, \quad \beta_- = \bar{\beta}_-, \\ p_\Omega &= p_+ = p_- = 0, \end{aligned} \tag{2.79}$$

in (2.72) and (2.74-2.77) with $|\psi\rangle = \sum_{k=1}^{N} c_k |k\rangle$, a linear combination of eigenstates of the quantum scalar field Hamiltonian. This gives the conditions

$$\begin{aligned} e^{-3\Omega_0}\Lambda + e^{-\Omega_0}V(\bar{\beta}_+,\, \bar{\beta}_-) & \\ + m\sum_{k=0}^{N} |c_k|^2 \,(k + 1/2) &= 0, && (2.80) \\ V_{,\beta_\pm} &= 0, && (2.81) \\ 3e^{-\Omega_0}\Lambda + e^{-\Omega_0}V(\bar{\beta}_+,\, \bar{\beta}_-) &= 0; && (2.82) \end{aligned}$$

all other equations vanish identically, as does the last term in (2.77).

From this it is evident that static solutions of the CQ equations require an extremum of the Bianchi potential V; with this, the last equation fixes the value of Λ, and the first fixes the expectation value of scalar Hamiltonian. Extrema of the potential occurs only for the Bianchi IX potential, and for this case, the extremum is a minimum.

Hence, the static solution is stable.

Lastly, we note that requiring a static solution of the corresponding classical equations involves setting $\phi =$ constant and $p_\phi = \dot{p}_\phi = 0$. For the massive scalar field, this imposes $\phi = 0$; hence there is no classical static solution for the same Bianchi potential.

This result on the existence of static solutions of the Bianchi IX model shows that there can be significant differences between CQ and classical models. An intuitive check of linear stability suggests that the directions corresponding to anisotropies are stable since the Bianchi IX has a minimum at $\beta_\pm = 0$; however, like the FRW CQ equations, there will be an unstable mode in the volume-state variables. This discussion is a first step toward a more complete numerical investigation of the Bianchi IX CQ equations (to be pursued elsewhere).

2.3 Summary and Discussion

We studied a "semiclassical" hybrid geometrodynamics defined by first-order Hamiltonian equations for classical geometry coupled to time-dependent Schrodinger equation for the state of a quantum scalar field. This system incorporates full backreaction of the quantum matter on classical geometry in a self-consistent manner.

We next applied the idea to study the dynamics of homogeneous isotropic and anisotropic cosmology with a truncation of the scalar field Hilbert space. We showed that there are static solutions for both cases with certain conditions, and that these solutions are linearly unstable.

That static spacetimes can arise in the semiclassical Einstein equation is curious from the physical point of view. It suggests that the backreaction of the (global) quantum matter state on a classical spacetime, through the effective Hamiltonian constraint,

can create a static classical-quantum bound state. From a mathematical perspective, the fact that the equations are non-linear in the state opens up the possibility of unusual solutions; such have been noted in the semiclassical spin-oscillator model [60].

For the isotropic case we studied numerically the full evolution of initial data that is a perturbation of the semiclassical static universe parameters, for both the classical-quantum and classical equations. This revealed some similarities and differences; the latter arise due to the oscillations of the classical scalar field at early times, and in the late time decay of the energy densities. Of particular interest is that the free data for the classical-quantum system is the initial scale factor and scalar quantum state. This raises the question of whether the issue of fine tuning of scalar field initial data of the classical system can be avoided in the classical-quantum equations; only an initial quantum state is required rather than initial values of the scalar field and its momentum.

That the past of an inflationary classical-quantum universe has a static 3-sphere attractor in the past may be compared with the purely classical "emergent universe" model proposed in [53], where the scalar field has an arbitrary scalar potential (unlike only the mass term here). Our analysis provides a similar model for the origin of inflation starting from a classical-quantum model with full backreaction.

It is useful to contrast our FLRW results with other works on the instability of emergent universes [61, 62, 63]: the first of these works argues that in a minisuperspace quantization without matter, an emergent universe would collapse; the second rules out oscillating solutions in loop quantum cosmology as the origin of an emergent universe; the third, unlike our case, considers the evolution of a scalar field wave packet on a fixed background (i.e. no backreaction). Including non-perturbative backreaction (as we do here) results in a static universe that has an unstable mode;

it is this mode that leads to inflation, while the other mode decays exponentially back to the semiclassical static universe. This applies where nonlinear effects are negligible, one interesting avenue to explore would be to compute how many e-folds of inflation can occur while the linear analysis holds.

For the aniotropic case we show that unstable static universes also arise for the Bianchi IX model; this is because one of the conditions for static solutions is the requirement of critical points of the curvature potential.

Thus, while we have shown that the semiclassical static universe derived here can inflate or stay stable, the question of how it might arise from quantum gravity remains, as does the validity of the semiclassical Einstein equation as a transitional theory between quantum gravity and quantum theory on curved spacetime; a recent discussion of this issue appears in [60], and a linear alternative is proposed in [64].

The numerical evolution of the CQ equations for the isotropic and Kasner cases shown in Figs. 2.1-2.4 show significant differences from classical evolution, especially concerning volume and energy density—for the CQ equations both quantities are larger than that for the classical equations. In particular, the scalar energy density energy tends to a constant, a fact following from the expression

$$\langle\hat{\rho}\rangle_\psi = \frac{\langle\hat{p}_\phi^2\rangle_\psi}{2v^6} + \frac{m^2}{2}\langle\hat{\phi}^2\rangle_\psi; \tag{2.83}$$

the second term dominates at late times and does not vanish, unlike for the classical scalar field. This suggests a possible contribution to dark energy if the CQ equations apply at sufficiently late times.

An important question is the domain of validity of the CQ approximation. In the absence of a quantum theory of gravity, this is hard to assess. However, there is indication from models such as the oscillator-spin [60] and the oscillator-oscillator

systems [65] that the CQ approximation is valid only for weak coupling and only for sufficiently small times. In the quantum gravity of cosmological models, which are solvable in several cases, a similar comparative investigation of the full quantum and CQ regimes is possible. (In field theory, the case of scalar quantum electrodynamics provides another testing ground for the regime of validity of CQ approximation: this has been partially investigated in [66] in the case of an evolving vacuum state.)

Beyond cosmological models, the Hamiltonian approach to semiclassical theory applied here opens up the possibility of studying the classical gravity-quantum scalar field theory in spherical symmetry, a recent study appears in [67]. This is a setting of particular interest for gravitational collapse generalizing the classical case [68], and for backreaction of Hawking radiation. A possible intuitive lesson from our study of the cosmological CQ system is that late time behaviour can differ significantly with full backreaction due to the expectation values of the $\hat{\phi}^2$.

Another possibility for further study concerns the CQ equations themselves. Here these were postulated. Can they be derived from the full quantum theory of the system with reasonably justified approximations? The case of coupled oscillators studied recently [65] provides an approach to consider for constrained Hamiltonian systems like gravity.

Chapter 3

Anisotropic Cosmology

The behavior of the universe close to the big bang singularity has been a question of much interest over the past decades. Despite several notable works, a widely accepted picture has yet to emerge. Seminal papers by Belinski, Khalitnikov, and Lifshitz conjectured that the approach to a spacelike singularity in Einstein gravity is homogeneous, dominated by time derivatives, and therefore described as a dynamical system of coupled non-linear ordinary differential equations (ODE) [46, 69]. This led to the study of homogeneous anisotropic Bianchi models that describe the evolution of scale factors moving in potentials that come from spatial curvature [49]. The most interesting of these is the Bianchi IX model, also termed the "Mixmaster Universe" [59]. It describes the universe as a billiard ball in a triangular potential with exponentially high expanding wall. Between the walls, the potential is negligible and the universe is described by the Kasner spacetime $ds^2 = -N^2dt^2 + \sum_{i=1}^{3} t^{2p_i}dx_i^2$, where the so-called Kasner exponents p_i satisfy the sum rules $\sum_i p_i = 1$ and $\sum_i p_i^2 = 1$ by virtue of the Einstein equations. These exponents transition to new ones at each collision with a wall of the potential, sending the universe into a new Kasner epoch with different exponents. The transitions are described by rules that have been the subject of many studies in vacuum [6] and with matter coupling [70]. This interest-

ing dynamics exhibits chaos, a feature that has led to many investigations over the years [71, 72, 73, 74, 75, 76, 77].

Despite these studies, the indicators that quantify chaos fail to be consistent when applied to the Mixmaster universe, giving varying numerical results; see e.g. [78, 79]. Furthermore, a question of covariance also arises: is chaos an actual physical feature or merely a coordinate artifact? This question has been addressed in by using the Kasner transition rules as an iterative map [80, 81], and by rewriting the evolution equations as a geodesic equation on an auxiliary geometry [82]. Both these methods confirm that the Bianchi IX model is chaotic.

The work presented here takes these past analyses further by including the quantum gravity effects of a bounce and quantization of matter, effects that should be important near the cosmological singularity. Several approaches to quantum gravity including supergravity indicate that chaotic dynamics persists with quantum effects [83]. There is a formulation of the BKL conjecture in the connection-triad formalism [84] using variables introduced in [85], and studies of singularity resolution in anisotropic models in symmetry reduced models in the Loop Quantum Gravity (LQG) approach [86, 87, 88, 89] (termed Loop Quantum Cosmology (LQC)). Another recent approach to semiclassical cosmological models is an effective approach where a truncated set of coupled classical equations for expectation values of products of powers of configuration and momentum operators in semiclassical states are studied [90, 91, 92]–these works indicate that chaos persists but is reduced in this semiclassical approach to the Bianchi IX model.

In this chapter we present a comparative study of three different approaches to "effective" and "semiclassical" cosmology applied to the Bianchi IX cosmology. The first is a canonical approach to the semiclassical Einstein equation, where gravity is classical and matter is quantum with an evolving state, a system that has full quan-

tum matter backreaction on a classical metric; such an approach has been studied for homogeneous isotropic cosmology [22, 45]; the second is the addition of spacetime discreteness using the LQG-inspired polymer quantization of volume, both with and without the quantization of a scalar field. In all cases we compare the resulting dynamics with the corresponding classical Bianchi IX model.

The structure of this chapter is as follows: In section II, we briefly review the canonical Mixmaster model, introduce the volume discreteness correction, and the effective Hamiltonian with quantum scalar field. In section III, we present numerical results for the three cases under study, together with results on characterizing chaos. We conclude in the final section with a summary and discussion of our results.

3.1 Mixmaster Cosmology

The starting point of our analysis is the homogeneous anisotropic line element

$$ds^2 = -N^2(t)dt^2 + \sum_{k=1}^{3} a_k^2(t)dx^k. \tag{3.1}$$

Misner's parameterization [59, 49] replaces the three scale factors by the volume and anisotropy variables (Ω, β_+, β_-) defined by

$$\nu = \ln(a_1 a_2 a_3), \tag{3.2}$$

$$\beta_+ = \frac{1}{3}\ln\left(\frac{a_1 a_2}{a_3^2}\right), \tag{3.3}$$

$$\beta_- = \frac{1}{\sqrt{3}}\ln\left(\frac{a_1}{a_2}\right), \tag{3.4}$$

The underlying topology for the Bianchi IX universe is $R \times S^3$, where S^3 is the 3-sphere. The canonical action for the Bianchi IX model with scalar field in these

variables is

$$S = \int dt \left[p_\nu \dot{\nu} + p_+ \dot{\beta}_+ + p_- \dot{\beta}_- + p_\phi \dot{\phi} + N(H_{IX} + H_\phi) \right]; \tag{3.5}$$

where $(p_\pm, p_\nu)$ are the momenta conjugate to $(\beta_\pm, \nu)$, (ϕ, p_ϕ) are the scalar field canonical variables, N is the lapse function, and

$$\begin{aligned} H_\phi &= \frac{p_\phi^2}{2\nu} + \nu\chi(\phi), & (3.6)\\ H_{IX} &= -\frac{3}{8}\nu p_\nu^2 + \frac{1}{24\nu}\left(p_+^2 + p_-^2\right) + \nu^{1/3}\, V_{IX}(\beta_+,\, \beta_-), & (3.7)\\ V_{IX}(\beta_+,\, \beta_-) &= e^{-8\beta_+} + 2e^{4\beta_+}\left[\cosh\Big(4\sqrt{3}\beta_-\Big) - 1\right] \\ &\quad -4e^{-2\beta_+}\cosh\Big(2\sqrt{3}\beta_-\Big). & (3.8) \end{aligned}$$

We restrict to the massive scalar field $\chi(\phi) = \frac{1}{2}m^2\phi^2$.

The evolution equation equations following from the Hamiltonian constraint $H_C \equiv H_{IX} + H_\phi = 0$ (it must vanish at all times) describe the universe as a point moving in a triangular potential $V_{IX}(\beta_+, \beta_-)$, which has exponentially high walls; the volume prefactor in (3.8) scales V_{IX}, shrinking the triangular potential as the singularity $\nu \to 0$ is approached. When the universe point is away from the potential walls, the dynamics is given by the Bianchi-I (Kasner) solution, which corresponds to $V_{IX} = 0$.

The Kasner Hamiltonian constraint in the phase space variables (a_k, π_k) (see e.g. [34, 70]) is

$$H_I = \frac{1}{4v}\left[\sum_k \mu_k^2 - \frac{1}{2}\left(\sum_k \mu_k\right)^2\right] = 0, \tag{3.9}$$

where $\mu_k = a_k p_k$ and $v = a_1 a_2 a_3 = e^{\nu}$; the evolution equations are

$$\dot{\mu}_i = \{\mu_i, H_K\} = 0, \tag{3.10}$$

$$\dot{v} = \{v, H_I\} = -\frac{1}{4}\sum_k \mu_k \equiv \sigma \tag{3.11}$$

$$h_k \equiv \frac{\dot{a}_k}{a_k} = \frac{1}{2v}\left(\mu_k + 2\sigma\right). \tag{3.12}$$

From these it follows that μ_k are constants of the motion,

$$v(t) = \sigma t + v_0, \tag{3.13}$$

$$a_k(t) = a_k(0)\left[\nu(t)\right]^{p_k}, \quad p_k \equiv 1 + \frac{\mu_k}{2\sigma}; \tag{3.14}$$

$\Sigma_{k=1}^{3} p_k = 1$ follows as an identity from the definition of p_k, and the Hamiltonian constraint $H_K = 0$ gives the non-trivial sum rule $\sum_{k=1}^{3} p_k^2 = 1$.

The exponents p_k thus specify a Kasner solution. A "Kasner transition" occurs when the universe point bounces off a wall of the potential, changing the exponents to new values. The number of Kasner transitions increase as the universe approaches the final singularity.

3.1.1 Effective equations

The main ingredient for defining effective equations arises from the idea of fundamental spacetime discreteness. In LQG this comes from the kinematical Hilbert space used for quantization, which is based on quantum states defined on graphs. This leads to a discrete spectra of area and volume operators. At the computational level in LQC, discreteness of volume amounts to the introducing of a volume lattice in the classical theory, followed by quantization of the discrete classical theory. An important element of the quantization is that the momentum conjugate to the vol-

ume is not defined as a derivative operator, but must be derived from the lattice translation operator. This feature makes the volume momentum bounded above.

This is formalized by introducing an alternative to Schrödinger quantization known as polymer quantization [93, 94, 95, 96]. The Hilbert space is the span of the basis set $\psi_\nu(x) = \langle x|\nu\rangle = e^{i\nu x}$ with inner-product

$$\langle \nu'|\nu\rangle = \lim_{L\to\infty} \frac{1}{2L}\int_{-L}^{L} dx\ e^{-i\nu' x} e^{i\nu x} = \delta_{\nu',\nu}. \tag{3.15}$$

The volume and translation operators act on this space as

$$\begin{aligned} \hat{v}|\nu\rangle &= \nu|\nu\rangle \\ \hat{U}_\lambda|\nu\rangle &\equiv \widehat{e^{i\lambda v}}|\nu\rangle = |\nu+\lambda\rangle. \end{aligned} \tag{3.16}$$

With this inner-product, the state $\psi(x) = \sum_{k=1}^{N} c_k e^{ix\nu_k}$ is non-zero at the N points ν_k; a Schrödinger state, such as a Gaussian, would require an uncountable superposition in this basis. Therefore in practical calculations, a lattice with fixed spacing is used, corresponding to a fixed λ in the translation operation. A "momentum operator" is constructed from the translation operator via, for instance $\hat{p}_\lambda := (\hat{U}_\lambda - \hat{U}_\lambda^\dagger)/(2i\lambda)$.

An effective classical theory is obtained by starting with Gaussian states peaked at a particular phase space point, taking expectation values of the Hamiltonian operator defined on the lattice, and imposing a Poisson bracket on the peaking values [97, 98, 99]. This procedure amounts to the replacement

$$p_\nu \ \to\ \frac{\sin(\lambda p_\nu)}{\lambda} \tag{3.17}$$

in the Mixmaster Hamiltonian constraint (3.7), giving

$$H_{IX}^{\text{eff}} \ \equiv\ -\frac{3}{8\lambda^2}\nu\sin^2(\lambda p_\nu) + \frac{1}{24\nu}\left(p_+^2 + p_-^2\right) + \nu^{1/3}\ V_{IX}(\beta_+,\,\beta_-) = 0. \tag{3.18}$$

In arriving at this expression, we made the choice that only the volume momentum is bounded above due to polymer quantization, and not the anisotropy variables or scalar field. This is motivated by work in the homogeneous isotropic models where it was found that the volume variable is responsible for the universe undergoing a bounce [100, 101, 99]. A similar effective approach that includes isotropy variables has been studied [102].

3.1.1.1 Effective cosmology with classical scalar field

The dynamics of the first model we consider follows from the effective constraint

$$H_C^{\rm eff} \equiv H_{IX}^{\rm eff} + H_\phi = 0, \tag{3.19}$$

where the scalar field part of the Hamiltonian constraint remains unmodified and $H_{IX}^{\rm eff}$ is defined in eqn.(3.18). The equations of motions are

$$\begin{aligned}
\dot{\nu} &= \{\nu,\, H_C^{\rm eff}\} = -\frac{3}{8}\nu\,\frac{\sin(2\lambda p_\nu)}{\lambda}, && (3.20)\\
\dot{p}_\nu &= \{p_\nu,\, H_C^{\rm eff}\} = \frac{3}{8}\frac{\sin^2(\lambda p_\nu)}{\lambda^2} + \frac{1}{24\nu^2}(p_+^2 + p_-^2) - \frac{1}{3}\nu^{-2/3}V_{IX}(\beta_+,\,\beta_-) \\
&\quad + \left(\frac{p_\phi^2}{2\nu^2} - \frac{1}{2}m^2\phi^2\right), && (3.21)\\
\dot{\beta}_\pm &= \{\beta_\pm,\, H_C^{\rm eff}\} = \frac{1}{12\nu}\,p_\pm && (3.22)\\
\dot{p}_\pm &= \{p_\pm,\, H_C^{\rm eff}\} = \nu^{1/3}\,\frac{\partial}{\partial\beta_\pm}V_{IX}(\beta_+,\,\beta_-) && (3.23)\\
\dot{\phi} &= \{\phi,\, H_C^{\rm eff}\} = p_\phi/\nu && (3.24)\\
\dot{p}_\phi &= \{p_\phi,\, H_C^{\rm eff}\} = -\nu\chi'(\phi). && (3.25)
\end{aligned}$$

3.1.1.2 Effective cosmology with quantum scalar field

The second model we study uses an effective constraint. In this, the scalar field is quantized and its quantum state evolves via the time dependent Schrödinger equation. This may be viewed as the canonical version of the semiclassical Einstein equation applied to cosmology, but with the polymer quantization corrections to the gravitational part. The effective constraint is now

$$H_Q^{\rm eff} \equiv H_{IX}^{\rm eff} + \langle\psi|\hat{H}_\phi|\psi\rangle = 0, \tag{3.26}$$

together with

$$i|\dot{\psi}\rangle = \hat{H}_\phi|\psi\rangle. \tag{3.27}$$

The gravitational Hamilton equations are identical to those $H_C^{\rm eff}$, with the exception of the $\dot{p}_\nu$ equation, which now reads

$$\begin{aligned}\dot{p}_\nu &= \{p_\nu,\, H_Q^{\rm eff}\} = \frac{3}{8}\frac{\sin^2(\lambda p_\nu)}{\lambda^2} + \frac{1}{24\nu^2}\,(p_+^2 + p_-^2) \\ &\quad -\frac{1}{3}\nu^{-2/3}\,V_{IX}(\beta_+,\,\beta_-) - \frac{\partial}{\partial\nu}\langle\psi|\hat{H}_\phi|\psi\rangle\end{aligned}$$

The last term of this equation can be expanded to give

$$\begin{aligned}\frac{\partial}{\partial\nu}\langle\psi|\hat{H}_\phi|\psi\rangle &= \frac{1}{\dot{\nu}}\left(\langle\dot{\psi}|\hat{H}_\phi|\psi\rangle + \langle\psi|\hat{H}_\phi\dot{\psi}\rangle\right) + \langle\psi|\frac{\partial}{\partial\nu}\hat{H}_\phi|\psi\rangle \\ &= -\frac{1}{2}\left(\frac{\langle\hat{p}_\phi^2\rangle}{\nu^2} - m^2\langle\hat{\phi}^2\rangle\right).\end{aligned} \tag{3.28}$$

It can be verified that the Hamiltonian constraint $H_Q^{\rm eff}$ is preserved: labeling the set of the configuration variables $\alpha_I = \{\nu, \beta_\pm\}$ and their canonically conjugate momenta

$\pi_J = \{p_\nu,\, p_\pm\}$,

$$\begin{aligned} \frac{d}{dt}H_Q^{\rm eff} &= \sum_I \frac{\partial H_Q^{\rm eff}}{\partial \alpha_I}\dot{\alpha}_I + \sum_J \frac{\partial H_Q^{\rm eff}}{\partial \pi_J}\dot{\pi}_J + \langle\dot{\psi}|\hat{H}_\phi|\psi\rangle + \langle\psi|\hat{H}_\phi|\dot{\psi}\rangle \\ &= 0. \end{aligned} \tag{3.29}$$

It is similarly verified that probability is conserved ensuring that the complete set of equations is self-consistent.

In the following we study numerically the dynamics of six models: the zero scalar field classical and effective cases H_{IX} and $H_{IX}^{\rm eff}$; the non-zero classical and quantum scalar field cases $H_C = H_{IX} + H_\phi$ and $H_Q = H_{IX} + \langle\psi|\hat{H}_\phi|\psi\rangle$; and $H_C^{\rm eff}$ and $H_Q^{\rm eff}$, where the volume momentum term comes from polymer quantization. The cosmological bounce is due to this last feature as may be seen by deriving the effective Hubble rate $H_\nu = \dot{\nu}/\nu$ from (3.20) and any one of effective Hamiltonian constraints:

$$H_\nu^2 = \frac{3}{2}\,\rho_T\left(1 - \frac{\rho_T}{\rho_{\rm crit}}\right) \tag{3.30}$$

where $\rho_{\rm crit} = 3/8\lambda^2$ and ρ_T is the sum of the energy densities of the scalar field and anisotropies, e.g.

$$\rho_T = \frac{1}{\nu}\left(\frac{1}{24\nu}(p_+^2 + p_-^2) + \nu^{1/3}\,V_{IX} + \frac{1}{\nu}H_\phi\right) \tag{3.31}$$

for the $H_C^{\rm eff}$ model.

3.2 Numerical Results

We used the Runge-Kutta-4 method to solve the set of coupled evolution equations for the six models. For useful comparisons of evolution, it is important to set up ini-

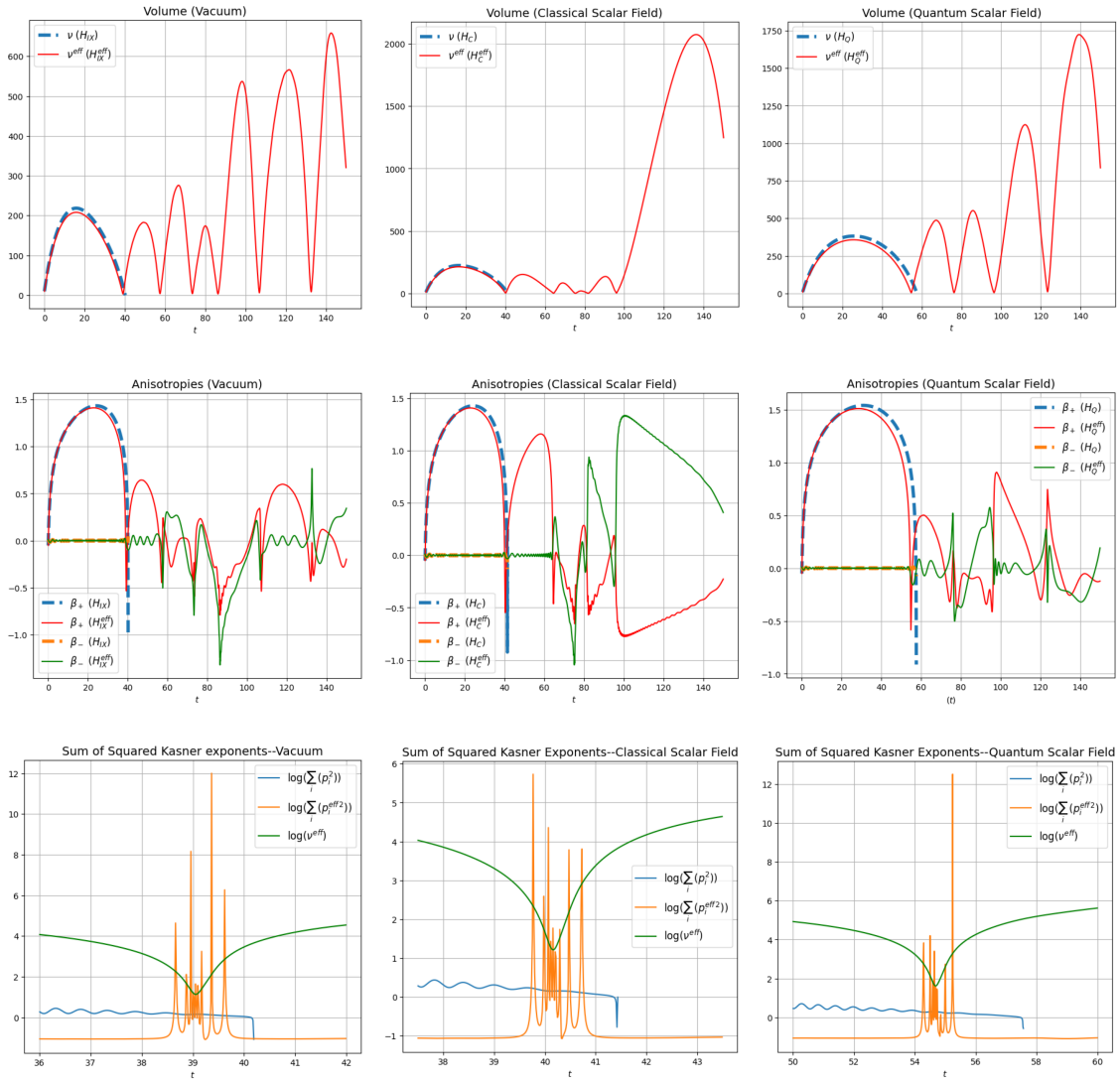


Figure 3.1: A typical evolution for the classical and effective Mixmaster universe in vacuum, and with classical and quantum scalar field. The dashed blue line is for the classical Bianchi IX Hamiltonian; the solid line represents the effective Bianchi IX Hamiltonian. The first row shows multiple bounces in the volume for the effective universe. The second row shows the evolution of the anisotropies $\beta_{\pm}$, and the third, the log of the Kasner squared sum rule overlayed with log of the volume.

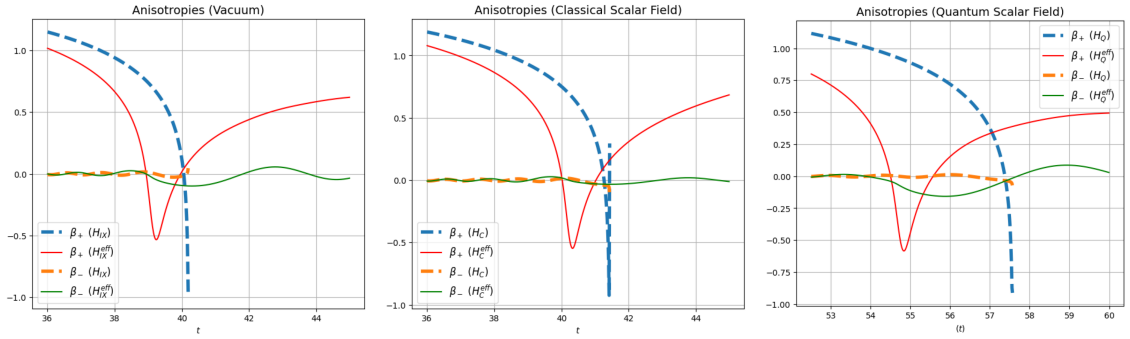


Figure 3.2: Anisotropy variables $\beta_\pm$ near the first bounce point for each of the models studied.

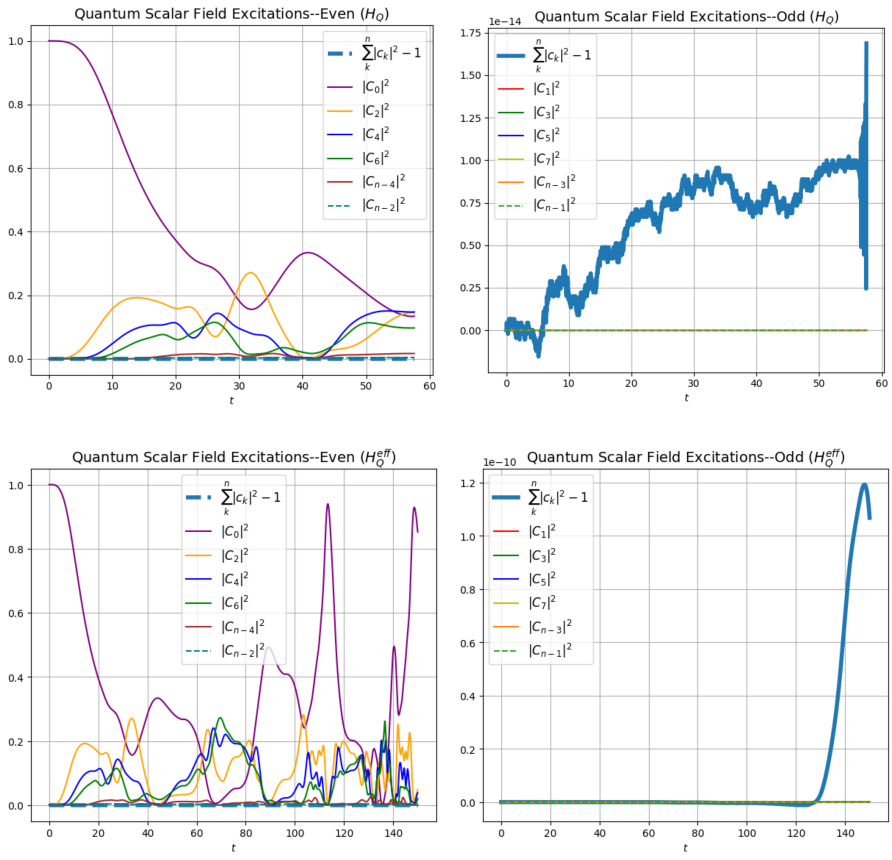


Figure 3.3: Scalar field state excitations for the Hamiltonians H_Q (classical gravity) top row, and H_Q^{eff} (effective gravity) bottom row, starting from the initial ground state. Both show excitations from the ground state as the singularity/bounce is approached, de-excitation as the universe expands after the bounce, and probability conservation.

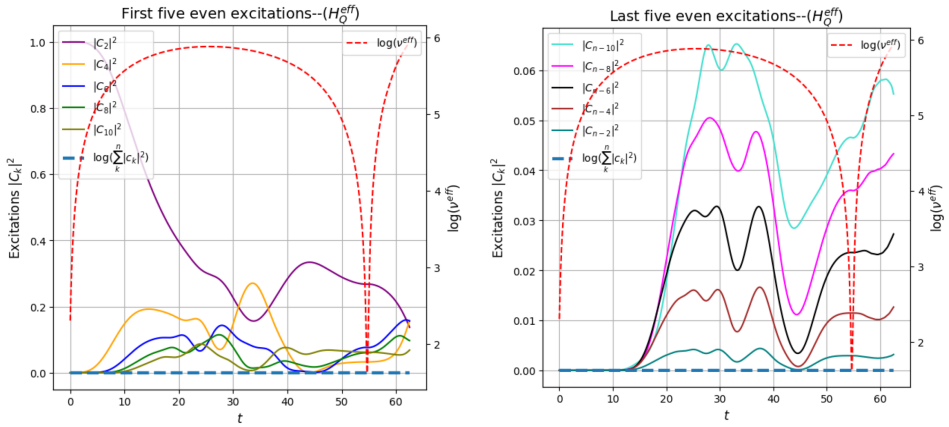


Figure 3.4: The first few and and the last few even-state excitations of the scalar field (with Hilbert space truncation $n = 30$) through the first bounce of the effective universe; the volume is overlaid (in red).

tial data that is as close as possible. This is straightforward for the vacuum and classical scalar field models $H_{IX}, H_{IX}^{\text{eff}}$ and H_C, H_C^{eff} respectively, since for these cases the initial data is solely configuration and momenta subject to the corresponding Hamiltonian constraint. For these cases we specify the set $\{\nu(0),\, p_\nu(0), \beta_\pm(0),\, p_-(0)\}$, and also $\{\phi(0), p_\phi(0)\}$ for non-zero scalar field, with $p_+(0)$ determined by the Hamiltonian constraint. This method provides identical data for all variables except for $p_+(0)$, since the Hamiltonian constraints differ.

In contrast, the initial data for the quantum scalar field cases H_Q and H_Q^{eff} require the initial quantum state of the scalar field; the data is $\{\nu(0),\, p_\nu(0), \beta_\pm(0),\, p_-(0), |\psi\rangle(0)\}$, again with $p_+(0)$ determined by solving the respective classical and effective Hamiltonian constraints. For comparison with the classical scalar field cases, we fix the data for the latter by setting

$$\phi(0) = \sqrt{\langle\hat{\phi}^2\rangle(0)}; \quad p_\phi(0) = \sqrt{\langle\hat{p}_\phi^2\rangle(0)}, \tag{3.32}$$

with the expectation values taken in the initial state. Lastly, for all illustrative numerical evolutions, we set the scalar field's mass to $m = 0.01$ and polymer scale

$\lambda = 0.1$. For the quantum scalar field we work in the fixed oscillator basis $\{|n\rangle_0\}$ at the initial time so that the evolved state at a subsequent time t is

$$|\psi\rangle\,(t) = \sum_n c_n(t)\,|n\rangle_{t=0}\,. \tag{3.33}$$

For state evolution, we write the scalar field Hamiltonian operator as a matrix in the oscillator representation with a truncation at level $n = 30$; the Schrödinger equation then becomes a set of 30 coupled equations for the coefficients $c_n(t)$. We confirm that changing truncation level does not significantly affect our results provided the initial state is the ground state, and the evolution time is such that probability remains conserved.

The following figures provide a sample of our numerical results. We have verified that the respective Hamiltonian constraints remain conserved up to order 10^{-9} and that the probability is conserved to a similar order for the quantum scalar field case.

3.2.1 Volume, anisotropy and Kasner sum evolution

Fig.3.1 shows the evolution of volume ν (first row), anisotropies (second row), and the log of the sum of the squared Kasner exponents $\sum_k p_k^2$ (third row), for the vacuum, and for the classical and quantum scalar fields coupled to (classical and effective) gravity; the initial state for the latter is the vacuum $|0\rangle_{t=0}$, this is chosen to keep our analysis simple. For each sub-figure, comparable initial data is chosen as described above; for all cases the data is $\{\nu(0) = 10,\, \beta_+(0) = -0.05,\, \beta_-(0) = 0.01,\, p_-(0) = -10,\, p_\nu(0) = -5\}$, with $p_+(0)$ determined by the respective hamiltonian constraints; the simulations run for the same time (with lapse $N = 1$); the dashed blue line is the case where the gravitational Hamiltonian is the classical (not the effective) one, which terminates in a singularity, e.g. near $t = 40$ in the first two frames, and near

$t = 55$ in the third frame of the first row. The small differences in the location of the bounce and singularity in these figures is due to the difference in the initial value $p_+(0)$ as determined by the respective Hamiltonian constraints.

Volume bounces: The first row shows that the bounces are asymmetric for each of the effective cases (vacuum, classical and quantum scalar field), with the most bounces occurring for the vacuum case; each case also indicates a higher rise in volume after a series of relatively smaller bounces and expansions; the quantum scalar case differs significantly from the classical scalar one in the number of initial bounces.

Anisotropies: The second row compares the anisotropies $\beta_\pm$ in each of the cases. The approach to the first bounce is noteworthy: all cases are very similar as the first bounce is approached, with anisotropies vanishing near $t = 40$. However after the bounce, the second and third frames (the cases H_C^{eff} and H_Q^{eff}) show higher anisotropies that rise rapidly near each bounce; it is also evident that the classical and quantum scalar field cases differ significantly in this respect. Fig. 3.2 is a view of the anisotropies at the first bounce point of Fig. 3.1; it shows that all three bounce cases are qualitatively similar. The evolutions of β_+ and β_- are quite different due to their definitions in (3.3) and (3.4): the former is a function of all three scale factors, while the latter depends on only two. Another reason for the difference is the different evolution equations p_+ and p_- have: the right-hand sides differ substantially for each, and this feeds into the solution for $\beta_\pm$. The different evolutions are a feature also of the exact Kasner solution where $\beta_+ \sim \ln\left(t^{p_1+p_2-p_3^2}\right)$ and $\beta_+ \sim \ln(t^{p_1-p_2})$, for Kasner exponents p_1, p_2, p_3 satisfying the sum rule.

Kasner sum rule: The third row of Fig.3.1 shows zoomed in plots of log of the Kasner sum $\sum_{i=1}^3 (p_i^2)$ and $\sum_{i=1}^3 (p_i^{\text{eff}\,2})$(blue and orange curves respectively), and log of the effective volume ν^{eff} (green curve), as the singularity/bounce point is approached. The blue curve shows that the Kasner sum tends to unity as the classical singular-

ity is approached for each of the vacuum, classical, and quantum scalar field cases (H_{IX}, H_C, and H_Q), supporting the BKL conjecture that "matter does not matter" as the singularity is approached; (the dip in these curves very close to the singularity point is due to break down of numerical evolution very close to the singularity).

However, the orange curves (corresponding to $H^{\rm eff}_{IX}$, $H^{\rm eff}_C$ and $H^{\rm eff}_Q$ —where there is a bounce) show that the sum rule is a constant away from the bounce point, but not unity due to the polymer scale $\lambda = 0.1$; it undergoes oscillations through the bounce (where the green volume curve dips); the differences in the three frames in this row show that "matter matters" when the universe bounces, and in particular whether matter is classical or quantum. Furthermore, the oscillations in the sum rule indicate that the approach to the volume bounce is not Kasner. This is in contrast with the BKL conjecture, which states that the approach to the classical singularity is Kasner-like; the conjecture is of course silent on the singularity free bouncing cosmologies we study here, perhaps more so due to departure from usual GR where the conjecture usually applies.

3.2.2 Scalar field excitation and density

Fig. 3.3 gives the results for the evolution of the scalar field quantum state, the coefficients $|c_n(t)|^2$ in (3.33) for the cases H_Q (classical gravity with quantum scalar field) in the first row, and $H^{\rm eff}_Q$ (effective gravity with quantum scaler field) in the second row, with initial state $|0\rangle_{t=0}$; the first and second columns show the even and odd level excitations (for Hilbert space truncation $n = 30$ in the fixed basis chosen at $t = 0$).

For H_Q (first row), the initial data is the same as in the for the dashed blue curve in the rightmost column of Fig. 3.1; the singularity is just before $t = 60$. The left frame shows the even state $|2k\rangle$ excitations (which connect with the initial state $|0\rangle_{t=0}$ due

to the quadratic Hamiltonian); as the singularity is approached, it is evident that higher states $k = 2, 4, 6$ are excited to nearly equal levels $|c_k|^2 \in (0.1, 0.2)$, but the states near the truncation point $n = 30$ are not significantly excited; the right frame shows the non-excitation of the odd states $|2k+1\rangle$ to order 10^{-14}. The total probability is numerically conserved to a similar order.

For $H_Q^{\rm eff}$ (second row), the initial data is the same as in the rightmost column of Fig. 3.1 (with the four bounces). The left frame shows the even excitations; the higher levels are excited through each bounce; $|c_0|^2$ drops and $|c_k|^2$ $(k = 2, 4, 6)$ rise; at later times these higher levels remain excited and the scalar field never returns to purely the ground state at maximum expansion. The right frame again shows that the odd levels are not excited to order 10^{-10}, and again total probability is numerically conserved.

Fig. 3.4 shows a zoomed in version of the even state excitations of the scalar field for $H_q^{\rm eff}$ near the first bounce; the left frame shows the lower levels, and the right frame shows the higher levels near the truncation $n = 30$; the log of the volume (dashed red line) is overlaid. This shows order 10^{-2} excitations of the higher levels with a similar pattern.

These results may be viewed as the quantum mechanics analog of particle production on a fixed time dependent background, with the difference that our calculation includes non-perturbative back reaction of the evolving scalar field state on the evolution of the gravitational variables.

Fig. 3.5 shows the evolution of the classical and quantum scalar field densities for $H_C^{\rm eff}$ and $H_Q^{\rm eff}$,

$$\rho = \frac{1}{\nu} H_\phi = \frac{p_\phi^2}{2\nu^2} + \frac{1}{2} m^2 \phi^2, \tag{3.34}$$

$$\rho_Q = \frac{1}{\nu} \langle \hat{H}_\phi \rangle = \frac{\langle \hat{p}_\phi^2 \rangle}{2\nu^2} + \frac{1}{2} m^2 \langle \hat{\phi}^2 \rangle, \tag{3.35}$$

again for the same initial data as in Fig. 3.1, with the cases H_C and H_Q (no bounce classical gravity) overlaid (dashed blue line). The bounded spikes in the densities are evident at each of the bounce points.

Lastly, Fig. 3.6 exhibits the conservation of the Hamiltonian constraint for each of the cases we study to order at least to order 10^{-7}. This shows the accuracy of our numerical evolutions, including the oscillations of the Kasner sum at the bounce point in Fig. 3.1. It also reflects probability conservation of the quantum scalar field case (third frame), where any probability violation would result in non-conservation of the Hamiltonian constraint through the expectation value of the matter contribution to this constraint.

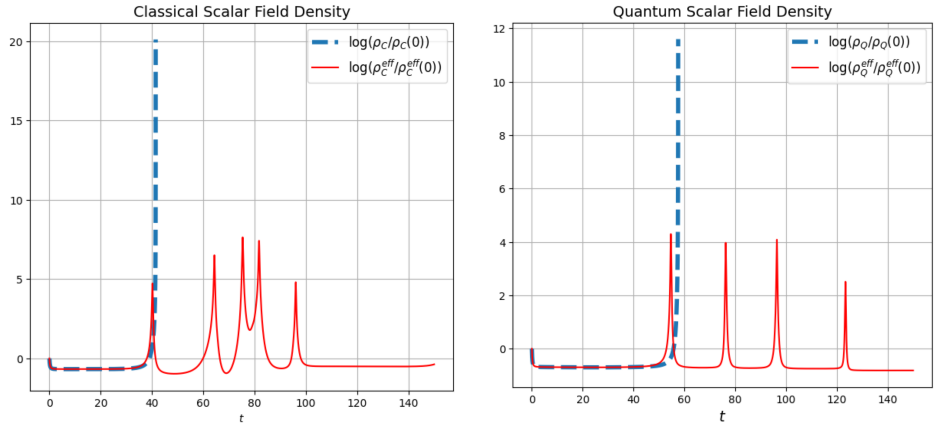


Figure 3.5: Scalar field densities in a classical and effective universe. In the former case (dashed blue line) the density diverges at the singularity; in the latter cases (orange line) the density spikes at a maximum at each bounce shown in Fig. 3.1

3.2.3 Chaos

Close to the singularity, the Mixmaster Universe is known to have chaotic dynamics [79, 80, 82]. We study this comparatively for the six models using two methods: computing Lyupanov exponents and the fractal dimension of trajectories in phase space.

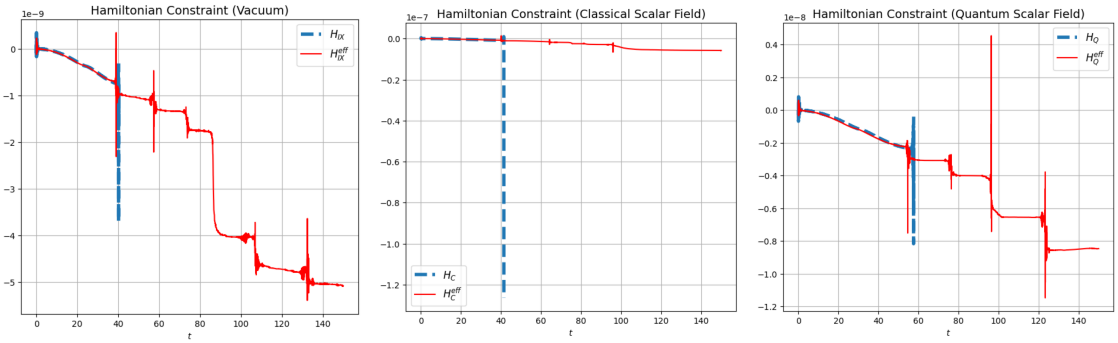


Figure 3.6: Numerical conservation of the Hamiltonian constraint for the evolutions shown in Figs. 3.1, 3.3, and 3.5.

3.2.3.1 Lyapunov exponents

One measure of chaos is the Lyapunov exponent: given two infinitesimally close initial data points $x_1(0)$ and $x_2(0)$ for a dynamical system, if the initial separation $\xi(0) = |x_2(0) - x_1(0)|$ grows as $\xi(t) \sim \xi(0)e^{\lambda t}$ with $\lambda > 0$ the system is considered to be chaotic, and λ is called the Lyapunov exponent. An $n-$dimensional phase space has n such exponents. One way to compute them is to linearize the dynamical system and solve the system

$$\frac{d}{dt}\xi_n(t) = J(f(x(t)))_{nm}\xi_m(t); \tag{3.36}$$

where J is the matrix that arises from linearization of the evolution equations. The Lyapunov exponents are given by

$$\lambda_n = \lim_{t\to\infty} \ln\left[\frac{\xi_n(t)}{\xi_n(0)}\right] \tag{3.37}$$

In the numeric integration of (3.36), it often happens that the $\xi_n(t)$ diverge in a short duration. To remedy this, Bennetin et al [103] introduced the the idea of re-orthonormalizing the vectors $\xi_n(t)$ at regular time intervals, and storing their corresponding scalings. This is the method we use to calculate the Lyapunov exponents

System	Lyapunov Exponent
H_{IX}	3.210
H_{IX}^{eff}	0.4093
H_C	4.4320
H_C^{eff}	2.100
H_Q	4.4320
H_Q^{eff}	1.024

Table 3.1: Maximal Lyapunov Exponents for the six models

for the six models studied. The results appear in Table 3.1.

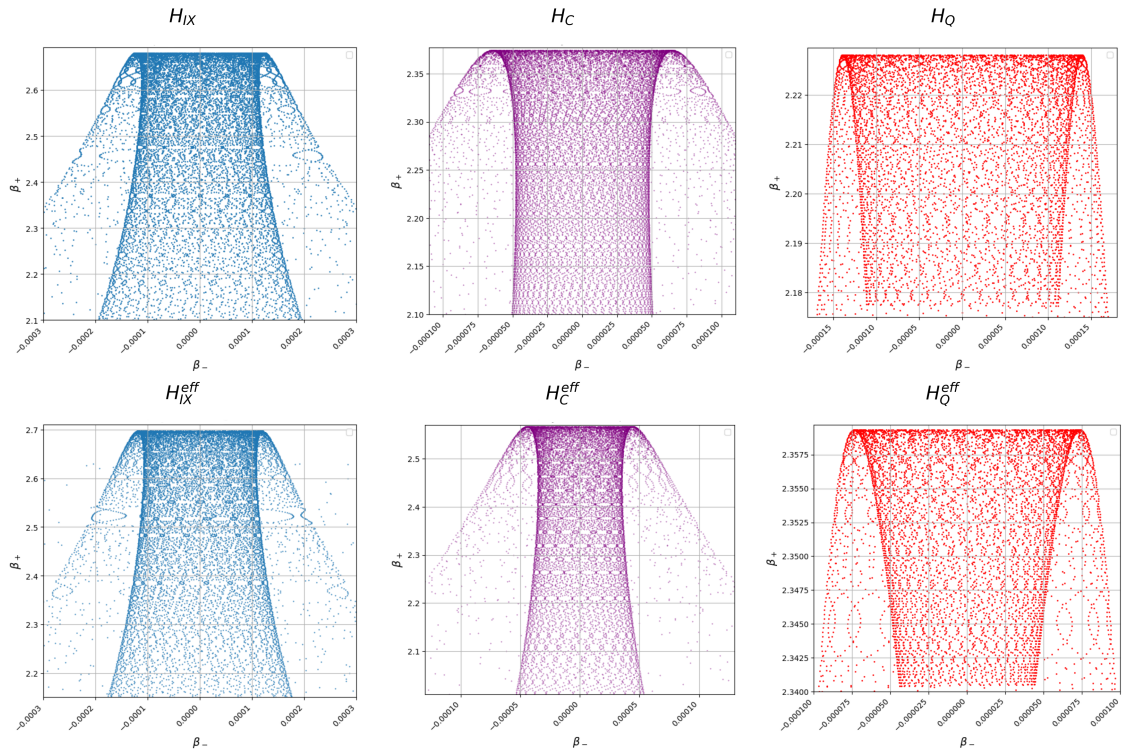


Figure 3.7: Zoomed-in phase plots of the anisotropies $\beta_\pm$ for each of the six models studied. Self-similarity and fractal-like structure is evident in each case; all are qualitatively similar, but with notable differences for the quantum scalar field.

These are computed from runs up to $t = 200$, keeping in mind that infinitesimally close initial trajectories first diverge, and then settle into a constant distance on average, forming an attractor set. The dimensions of the matrix are different in each of the six cases due to the number of dynamical equations, with the largest dimension occurring for the quantum scalar field cases with truncation (at $n = 30$). Notable in

the table is that the Lyapunov exponents for the effective gravity cases are smaller than for classical gravity, providing evidence that chaos is reduced, at least by this measure. In particular, there is a nearly factor of four difference in the exponents between H_C (classical gravity with classical scalar field) and H_Q^{eff} (effective gravity with quantum scalar field).

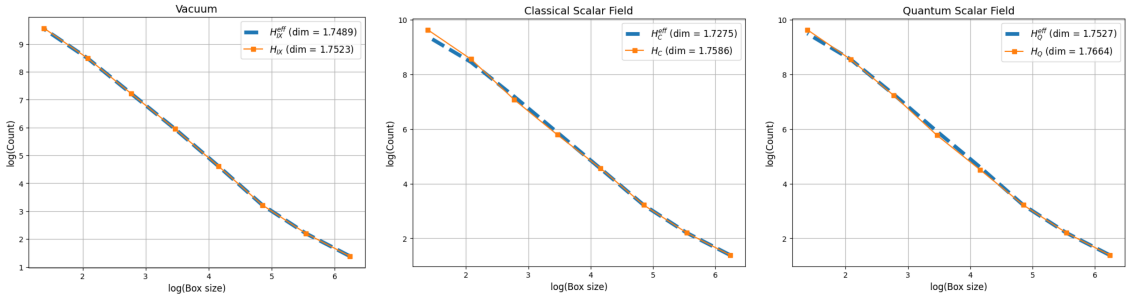


Figure 3.8: We see here the results of the box-counting analysis to compute the dimensions of the plots in Figure 3.7. For each plot in the figure, we use the polymerized and unpolymerized counterparts for each species (vacuum, classical scalar field, and quantum scalar field). We see that in each case, polymerization reduces the fractal dimension of the image, rendering the system to be less chaotic.

3.2.3.2 Fractal dimension

There are several methods for estimating the fractal dimension of attractor sets in phase space [104, 80]. One of these is the so-called box counting method computed from images of the fractal. For a fractal set F, the number N of boxes of size ϵ it takes to cover F scales as

$$\log(N(\epsilon)) = -D\log(\epsilon). \tag{3.38}$$

Here, D, is the dimension of the fractal . We apply this to the phase space plots in Fig. 3.7, which show evolution in the $\beta_+ - \beta_-$ plane for each of the six Hamiltonians we studied. Specifically, we place a sequence of finer and finer square grids on the gray scale images in this figure, and count the number of pixels above a certain gray

scale threshold (90%) in each grid box. The aim is to obtain a comparison of fractal dimension for each of the six cases to see how they compare with the Lyapunov exponents, for a relative ranking of degree of chaos.

The results of this are shown in Fig. 3.8. The fractal dimensions are all very close to one another in the range $[1.72, 1.77]$, but with the effective Hamiltonian cases having slightly smaller dimensions than the classical case. As such this method does not provide a significant differentiation of chaos in the six models we studied.

Our main result of this subsection is evidence of significant chaos reduction in the cases where there is a bounce, as exhibited in Table 3.1. These results are intuitively reasonable from the perspective that a minimum volume effectively saturates the number of collisions of the universe particle with the walls of the Bianchi IX potential, compared to the case where there is no minimal volume and the singularity is present. This in turn means that a more pervasive exploration of the phase space is thwarted by the bounce in volume, thereby reducing the degree of chaos. As this intuition is broad, it likely applies to a͡ny mechanism that replaces the singularity with a bounce; see e.g. [105, 106] for other approaches where chaos is either reduced or eliminated altogether.

3.3 Summary and Discussion

We presented a comparative study of six Bianchi-IX models, with classical and effective gravity, and with classical and quantum massive scalar field. The effective gravity case used space discreteness only in the volume variable, in a manner similar to that used in LQC models [88]. We saw that this is sufficient for producing bouncing dynamics, both analytically and numerically. The model with the quantum scalar field used the Schrödinger equation for state evolution, and a modified Hamil-

tonian constraint where the scalar field contribution is replaced by its expectation value; this is a non-perturbative and self-consistent method for back reaction.

Our simulations show a number interesting features: (i) multiple bounces occur with the effective gravity Hamiltonian cases, with expansion to larger volume after successive bounces; (ii) all bounces are asymmetric; (iii) anisotropies are relatively larger with classical and quantum matter than in vacuum as the universe emerges from a bounce; (iv) away from the bounce, the effective gravity quadratic Kasner exponent sum is a constant of the motion, but undergoes oscillations through the bounce, whereas it is conserved and approaches unity (with or without matter) in the classical case; (v) the quantum scalar field undergoes excitations from the initial ground state as the singularity/bounce is approached, and partial de-excitation after the bounce; (vi) chaos persists in the effective gravity case, but the Lyapunov exponents indicate that it is "reduced" in the effective gravity cases, with the largest reduction occurring for the vacuum effective case $H_{IX}^{\rm eff}$, a result at least qualitatively consistent with results for vacuum Bianchi IX using entirely different methods [91]; (vii) the box counting method in phase space also provides evidence for chaos with a fractal dimension of between 1.72 and 1.77 for all six models, but with only marginal differences between them.

As noted above, the observation that chaos is reduced in effective gravity is not surprising, since chaos is produced by the increasing number of bounces off the triangular potential walls as the singularity is approached. If the universe achieves a minimum volume, the potential walls stop closing in, and it is reasonable to expect that the number of collisions with the walls reaches a maximum, and then starts to reduce through the bounce. The presence of matter affects this only in the transfer of some "energy" between the matter and gravity terms in the Hamiltonian constraint; the reduction in chaos appears to be mainly due to the bounce in the effective gravity cases. This argument also suggests that chaos is not merely a coordinate artefact,

and that although Lyapunov exponents may differ if other phase space variables and time coordinates are used, it appears unlikely that all exponents would become zero or negative, given the nature of the potential. In contrast, the fractal dimension calculation for images generated of zoomed in anisotropies are more 'robust' up to numerical accuracy– similarly generated fractal images would return comparable fractal dimensions D.

This work extends the much-studied vacuum Bianchi IX model in two ways – by introducing effective gravity via fundamental discreteness corrections and quantum matter with back reaction. The same methods may be used for the other Bianchi models, with their somewhat simpler potentials. More interesting from a quantum gravity perspective are inhomogeneous models, the simplest of which are the Gowdy cosmologies with one local degree of freedom. Introducing quantum matter with back reaction in the manner we have done here would require introducing matter expectation value terms in both the Hamiltonian and diffeomorphism constraints, and ensuring their algebra remains consistent. This remains to be seen.

Chapter 4

Exact RG for minisuperspace cosmology

Renormalization group (RG) methods are foundational in modern quantum field theory (QFT), offering a framework to understand how physical laws change with scale. Wilson's insights showed that high-energy degrees of freedom can be integrated out gradually, yielding effective theories for low-energy phenomena [26]. This idea culminated in the development of exact renormalization group (ERG) equations – functional differential equations that encode the scale dependence of the quantum effective action in a non-perturbative way. Among several formulations of ERG, Wetterich's approach stands out for its use of the scale-dependent effective average action, which satisfies a flow equation now commonly known as the Wetterich equation [27]. This approach is complementary to Polchinski's, related by a Legendre transform [26], and has been further developed by Ellwanger [107], and Morris [108, 109]. The ERG framework allows a continuum of effective theories between the ultraviolet (UV) and infrared (IR), providing a powerful tool for analyzing strongly-coupled systems beyond perturbation theory.

The ERG formalism has been particularly influential in the asymptotic-safety programme of quantum gravity. Weinberg conjectured that gravity could remain well defined at arbitrarily high energies – even though it is perturbatively non-renormalizable – if the RG flow of all diffeomorphism-invariant couplings runs into a non-Gaussian UV fixed point with only a finite number of relevant directions [18]. At such a point every dimensionless coupling approaches a finite value as the high energy cutoff scale goes to infinity; no parameter diverges, and the theory stays predictive because only those few relevant couplings must be fixed by experiment. This search for a UV fixed point is, in essence, the asymptotic-safety programme for quantum gravity.

Concretely, Reuter pioneered the application of the Wetterich Equation to gravity, formulating a flow equation for a scale-dependent effective action in a gravitational context [28]. This approach, often termed Quantum Einstein Gravity (QEG), provided the first concrete evidence of a non-Gaussian UV fixed point. Subsequent studies confirmed the robustness of this fixed point across different truncations and matter couplings [29, 30, 110, 111, 112]. Reviews by Percacci and Eichhorn summarize much of this progress and underline the theoretical viability of asymptotically safe gravity [113, 114].

Despite these advances, the application of ERG techniques to symmetry-reduced gravitational models remains largely unexplored. These minisuperspace models are more amenable than the full theory, the symmetry truncation simplifies the quantization process. For instance, in such homogeneous models (cosmology) one does not have to worry about the diffeomorphism constraint and the ensuing quantum constraint algebra. Notably, Misner introduced the idea of using such models in the context of quantum cosmology [6]. In the minisuperspace framework, the dynamics of homogeneous and isotropic cosmologies can be reduced to finite-dimensional systems, making them analytically and numerically tractable; for more details see [49]. Constructing these models entails restricting the infinite degrees of freedom of

general relativity to a finite number by imposing strong symmetry conditions.

However, the validity of minisuperspace quantization has been a subject of long-standing debate. Kuchař and Ryan famously argued that minisuperspace truncations may not capture essential features of the full theory, as they simultaneously set inhomogeneous modes to zero in both configuration and momentum space, violating the uncertainty principle. Further analyses demonstrated that such models can fail to reproduce the dynamics of more complete theories, raising concerns about the physical reliability of conclusions drawn from them [115].

Nevertheless, symmetry-reduced models remain a useful theoretical laboratory, especially when used judiciously. They have been employed to great effect in canonical quantum gravity and loop quantum cosmology. In this spirit, we explore the use of the ERG in a highly symmetric setting: a Friedmann–Robertson–Walker (FRW) universe minimally coupled to a massless scalar field and pressureless dust. The scalar field serves as simple matter content, while the dust – introduced following Brown–Kuchař, and Husain-Pawlowski – provides a relational time variable [10, 13]. This allows for a well-defined notion of scale flow even in a cosmological context.

Our goal is to apply the ERG to this minisuperspace model and examine whether fixed-point behavior akin to that seen in the asymptotic safety program persists. By recasting the dynamics in terms of harmonic oscillator variables, we gain new insights into the renormalization structure of the theory. Most notably, our results indicate the absence of UV fixed points in this truncated setting, challenging assumptions about the validity of using minisuperspace models to draw conclusions about full quantum gravity. Moreover, we find that in the quantum limit ($k \to 0$), the dimensionless gravitational constant g_k goes to zero, while the dimensionless cosmological constant Λ_k diverges. In other words, gravity itself becomes free (non-interacting), yet the cosmological coupling runs off to infinity – an RG runaway that

signals our minisuperspace trajectory never lands on the non-Gaussian fixed surface and therefore does not realize asymptotic safety within this truncation. In this sense, our work complements existing studies by critically evaluating the interplay between truncation and non-perturbative RG flow. It also opens avenues for future research involving more complex midisuperspace models, where partial inhomogeneities are retained and more realistic dynamics can be probed using the ERG framework.

In section II, we outline the Exact Renormalization Group *á la* Wetterich starting from the generating functional for a Euclidean QFT in the presence of a source $J(x)$. In the next section (III), we describe and outline the dust time gauge to get physical evolution by solving the constraints; in section IV, describe the FRG as applied to FRW cosmology. We conclude by giving our results in section VI, followed by a summary and discussion in section VII.

4.1 Exact Renormalization Group

The Exact Renormalization Group (ERG) equation, also called the Wetterich Equation, is applied on the quantum effective average action (QEAA) describing a quantum field theory (QFT). We shall briefly review the derivation for the ERG equation starting from the generating function of correlation functions in QFT. For a Euclidean QFT ($t \to i\tau$) with bare action functional $S[\varphi]$ and and external source $J(x)$, the generating functional is given

$$Z[J] = \int \mathcal{D}\varphi \, e^{-S[\varphi]+\int d^d x J(x)\varphi(x)}. \tag{4.1}$$

The n^{th} functional derivative of the generating functional (4.1) is the $n-$point function for the QFT.

$$\langle\varphi(x_1)\varphi(x_2)\ldots\varphi(x_n)\rangle = \frac{1}{Z[J]}\frac{\delta^n Z[J]}{\delta J(x_1)\delta J(x_2)\ldots\delta J(x_n)}. \tag{4.2}$$

From $Z[J]$ above, we can define the Schwinger functional $W[J]$,

$$W[J] = \ln Z[J], \tag{4.3}$$

the functional derivatives of this are the *connected* $n-$point functions. An even more efficient way to store the information of a quantum theory is the effective action. This is the Legendre transformation of the Schwinger functional with respect to the mean field $\phi(x) = \langle\varphi\rangle$,

$$\begin{aligned}\Gamma[\phi] &= \sup_J\left[\int_x J(x)\phi(x) - W[J]\right] \\ &= J_{\text{sup}}(x)\phi(x) - W[J_{\text{sup}}].\end{aligned} \tag{4.4}$$

Here, we pick a configuration which maximizes the Legendre transformation. The supremum of the source is a function of the mean field $J_{\text{sup}}[\phi(x)]$. This definition guarantees that $\Gamma[\phi]$ is convex, in that we can now see that not only is ϕ equal to $\langle\varphi\rangle$, but also is conjugate to $W[J]$. That is, at $J = J_{\text{sup}}$

$$\begin{aligned}&\frac{\delta}{\delta J(x)}\left(\int d^dx J(x)\phi(x) - W[J(x)]\right) \overset{\text{def.}}{=} 0 \\ &\implies \phi = \frac{\delta W[J]}{\delta J(x)} = \langle\varphi\rangle_J,\end{aligned} \tag{4.5}$$

where the overset on the equals sign in the first line signifies that the equality holds at only the supremum of the source. It is also instructive to see the opposite direction,

that is the derivative of the effective action with respect to the mean field.

$$\begin{aligned}\frac{\delta\Gamma[\phi]}{\delta\phi(x)} &= -\frac{\delta W[J]}{\delta\phi(x)} + \int dx' J_{\rm sup}(x')\frac{\delta\phi(x')}{\phi(x)} + \int dx'\frac{\delta J(x')}{\delta\phi(x)}\phi(x) \\ &= J_{\rm sup}(x) + \int dx'\frac{\delta J(x')}{\delta\phi(x)}\underbrace{\left(\phi(x) - \frac{\delta W[J(x')]}{\delta J(x)}\right)}_{=0} \\ &= J_{\rm sup}(x). \end{aligned} \tag{4.6}$$

Here we have used the definition and conclusion of (4.5), to establish that $W[J(x)]$ and $\phi(x)$ (mean field) are conjugate variables. This is also the *quantum equation of motion*: the effective action $\Gamma[\phi]$ encodes all dynamics of the field expectation values and their functions thereof, taking into account all quantum fluctuations. The effective action generates one-particle irreducible $n-$point functions. 1PI correlation functions are generated from the effective action by functional differentiation with respect to the mean field. This is done by taking n derivatives of the effective action with respect to $\phi(x)$. Here, one-particle irreducible means that the corresponding Feynman diagrams cannot be cut into two diagrams by the cut of a single internal line.

$$\begin{aligned}\Gamma^{(n)}(\phi(x)) &= \frac{\delta^{(n)}\,\Gamma(\phi(x))}{\delta\phi(x_1)\delta\phi(x_2)\,\ldots\,\delta\phi(x_n)} \\ &= \langle\phi(x_1)\,\phi(x_2)\,\ldots\,\phi(x_n)\rangle_{\rm 1PI} \end{aligned} \tag{4.7}$$

4.1.1 Wetterich Equation

One way to get to the effective action Γ is to employ renormalization group techniques by making use of an scale-dependent interpolating action Γ_k, termed the effective average action (EAA), the k here is a momentum-shell parameter denoting scale. The scale k can be seen as a 'dial' that interpolates between the classical (bare)

action and the quantum effective action (at $k \to 0$). We have for some UV cutoff λ

$$\Gamma_{k\to\lambda} = S_{\text{bare}}, \qquad \Gamma_{k\to 0} = \Gamma. \tag{4.8}$$

We can get to the interpolating action Γ_k by following exactly the same procedure outlined previously; the only difference here being that the generating functional we start with is now infrared regulated via a scale-dependent term. Restricting the path integral in this way (or any other way that 'does away' with a finite number of modes) usually does not respect the symmetries (Lorentz, diffeomorphism, $O(N)$, etc) of the full QFT. The breaking of said symmetries depends upon the anomaly associated to the symmetry. We assume that the theories we deal with here are anomaly-free, and symmetries preserved upon quantization, for more details see [116].

From the scale-dependent generating functional $Z_k[J]$, we switch to the Schwinger functional and eventually transform to the quantum effective average action, all of whom would now be scale-dependent. We denote the generating functional with suppressed IR modes by,

$$Z_k[J] = \frac{1}{N} \int_{p^2 \geq k^2} \mathcal{D}\varphi \, e^{-S[\varphi] - \int J(x)\varphi(x)}, \tag{4.9}$$

here the subscript, $p^2 \geq k^2$ indicates that we only include momentum modes above the scale k. This is implemented by using a function that smoothly suppresses these modes. We define,

$$\int_{p^2 \geq k^2} \mathcal{D}\varphi = \int \mathcal{D}\varphi e^{-\Delta S_k[\varphi]}, \tag{4.10}$$

where,

$$\Delta S_k[\varphi] = \frac{1}{2} \int_p \varphi(p) R_k(p^2) \varphi(-p). \tag{4.11}$$

Here, we have defined $\int_p = \int \frac{d^d p}{(2\pi)^d}$ and R_k is the regulator function that suppresses modes with $p^2 \leq k^2$ but leaves modes with $p^2 \geq k^2$ unaffected, and ΔS_k is called the cut-off action. This can be viewed as a momentum-dependent mass term. The regulator function is required to have three properties:

1. Suppression of the IR modes:

$$\lim_{p^2 \to 0} R_k(p^2) > 0$$

2. Physical limit to ensure $Z_{k=0} = Z$:

$$\lim_{k \to 0} R_k(p^2) = 0$$

3. UV limit to ensure that $\Gamma_{k=\Lambda} = S$:

$$\lim_{k \to \Lambda \to \infty} R_k(p^2) \to \infty$$

Adding the cut-off action with an appropriate regulator function (one with the correct limiting behavior) to the generating functional as in (4.9), using the previous definitions, we get the scale-dependent Schwinger functional

$$W_k[J] = \ln(Z_k[J]), \tag{4.12}$$

and through a 'modified' Legendre transformation, the scale-dependent QEAA:

$$\Gamma_k[\phi] = \int dx\, J(x)\phi(x) - W_k[J] - \Delta_k S[\phi]. \tag{4.13}$$

Note that, (4.13) is not the Legendre transformation of the Schwinger functional (4.12) because of the additional term $\Delta_k S[\phi]$; the limit $k \to 0$ implying $\Delta_k S[\phi] \to 0$

would render (4.13) back to the expected convex Legendre transform of $W_k[J]$. We seek the flow of scale-dependent couplings through the $k-$derivative of the now scale-dependent QEAA, $\Gamma_k[\phi]$, $\partial_k\Gamma_k[\phi]$. We define the 'RG-time' t and dimensionless scale derivative ∂_t

$$t = \ln\left(\frac{k}{\lambda}\right) \qquad\qquad \partial_t = k\frac{d}{dk}. \tag{4.14}$$

Starting with the scale-dependent Schwinger functional, we compute the derivative $\partial_t W_k[J]$:

$$\begin{aligned} \partial_t W_k[J] &= -\frac{1}{2}\int \mathcal{D}\varphi \int_p \varphi(p)\partial_t R_k(p^2)\varphi(-p)e^{-S-\Delta_k S+\int dx J(x)\varphi(x)} \\ &= -\frac{1}{2}\int \frac{d^dp}{(2\pi)^d} G_k(p)\partial_t R_k(p^2) + \partial_t\Delta_k S[\varphi] \end{aligned} \tag{4.15}$$

where we have defined the connected propagator (source derivatives of the Schwinger functional)

$$G_k(p) = \frac{\delta^2 W_k[J]}{\delta J(p)\delta J(-p)} = \langle\varphi(p)\varphi(-p)\rangle - \langle\varphi(p)\rangle\langle\varphi(-p)\rangle. \tag{4.16}$$

Subsequently, we get modification in the relationship between the mean field and the derivative of the now scale-dependent Schwinger functional. Note that, the right-hand side of (4.13) is now the Legendre transform of $\Gamma_k[\phi] + \Delta_k S[\phi]$, this follows from the definition in (4.13) (again, at the supremum of the source, J):

$$\frac{\delta(\Gamma_k + \Delta_k S)}{\delta\phi(x)} = J_{\sup}(x), \qquad \frac{\delta W_k[J_{\sup}(x)]}{\delta J(x)} = \phi(x). \tag{4.17}$$

Consequently, the connected propagator (4.16) gets the corresponding scale-dependent

modification:

$$G_k(p) = \frac{\delta^2 W_k[J]}{\delta J(p)\delta J(-p)} = \left(\frac{\delta^2(\Gamma_k + \Delta_k S)}{\delta\phi(p)\delta\phi(-p)}\right)^{-1} \tag{4.18}$$

In the second equality above, we have used the fact that the propagator is the inverse of the 1PI two-point function. We have

$$\int dy \frac{\delta^2 W}{\delta J(x_1)\delta J(y)} \cdot \left(\frac{\delta^2 \Gamma}{\delta\phi(y)\delta\phi(x_2)}\right) = \int dy \frac{\partial\phi(y)}{\partial J(x_1)} \frac{\partial J(x_2)}{\partial\phi(y)} = \delta(x_1 - x_2) \tag{4.19}$$

which leads us to conclude

$$\begin{aligned} \frac{\delta^2 W}{\delta J(x_1)\delta J(x_2)} = G(x_1,\, x_2) &= \left(\frac{\delta^2 \Gamma}{\delta\phi(x_1)\delta\phi(x_2)}\right)^{-1} \\ &= \frac{1}{\Gamma_k^{(2)}[\phi] + R_k(\phi)}. \end{aligned} \tag{4.20}$$

Using results from (4.15), (4.16), (4.18), (4.17), (4.20) (in momentum space), and the definition of the scale derivative in (4.14), we compute the change in the interpolating, effective average action, with scale:

$$\begin{aligned} \partial_t \Gamma_k[\phi] &= -\partial_t W_k[J] - \partial_t \Delta_k S[\phi] \\ &= \frac{1}{2}\int \frac{d^d p}{(2\pi)^d} G_k(p) \partial_t R_k(p^2) \\ &= \frac{1}{2}\int \frac{d^d p}{(2\pi)^d} \frac{\partial_t R_k(p^2)}{\Gamma_k^{(2)}[\phi] + R_k(\phi)}. \end{aligned} \tag{4.21}$$

The fact that that the scale derivative of the cut-off action cancels in the first line provides a further motivation of the modified Legendre transformation (4.13). The final Wetterich Equation incorporates the integral over all relevant momenta and (if any other) continuous indices, plus a sum over all possible discrete indices via a

'super-trace' operator STr, we get the final Wetterich Equation in a compact form

$$\partial_t \Gamma_k[\phi] \;=\; \frac{1}{2}\,\mathrm{STr}\left[\frac{\partial_t R_k(p^2)}{\Gamma_k^{(2)}[\phi] + R_k(\phi)}\right]. \tag{4.22}$$

It is important to note a few properties of the Wetterich Equation. The Wetterich equation is a functional differential equation for the interpolating action Γ_k. The limits of which are the bare action $k \to \lambda$ in the UV (λ here being the UV cutoff for a regularized theory), and the full quantum effective action Γ in the IR ($k \to 0$). These correct limits are enforced by the choice of the regulator function R_k, which is completely arbitrary up to the choice of limiting behavior outlined above. These properties serve to not only ensure the correct limiting behavior, but also renders the Wetterich equation finite in both the UV and the IR. The occurence of the regulator in the denominator ensures IR finiteness, while the derivative occurring in the numerator ensures, by integrating momenta $p^2 \sim k^2$ out, UV finiteness.

The solution to the Wetterich equation is an interpolating trajectory in theory space (space of all possible couplings) between the bare action and a quantum effective action. These trajectories, however, depend on the choice of the regulator, but since they are meant to describe the same QFT– they have the same end-points. However, while this is true in theory, in practice we truncate our coupling space for the problem at hand, this results in a different quantum effective action–with this, faster convergence becomes a priority of the problem.

4.2 Matter Time in General Relativity

We will couple our eventual system of interest (FRW cosmology + massless quantum scalar field) to a matter field clock. General Relativity is a theory with constraints. That is, it is described in terms of more variables than actual degrees of freedom.

Due to this fact, the Hamiltonian for gravity, H_G, vanishes. This reflects the time reparameterization invariance of GR. This is in contrast to time in quantum theory where time is an external parameter. We consider introducing 'physical time' as a clock to circumvent the problem of time faced in quantizing GR. This physical time is to use one of the phase space variables that is second-class with the full Hamiltonian Constraint, i.e. $\{t,\, H_G\} \not\approx 0$.

For any such choice of physical time, we have the physical Hamiltonian as,

$$H_p = -p_t, \tag{4.23}$$

where p_t is the momentum conjugate to t, that is, $\{t,\, p_t\} = 1$. We shall now discuss how can we use matter, such as pressure-less dust, as physical time. The action for GR coupled to dust field, T, is given by

$$\begin{aligned} S &= S_G + S_D \\ &= \frac{1}{2\pi}\int d^4x\sqrt{-g}\, R - \frac{1}{4\pi}\int d^4x\sqrt{-g}\, M(g^{\mu\nu}\partial_\mu T\partial_\nu T + 1) \end{aligned} \tag{4.24}$$

The second term describes the dust part of the action. The parameter M enforces the constraint that the gradient of the dust field T is timelike. The corresponding ADM action obtained from this theory is,

$$S = \frac{1}{2\pi}\int dt d^3x \left(\pi^{ab}\dot{q}_{ab} + p_T\dot{T} - N\mathcal{H} - N^a C_a\right), \tag{4.25}$$

here $(q_{ab},\, \pi^{ab})$ and $(T,\, p_T)$ are canonically conjugate variables for gravity and dust, respectively. N is the lapse, N^a is the shift. These appear as Lagrange multipliers

in the action.

$$\begin{aligned} H &= H^G + H^D, && (4.26)\\ C_a &= C_a^G + C_a^D && (4.27)\\ &= -2D_b\pi_a^b + p_T\partial_a T. && (4.28) \end{aligned}$$

where H^G is the gravitational part of the Hamiltonian constraint, and

$$H^D = \frac{1}{2}\left(\frac{p_T^2}{M\sqrt{q}} + M\sqrt{q}\left(q^{ab}\partial_a T\partial_b T + 1\right)\right). \quad (4.29)$$

Since M appears as a Lagrange multiplier in the action, the momentum conjugate to it is zero. We can vary H^D with respect to M

$$\begin{aligned} \frac{\delta H^D}{\delta M} &= -\frac{p_T^2}{2M^2\sqrt{q}} + \frac{\sqrt{q}}{2}\left(q^{ab}\partial_a T\partial_b T + 1\right) && (4.30)\\ &= 0 && (4.31)\\ \frac{p_T^2}{2M^2\sqrt{q}} &= \frac{\sqrt{q}}{2}\left(q^{ab}\partial_a T\partial_b T + 1\right) && (4.32)\\ \implies M &= \pm\frac{p_T}{\sqrt{q\left(q^{ab}\partial_a T\partial_b T + 1\right)}}. && (4.33) \end{aligned}$$

Substituting (4.33) back in the Hamiltonian constraint for the dust (4.29) we get:

$$H^D = \mathrm{sgn}(M)p_T\sqrt{q^{ab}\partial_a T\partial_b T + 1} \quad (4.34)$$

4.2.1 The Dust time gauge

We now reduce the theory by fixing a time gauge. That is choosing that level surfaces of the dust field give physical time.

$$T = \epsilon t; \qquad \epsilon = \pm 1. \quad (4.35)$$

Substituting this back in to (4.29), we get

$$q^{ab}\partial_a T\partial_b T = 0; \tag{4.36}$$

allowing us to write,

$$H = H^G + H^D = H^G + \mathrm{sgn}(M)p_T. \tag{4.37}$$

This leads us to write the physical Hamiltonian density

$$H_p := -\epsilon p_T = \mathrm{sgn}(M)\,\epsilon H^G. \tag{4.38}$$

For the validity of the gauge choice, we want it to be preserved in time. This requires

$$\dot{T} = \epsilon = \{T,\, \int d^3x N H\}|_{T=t} = \mathrm{sgn}(M)N. \tag{4.39}$$

Substituting (4.39) into (4.38) gives us:

$$H_p = N\mathcal{H}^G. \tag{4.40}$$

Lastly, we choose lapse for this physical Hamiltonian. We go back to the dust action,

$$L_D = \frac{M\sqrt{q}}{2N}\left[\left(\dot{T} + N^a\partial_a T\right)^2 - N^2\left(q^{ab}\partial_a T\partial_b T + 1\right)\right]. \tag{4.41}$$

The dust momentum is

$$p_T = \frac{\partial L_D}{\partial \dot{T}} = \sqrt{q}\frac{M}{N}\left(\dot{T} + N^a\partial_a T\right). \tag{4.42}$$

Substituting conditions (4.39) and (4.35) results in

$$p_T = \epsilon\sqrt{q}\frac{M}{N} = \epsilon\frac{\text{sgn(M)}}{N}|M| = \sqrt{q}|M|. \tag{4.43}$$

Positive dust energy density thus corresponds to a positive physical Hamiltonian density if $N = -1$, implying $\epsilon = -1$, and thus,

$$H_p = -\frac{1}{2\pi}\int d^3x H^G. \tag{4.44}$$

Several key features follow from this gauge fixing. First of which is the obvious, but all-important that the dynamics are now physical that come from a physical Hamiltonian that is not a constraint. Moreover, the physical Hamiltonian is not a square root as was the case for several previous attempts, see [49] for examples in the homogeneous context. On top of that, the algebraic form of the physical Hamiltonian is the same as in the Hamiltonian constraint (up to sign). We now study the physical dynamics of systems coupled with dust. We now couple dust with Friedman cosmology and use it as matter time.

4.3 Universe as an oscillator

The eventual goal of this work is to compute the fixed points (if any) of the exact RG flow equations for FRW cosmology and compare them to the fixed points found in the asymptotic safety program by Reuter [28]. Assuming we have reviewed the computation of the Wetterich equation for a quantum mechanical system in Appendix A, we analogously derive the flow equation(s) for cosmology, where akin to quantum mechanics, we have one degree of freedom–namely the scale factor. Our starting point for this analysis would be canonical action for FRW cosmology with a cosmological constant Λ coupled with a dust field, T; the gauge fixed action in units

where $\hbar = c = 1$ is,

$$S = \int dt \left(\frac{1}{16\pi G} \left(R - 2\Lambda \right) + \mathcal{L}_{\text{matter}} + \mathcal{L}_{\text{Dust}} \right). \tag{4.45}$$

In ADM variables, and after symmetry-reducing to homogeneous and isotropic cosmology this becomes,

$$S = \frac{V_0}{16\pi G} \int dt \, \left(p_a \dot{a} - N H_G \right) + V_0 \int dt \, \left(p_\phi \dot{\phi} - N H_\phi \right) \tag{4.46}$$

where,

$$H_G = -\frac{p_a^2}{24a} + a^3 \Lambda \tag{4.47}$$

$$H_\phi = \mu \frac{p_\phi^2}{2a^3}. \tag{4.48}$$

H_G, is the physical Hamiltonian for cosmology, and $V_0 = \int d^3x$ is the fiducial volume; and the lapse $N = 1$.

In the variables above (a, p_a), the eventually computed flow equations are not particularly insightful. Among several choices of suitable variables for our subsequent analysis, we turn to one outlined in [117]. We perform the canonical transformation,

$$x = \frac{4}{\sqrt{3}} a^{3/2} \qquad\qquad p = \frac{p_a}{\sqrt{12a}} \tag{4.49}$$

In these variables, the physical Hamiltonian becomes

$$\tilde{H} = -\frac{p^2}{2\tilde{G}} + \frac{\Lambda}{2\tilde{G}} x^2 \tag{4.50}$$

where we rescale $\Lambda \to \frac{8}{3}\Lambda$, and define $\tilde{G} = \frac{1}{16\pi G}$. Using (4.50), we find

$$\dot{x} = \{x,\, \tilde{H}\} = \frac{\partial \tilde{H}}{\partial p} = -p. \tag{4.51}$$

This allows us to write the gravity part of the gauge fixed canonical action,

$$S_G = V_0 \int dt \, \left(-\frac{\dot{x}^2}{2\tilde{G}} - \frac{\Lambda}{2\tilde{G}} x^2 \right). \tag{4.52}$$

For the scalar field part, in the new variables, we have

$$H_\phi = \mu \frac{8}{3} \frac{p_\phi^2}{x^2} \implies \dot{p}_\phi = \frac{3}{16\mu} \dot{\phi} x^2 \tag{4.53}$$

Substituting (4.53), in the canonical scalar field action, and rescaling $\mu \to \frac{3}{16}\mu$, we get

$$S_\phi = V_0 \int dt \, \left(\frac{1}{2\mu} \dot{\phi}^2 x^2 \right). \tag{4.54}$$

Our full system of interest, is symmetry-reduced gravity minimally coupled to the massless scalar field. Canonically, this is the sum of the two actions (4.52) and (4.54). Identifying $1/\mu \to \bar{\mu}$

$$\begin{aligned} S &= S_G + S_\phi \\ &= V_0 \int dt \left[\left(-\frac{1}{2G} \dot{x}^2 - \frac{\Lambda}{2G} x^2 \right) + \left(\frac{\bar{\mu}}{2} \dot{\phi}^2 x^2 \right) \right] \end{aligned} \tag{4.55}$$

In subsequent analysis, we drop the overbar on $\bar{\mu}$ and Euclideanize this total action for use in the Wetterich equation

$$S^E = -iV_0 \int d\tau \, \left(\frac{\dot{x}^2}{2G} - \frac{\Lambda}{2G} x^2 - \frac{\mu}{2} x^2 \dot{\phi}^2 \right). \tag{4.56}$$

4.4 FRG for Cosmology with a Scalar Field

We now derive the flow equations for FRW cosmology minimally coupled to a scalar field. Here, we have two configuration variables, $x(\tau)$ and $\phi(\tau)$. In this we also assume that that the scalar field we have is homogeneous, this implies it only depends on time, and the spatial derivatives vanish. Our starting point for the analysis is the scale-dependent Euclideanized action S_k^E, with an additional term $\epsilon_k x^4$ term, where all couplings are now dependent on scale k. This is the analong of the interpolating average action Γ_k in standard QFT:

$$S_k^E = V_0 \int d\tau \left(\frac{1}{2G_k}\dot{x}^2 + \frac{1}{2}\frac{\Lambda_k}{G_k}x^2 + \frac{\epsilon_k}{12}x^4 - \mu_k x^2 \dot{\phi}^2 \right) \tag{4.57}$$

Here, the set of couplings $\{G_k,\, \Lambda_k,\, \epsilon_k\}$ are dimensionful, while μ_k is dimensionless. The dimension of the first three in terms of scale k is,

$$[\Lambda_k] = k^2 \qquad [G_k] = 1/k^2 \qquad [\epsilon_k] = k^4. \tag{4.58}$$

Moreover, the addition of the x^4 term serves a bipartite purpose: first, it allows us to construct a direct analogy with the anharmonic oscillator [118], second it allows us to extract the flow for Λ_k by comparing powers in the x^2 term on the left and right-hand sides of the Wetterich equation below; this arises due to two functional derivatives of S_k^E on the right-hand side.

In terms of (4.57) the Wetterich equation for the full system would be

$$\partial_t S_k^E \;=\; \mathrm{STr}\left[\frac{\partial_t (Z_k^x R_k)}{S^{(2)}_{,x} + Z_k^x R_k} + \frac{\partial_t (Z_k^\phi R_k)}{S^{(2)}_{,\phi} + Z_k^\phi R_k} \right]. \tag{4.59}$$

On the right hand side, we have two terms: one for gravity (labelled with sub- and super-script x), and one for the scalar field (labelled with sub- and super-script ϕ).

As with the harmonic oscillator outlined in the appendix below, we choose for our computations the optimized regulator

$$R_k(p^2) = (k^2 - p^2)\Theta(k^2 - p^2) \tag{4.60}$$

For completeness, we have above the form of the Wetterich equation with the wave-function renormalization terms for each species, see [119] for more details. These are the coefficients of the kinetic terms in the respective actions. For the first (gravity) term this is, $Z_k^x = 1/G_k$ and for the scalar field it is $Z_k^\phi = -\mu_k x^2$. From here, we follow the procedure outlined in section II, to compute the second functional derivatives of (4.57) with respect to x and ϕ. We have

$$\begin{aligned} S^{(2)}_{,x} &= Z_k p^2 - \frac{\Lambda_k}{G_k} + \epsilon_k x^2 - \mu_k \dot{\phi}^2 \\ S^{(2)}_{,\phi} &= -\mu_k x^2 p^2. \end{aligned} \tag{4.61}$$

The derivative of the regulator is,

$$\partial_t R_k = 2k\Theta(k^2 - p^2). \tag{4.62}$$

Substituting results from (4.61), 4.61), (4.62), we get the final constituents of the Wetterich equation are,

$$\int d\tau\, \partial_k S^x_k = \frac{1}{3\pi}\int d\tau \frac{(\partial_t Z_k + 3Z_k)\, k^3}{Z_k k^2 - \frac{\Lambda_k}{G_k} + \epsilon_k x^2 - \mu_k \dot{\phi}^2},, \tag{4.63}$$

$$\int d\tau\, \partial_k S^\phi_k = \frac{1}{3\pi}\int d\tau\, \frac{(k\partial_k \mu_k + 3\mu_k)\, k}{\mu_k}. \tag{4.64}$$

Expanding out the right-hand side of the (4.63) equation around $\{x = 0,\, \dot{\phi} = 0\}$ and comparing powers, we get the auxiliary flow equations for all couplings. These would not be the final equations as all couplings are still dimensionful. We extract

all relevant flows in the next subsection.

4.4.1 RG Flow Equations

Before writing down the final set of RG flow equations, we must ensure that they are dimensionless. These dimensionless couplings (and their flows) can be obtained by appropriate multiplication with powers of k. In the foregoing we relabel the dimensionful couplings, with dimensions defined in (4.58), to be

$$\Lambda_k \to \tilde{\Lambda}_k \qquad G_k \to \tilde{G}_k \qquad \epsilon_k \to \tilde{\epsilon}_k \qquad \mu_k \to \tilde{\mu}_k, \tag{4.65}$$

and then define the dimensionless couplings,

$$\Lambda_k \equiv \tilde{\Lambda}_k/k^2 \qquad g_k \equiv k^2\tilde{G}_k \qquad \epsilon_k \equiv \tilde{\epsilon}_k/k^4 \qquad \mu_k \equiv \tilde{\mu}_k. \tag{4.66}$$

We use these dimensionless coupling in all the subsequent analysis. The final renormalization group (RG) flow equations for dimensionless couplings are given by

$$\partial_k g_k = \frac{2}{k} g_k \tag{4.67}$$

$$\partial_k \Lambda_k = \frac{2}{\pi}\frac{1}{k^4 V_0}\left(\frac{g_k^2 \epsilon_k}{(\Lambda_k - 1)^2}\right) - \frac{6}{k}\Lambda_k \tag{4.68}$$

$$\partial_k \epsilon_k = \frac{12}{\pi}\frac{1}{k^4 V_0}\left(\frac{g_k^2 \epsilon_k^2}{(1 - \Lambda_k)^3}\right) - \frac{4}{k}\epsilon_k \tag{4.69}$$

$$\partial_k \mu_k = -\frac{4}{k^4 V_0 \pi}\left(\frac{g_k^2 \mu_k\, \epsilon_k}{(\Lambda_k - 1)^3}\right) \tag{4.70}$$

$$\partial_k E_k = \frac{1}{3k^3 V_0 \pi}\left(\frac{\partial_k \mu_k}{\mu_k}\right) + \frac{1}{k^4 V_0 \pi} + \frac{1}{k^4 V_0}\left(\frac{1}{1 - \Lambda}\right) - \frac{4E_k}{k}. \tag{4.71}$$

At a fixed point we require that all beta functions vanish. Analytically, this cal-

culation shows an absence of any fixed points. We verify this in the next section numerically.

4.5 Results

We now present the results of our numerical evolution of the dimensionless flow equations derived in the previous section. We use a standard Runge-Kutta 4 to solve the ODE system. The initial data comprises of set of values of couplings at the UV cut-off, or their values in the bare action. Since, in our truncation of the interpolating action (4.57), we added in the x^4 term with the coupling ϵ_k, we start with, at the bare level $\epsilon_k(0) = 0.0001$.

In Fig. 4.1 we present results for the flow for the dimensionless couplings g_k and Λ_k. We start in the IR at arbitrary large k, here taken to be $k = 2$, and then evolve the set of ODEs (4.69), (4.67), (4.71), (4.68) for various initial data. There is a pole at $\Lambda_k = 1$ which renders our system singular, in that we avoid $\Lambda_k(0) = 1$ as initial data. We test the equations for various initial data but get results that are qualitatively similar: we see that in the UV our theory is free, that is, as $k \to 0$, and we go to the scales where all quantum fluctuations are incorporated, any value of initial gravitational constant vanishes. Conversely, at these higher energies, the cosmological constant blows up.

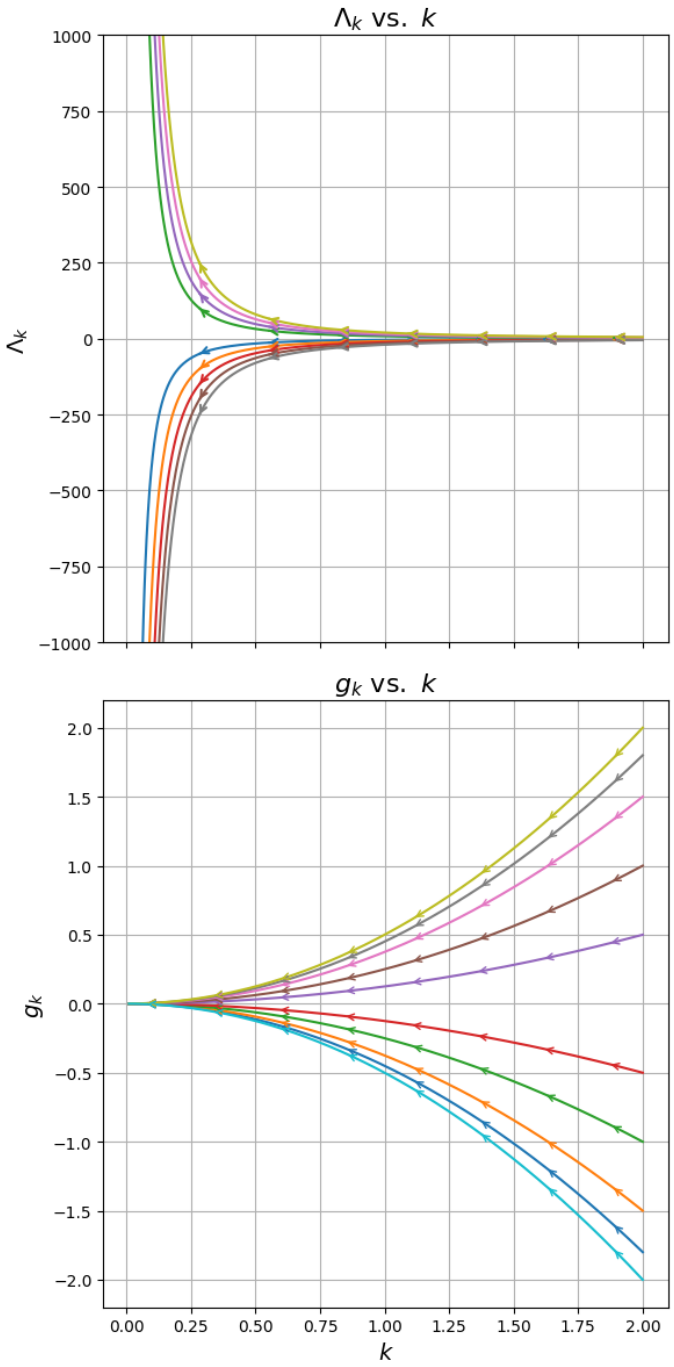


Figure 4.1: Renormalization group flows of the dimensionless cosmological constant Λ_k (top panel) and the dimensionless Newton coupling g_k (bottom panel) as functions of the RG scale k. Arrows indicate the direction of decreasing k (i.e. the UV flow). Although both couplings start from finite values in the infrared ($k \simeq 2$), their UV behavior is radically different: as $k \to 0$, the Newton coupling vanishes, signaling the effective disappearance of gravitational interactions, whereas the cosmological constant grows without bound, indicating a divergent vacuum energy in the deep UV.

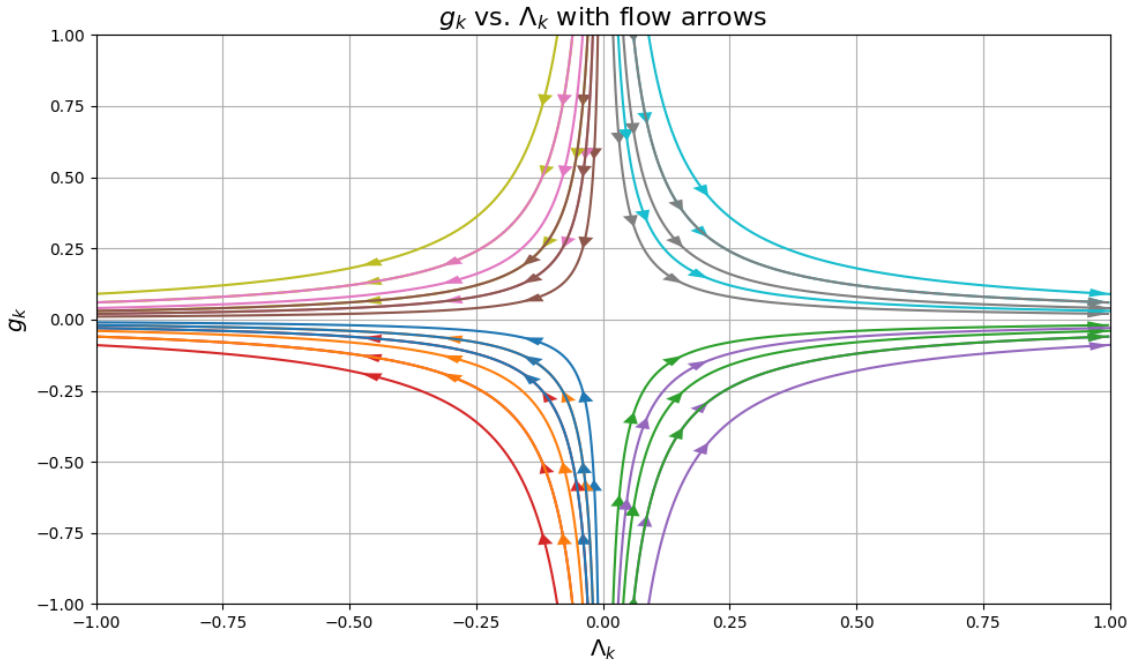


Figure 4.2: Renormalization group flow trajectories in the dimensionless coupling plane (Λ_k, g_k) for a variety of infrared initial conditions. Arrows mark the direction of decreasing RG scale k (toward the UV). Although all flows emanate from the vicinity of the Gaussian point $(\Lambda, g) = (0, 0)$ at high k, they do not settle at any non-trivial fixed point as $k \to 0$. Instead, g_k universally tends toward zero while Λ_k diverges positively or negatively depending on the chosen trajectory. The lack of any vanishing arrow vectors in the plotted region confirms the absence of additional fixed points.

4.6 Summary and Discussion

In this work we applied the exact renormalization group (ERG) to a symmetry-reduced (minisuperspace) cosmological model: a homogeneous FRW universe minimally coupled to a massless scalar field and pressureless dust. Our analysis was motivated by the asymptotic safety program in full quantum gravity, which posits a non-Gaussian ultraviolet (UV) fixed point that renders gravity finite at high energies [28, 114]. Here, we investigated whether such nontrivial fixed-point behavior persists in a highly truncated cosmological setting. The minisuperspace model allowed us to derive and study the renormalization-group flow of the gravitational couplings (Newton's constant g_k and the cosmological constant Λ_k) and matter couplings in a simplified context, treating the dust field as a reference fluid to define a proper time coordinate [10]. We emphasize that our "exact" RG treatment is still a severe truncation of the full theory, capturing only the dynamics of the homogeneous mode of the universe.

Our key findings are as follows. First, we find no evidence of a non-Gaussian UV fixed point in this minisuperspace model – the only fixed point of the flow equations is the Gaussian one, where the dimensionless couplings g_k and Λ_k go to zero. This stands in contrast to the full 4D theory, where functional RG studies have repeatedly found an interacting UV fixed point [28, 110]. For our truncated cosmological model the RG flow never settles into a finite, non-zero set of constant couplings and thus the theory never becomes scale-invariant. The absence of a UV fixed point suggests that critical gravitational dynamics may not be captured when only homogeneous modes are present.

Second, when we raise the RG scale into the ultraviolet we find that the dimensionless Newton coupling $g_k = k^2 G(k)$ runs to zero, whereas the dimensionless cosmological constant $\Lambda_k = \tilde{\Lambda(k)}/k^2$ grows without bound. This is in contrast to findings from

what full ERG studies typically report, namely a finite non-Gaussian fixed point with $g_k \to g^* \neq 0$ and $\Lambda_k \to \Lambda^*$ [29, 30]. In our minisuperspace truncation the gravitational self-interaction effectively fades out at high energies while the cosmological term dominates. The runaway of Λ_k is plausibly an artefact of the symmetry reduction: with massive and inhomogeneous modes frozen out, no threshold effects remain to balance the flow and stabilize the coupling.

Third, we find that the scalar field coupling μ_k is nearly constant across the entire flow. The scalar field is massless and minimally coupled, and its kinetic coefficient shows negligible running. This result is consistent with results from full asymptotic safety studies, where minimally coupled free scalars continue to act like non-interacting fields – their couplings stay essentially unchanged – even when gravity itself sits at a fixed point [110].

Together, these results highlight both the strengths and limitations of minisuperspace ERG analyses. On the one hand, the simplicity of the model enables us to obtain a self-consistent picture of RG flow in a quantum cosmological setting. On the other hand, the absence of an interacting UV fixed point and other unconventional UV behavior of the couplings signal that the symmetry reduction removes crucial dynamical content. This echoes the longstanding critiques of minisuperspace models that cautioned that truncating to homogeneous configurations neglects essential degrees of freedom and may produce misleading results [115].

The lack of a fixed point in the minisuperspace ERG flow does not falsify the asymptotic safety scenario, but rather underscores the limitations of overly symmetric truncations. The inhomogeneous gravitational degrees of freedom, which are absent in minisuperspace, appear to play a central role in driving the characteristics of gravity that lead to a UV fixed point. These modes may also regulate the UV dynamics in more complete settings. Future work should extend the ERG analysis to include in-

homogeneities or midisuperspace models to investigate the emergence of fixed points and more realistic running behavior.

Moreover, there also remains the crucial question of the entire analysis being carried out in Euclidean signature: although one can often recover observables by analytically continuing back to Lorentzian time, this step is not rigorously justified when the metric itself fluctuates. Moreover, while the Euclidean fixed point found by Reuter et al. in the full theory is strong evidence that gravity can be asymptotically safe, a definitive proof would require a Lorentzian – or at least signature-independent – derivation. Consequently, it is still unclear whether the fixed-point structure seen in the Euclidean flow even survive in the genuinely Lorentzian, and therefore causal, quantum theory.

Lastly, while minisuperspace models provide valuable theoretical insight in other areas of the quantum gravity programme such as loop quantum cosmology, spin-foam cosmology, and studies of quantum black-hole interiors, our findings reinforce the view that their predictive power is limited when addressing the full structure of quantum gravitational renormalization.

Chapter 5

Conclusion

In this thesis we studied a few aspects of the nonperturbative quantum gravity programme:

- Hamiltonian semiclassical cosmology: We developed a self-consistent framework in which fully quantized matter fields backreact on homogeneous (both isotropic and anisotropic) cosmological metrics, tracking how quantum stress–energy modifies early- and late-time dynamics.
- Renormalization-group flow of gravity: Using Exact RG techniques we followed the scale dependence of gravitational couplings in an FRW universe, testing whether the ultraviolet fixed point predicted by the asymptotic-safety programme survives in symmetry-reduced models of gravity with quantum matter.

In the first part we explored semiclassical gravity, allowing fully quantum matter fields to backreact on a dynamical yet classical spacetime metric. Towards the end, we applied the Functional Renormalization Group to cosmological minisuperspace models, investigating how the non-Gaussian ultraviolet fixed point discovered by

Reuter behaves – or fails to appear – in this symmetry-reduced setting. More detailed outlooks and summaries of these issues can be found at the end of each chapter.

Chapters 2 and 3 made use of the Hamiltonian SCG framework and applied it to homogeneous spacetimes. In chapter 2, we exclusively dealt with the isotropic universe (FRW), and segued briefly with a discussion on the Kasner universe, introducing the most basic notions of anisotropy in a minisuperspace setting into the analysis. We find for the FRW universe, that a semiclassical treatment, where the quantum matter is represented by a massive quantum scalar field, allows for static solutions. Linear stability analysis revealed that the unstable mode led naturally to inflation. Moreover, in addition to limiting towards the classical results at late times, the classical-quantum (CQ) system showed several interesting features. Particularly striking was the difference in the evolution of the scalar field density, which in the case of the CQ equations settled to a minimum constant value – a possible hint towards Dark Energy. As for the treatment of the Kasner universe, adding matter rendered the Kasner sum rules violated – as these, arising from the Hamiltonian constraint, are valid in regimes without matter. As the universe expands we see that all the individual exponents converge to a common value, signaling as expected, the isotropization of the universe at late times.

In Chapter 3 we extend this semiclassical framework to the mixmaster, or Bianchi-IX, universe. The mixmaster universe presents its own host of complexities induced in the form a triangular potential via scale-factor interactions. The classical mixmaster universe, even without matter, presents rich dynamics that follow from a particle in a potential picture. These interesting dynamics include chaos [80, 82]. We studied two important aspects here, first, the effect of adding quantum matter in the analysis similar to how we did in chapter 2, and second, to assess the implications of polymerizing (introducing discreteness corrections) the background. This allowed us to probe the theory close to the singularity (or bounce) and study several

features. We found that polymerizing resolves the initial singularity by replacing it with successive, asymmetric bounces. Each minimum volume occurs at a critical density that is proportional to the inverse squared size of the discreteness correction λ. Moreover, the quantum scalar field excites higher states as the universe volume decreases towards the bounce, and de-excites partially after a bounce. We also find that the chaos reduces in models where we add quantized matter and introduce polymer corrections in the background.

Finally, Chapter 4 shifts focus to the functional renormalization group and examines its application to a cosmological context. We start from the Euclidean action recast in variables that allows us to make a direct analogy with the harmonic oscillator, simplifying the resulting functional derivatives and flow equations. Here, we do a partial gauge fixing initially to ensure our evolution in time is physical: that the Hamiltonian is not constrained to vanish. We minimally couple the FRW universe with a massless scalar field and derive the flow equations. The resulting, dimensionless, flow equations reveal that there is no non-trivial fixed point in the UV as speculated by Weinberg [18], and shown by Reuter in the full theory [28]. This raises questions on the conclusions drawn about full quantum gravity from analyses conducted in the symmetry-reduced sectors of the theory. As for the flow of the dimensionless couplings, we find that the gravitational constant goes to zero at the quantum level ($k \to 0$), and the cosmological constant diverges.

These findings open several promising avenues for further study. Within the semi-classical gravity framework, a natural next step is to include inhomogeneous degrees of freedom – for example, by extending the analysis to Gowdy cosmologies. These are solutions to the Einstein's fields equation that admit two (out of a maximum three) spatial killing vector fields – the metric admits a continuous isometry along these directions, and would only depend on time and one other spatial coordinate. Thus, these models are two-dimensional field theories. Analyzing our classical–quantum

(CQ) equations in this setting could reveal how backreaction modifies the production and amplification of inhomogeneous scalar quanta and could test whether quantum stress–energy dampens or enhances the classical Gowdy 'spikes'[1] known from numerical relativity. Furthermore, introducing discreteness correction in the quantum matter as well, as in [120], in combination with some permutation of polymerized volume and anistropies could be a good numerical exercise in providing a more robust picture of the early universe and inflationary dynamics.

One could then move on to spherically symmetric spacetimes and study black hole spacetimes. In that setting one can begin with test problems scalar collapse in Painlevé–Gullstrand or Eddington–Finkelstein coordinates for the static or dynamical cases. The static problem here would be study the behaviour of the horizon for a static Schwarzchild geometry once backreaction by a quantum scalar field is included. In the full dynamical problem, one can follow a scalar field shell computed in a suitable state through the collapse process. Tracking the solution until curvatures approach the Planck scale could reveal whether the semiclassical approximation predicts (i) complete evaporation, (ii) a long-lived remnant, or (iii) a bounce that avoids the singularity. Each outcome feeds directly into the information-loss paradox – does information escape with the Hawking flux, remain in a remnant, or return after a bounce?

On the functional renormalization group front, a promising way to tighten the link between our minisuperspace ERG calculation and full Quantum Gravity is to thaw the frozen geometry one spatial direction at a time and study what happens to the RG flow. The first step could be an axisymmetric Bianchi-I metric with two independent scale factors; this slight relaxation already lets us test whether the non-Gaussian fixed point that eluded the isotropic model re-emerges once even a

[1] Gowdy spikes are narrow, rapidly growing inhomogeneities that appear in some numerical and analytic solutions of vacuum Gowdy cosmologies in the approach to a singularity.

single anisotropy direction is allowed. One can then upgrade to the full Bianchi-IX ("mixmaster") geometry, whose three scale factors and spatial curvature make its dynamics resemble that of the full theory.

One can then also consider systematically introducing gradient expansions – adding operators with spatial derivatives. This would progressively restore genuine inhomogeneous modes, turning the minisuperspace flow into an increasingly faithful proxy for the complete diffeomorphism-invariant action. At each stage the goals are the same: determine whether a stable UV fixed point with finitely many relevant directions appears; analyze the stability matrix to see how quickly the new anisotropy or gradient couplings are attracted to (or repelled from) that point; and check that the outcome is robust against changes in gauge fixing or regulator choice. Once the running of anisotropy couplings is known, it can be fed back into effective Friedmann equations, yielding RG-improved predictions for quantities such as primordial shear, gravitational-wave backgrounds, or CMB quadrupole constraints and other phenomenological aspects of GR.

Bibliography

[1] Claus Kiefer. *Quantum gravity*, volume 124. Clarendon, Oxford, 2004.

[2] C. J. Isham. Prima facie questions in quantum gravity. *Lect. Notes Phys.*, 434:1–21, 1994.

[3] Carlo Rovelli. Time in quantum gravity: An hypothesis. *Phys. Rev. D*, 43:442–456, Jan 1991.

[4] C. J. Isham. Canonical quantum gravity and the problem of time. *NATO Sci. Ser. C*, 409:157–287, 1993.

[5] Laura Ruetsche. *Interpreting quantum theories*. Oxford University Press, 2011.

[6] Charles W. Misner. Quantum cosmology. I. *Phys. Rev.*, 186:1319–1327, Oct 1969.

[7] James W York Jr. Role of conformal three-geometry in the dynamics of gravitation. *Physical review letters*, 28(16):1082, 1972.

[8] Claus Kiefer and Tejinder P Singh. Quantum gravitational corrections to the functional Schrödinger equation. *Physical Review D*, 44(4):1067, 1991.

[9] Julian Barbour, Tim Koslowski, and Flavio Mercati. Identification of a gravitational arrow of time. *Physical review letters*, 113(18):181101, 2014.

[10] Viqar Husain and Tomasz Pawlowski. Time and a physical Hamiltonian for quantum gravity. *Phys. Rev. Lett.*, 108:141301, 2012.

[11] Carlo Rovelli and Lee Smolin. The physical hamiltonian in nonperturbative quantum gravity. *Physical review letters*, 72(4):446, 1994.

[12] Bernard F Schutz Jr. Hamiltonian theory of a relativistic perfect fluid. *Physical Review D*, 4(12):3559, 1971.

[13] J. D. Brown and K. V. Kuchař. Dust as a standard of space and time in canonical quantum gravity. *Phys. Rev. D*, 51:5600–5629, 1995.

[14] C. J. Isham. Structural issues in quantum gravity. In *14th International Conference on General Relativity and Gravitation (GR14)*, pages 167–209. World Scientific, Singapore, 8 1997.

[15] Masooma Ali. *Forks on a dusty road - Studies in Classical and Quantum Gravity*. PhD thesis, New Brunswick U., 2019.

[16] Marc Henneaux and Claudio Teitelboim. *Quantization of gauge systems*. Princeton university press, 1992.

[17] Paul AM Dirac. *Lectures on quantum mechanics*. Courier Corporation, 2013.

[18] S. Weinberg. Ultraviolet divergences in quantum theories of gravitation. In S. W. Hawking and W. Israel, editors, *General Relativity: An Einstein Centenary Survey*, pages 790–831. Cambridge University Press, Cambridge, 1979.

[19] Juan Maldacena. The large-n limit of superconformal field theories and supergravity. *International journal of theoretical physics*, 38(4):1113–1133, 1999.

[20] Edward Witten. Anti de sitter space and holography. *arXiv preprint hep-th/9802150*, 1998.

[21] Renate Loll, Giuseppe Fabiano, Domenico Frattulillo, and Fabian Wagner. Quantum gravity in 30 questions. *PoS*, CORFU2021:316, 2022.

[22] Viqar Husain and Suprit Singh. Quantum backreaction on a classical universe. *Phys. Rev. D*, 104:124048, Dec 2021.

[23] Michael E Peskin. *An Introduction to quantum field theory*. CRC press, 2018.

[24] Humphrey J Maris and Leo P Kadanoff. Teaching the renormalization group. *Am. J. Phys*, 46(6):653–657, 1978.

[25] Kenneth G Wilson. Renormalization group and critical phenomena. I. renormalization group and the Kadanoff scaling picture. *Physical review B*, 4(9):3174, 1971.

[26] J. Polchinski. Renormalization and effective lagrangians. *Nucl. Phys. B*, 231:269–295, jan 1984.

[27] Christof Wetterich. Exact evolution equation for the effective potential. *Physics Letters B*, 301(1):90–94, 1993.

[28] M. Reuter. Nonperturbative evolution equation for quantum gravity. *Phys. Rev. D*, 57(2):971–985, jan 1998.

[29] D. F. Litim. Fixed points of quantum gravity. *Phys. Rev. Lett.*, 92:201301, 2004.

[30] R. Percacci and D. Perini. Asymptotic safety of gravity coupled to matter. *Phys. Rev. D*, 68:044018, Aug 2003.

[31] Dario Benedetti, Pedro F. Machado, and Frank Saueressig. Asymptotic safety in higher-derivative gravity. *Mod. Phys. Lett. A*, 24:2233–2241, 2009.

[32] Pietro Donà, Astrid Eichhorn, and Roberto Percacci. Matter matters in asymptotically safe quantum gravity. *Phys. Rev. D*, 89:084035, 2014.

[33] Kevin Falls, Daniel F. Litim, Konstantinos Nikolakopoulos, and Christoph Rahmede. On de sitter solutions in asymptotically safe *f(R)* gravity. *Class. Quant. Grav.*, 33:065004, 2016.

[34] Viqar Husain and Muhammad Muzammil. Semiclassical geometrodynamics of homogeneous cosmology. *Phys. Rev. D*, 109(4):044063, 2024.

[35] Muhammad Muzammil and Viqar Husain. Semiclassical mixmaster universe. *Phys. Rev. D*, 111(8):084071, 2025.

[36] N. D. Birrell and P.C.W Davies. *Quantum fields in curved space*. Cambridge University Press, 1984.

[37] Leonard Parker and David Toms. *Quantum field theory in curved spacetime: quantized fields and gravity*. Cambridge University Press, 2009.

[38] Stephen A Fulling et al. *Aspects of quantum field theory in curved spacetime*. Number 17. Cambridge University Press, 1989.

[39] Don N. Page and C. D. Geilker. Indirect evidence for quantum gravity. *Phys. Rev. Lett.*, 47:979–982, 1981.

[40] T Padmanabhan. Semiclassical approximations for gravity and the issue of backreaction. *Classical and Quantum Gravity*, 6(4):533, 1989.

[41] Tanmay Vachaspati. Quantum backreaction on classical dynamics. *Phys. Rev. D*, 95:125002, Jun 2017.

[42] L. H. Ford. Spacetime in semiclassical gravity. *100 Years Of Relativity : space-time structure: Einstein and beyond*, pages 293–310, 2005.

[43] Jonathan Z. Simon. No Starobinsky inflation from selfconsistent semiclassical gravity. *Phys. Rev. D*, 45:1953–1960, 1992.

[44] Benito A. Juárez-Aubry. Semiclassical Gravity in Static Spacetimes as a Constrained Initial Value Problem. *Annales Henri Poincare*, 23(4):1451–1487, 2022.

[45] Viqar Husain and Suprit Singh. Semiclassical cosmology with backreaction: The Friedmann-Schrödinger equation and inflation. *Phys. Rev. D*, 99(8):086018, 2019.

[46] VA Belinskiĭ, EM Lifshitz, and Isaak M Khalatnikov. Oscillatory approach to the singular point in relativistic cosmology. *Soviet Physics Uspekhi*, 13(6):745, 1971.

[47] George FR Ellis and Malcolm AH MacCallum. A class of homogeneous cosmological models. *Communications in Mathematical Physics*, 12(2):108–141, 1969.

[48] M. A. H. MacCallum. A class of homogeneous cosmological models III: Asymptotic behaviour. *Communications in Mathematical Physics*, 20(1):57–84, 1971.

[49] Michael P. Ryan and Lawrence C. Shepley. *Homogeneous relativistic cosmologies*. Princeton Series in Physics. Princeton University Press, Princeton, 1975.

[50] Sanjeev S Seahra and Christian G Boehmer. Einstein static universes are unstable in generic $f(R)$ models. *Physical Review D*, 79(6):064009, 2009.

[51] Christian G Boehmer and Francisco SN Lobo. Stability of the einstein static universe in modified Gauss-Bonnet gravity. *Physical Review D*, 79(6):067504, 2009.

[52] Puxun Wu and Hongwei Yu. The stability of the Einstein static state in $f(T)$ gravity. *Physics Letters B*, 703(3):223–227, 2011.

[53] George F. R. Ellis and Roy Maartens. The emergent universe: inflationary cosmology with no singularity. *Class. Quant. Grav.*, 21:223–232, 2004.

[54] John D Barrow, George FR Ellis, Roy Maartens, and Christos G Tsagas. On the stability of the Einstein static universe. *Classical and Quantum Gravity*, 20(11):L155, 2003.

[55] Saulo Carneiro and Reza Tavakol. Stability of the Einstein static universe in the presence of vacuum energy. *Physical Review D*, 80(4):043528, 2009.

[56] Rosangela Canonico and Luca Parisi. Stability of the Einstein static universe in open cosmological models. *Physical Review D*, 82(6):064005, 2010.

[57] Daniel Müller and Alexey Toporensky. Static cosmological solutions in quadratic gravity. *General Relativity and Gravitation*, 53(6), June 2021.

[58] F Darabi, Y Heydarzade, and F Hajkarim. Stability of Einstein static universe over lyra geometry. *Canadian Journal of Physics*, 93(12):1566–1570, 2015.

[59] Charles W Misner. Mixmaster universe. *Physical Review Letters*, 22(20):1071, 1969.

[60] Viqar Husain, Irfan Javed, and Suprit Singh. Dynamics and entanglement in quantum and quantum-classical systems: lessons for gravity. *Phys. Rev. Lett.*, 129(11):111302, 2022.

[61] Audrey Mithani and Alexander Vilenkin. Did the universe have a beginning? 4 2012.

[62] Audrey T. Mithani and Alexander Vilenkin. Instability of an emergent universe. *JCAP*, 05:006, 2014.

[63] Anthony Aguirre and John Kehayias. Quantum instability of the emergent universe. *Phys. Rev. D*, 88:103504, Nov 2013.

[64] Jonathan Oppenheim. A post-quantum theory of classical gravity? 11 2018.

[65] Viqar Husain, Irfan Javed, Sanjeev S. Seahra, and Nomaan X. Motivating semiclassical gravity: A classical-quantum approximation for bipartite quantum systems. *Phys. Rev. D*, 108(8):086033, 2023.

[66] Claus Kiefer. Functional Schrodinger equation for scalar QED. *Phys. Rev. D*, 45:2044–2056, 1992.

[67] Irfan Javed and Viqar Husain. Regular black holes and boson stars in semiclassical gravity, 2025.

[68] Matthew W. Choptuik. Universality and scaling in gravitational collapse of a massless scalar field. *Phys. Rev. Lett.*, 70:9–12, 1993.

[69] Vladimir A Belinskii and Isaak Markovich Khalatnikov. On the nature of the singularities in the general solution of the gravitational equations. *Sov. Phys. JETP*, 29(5):911–917, 1969.

[70] Masooma Ali and Viqar Husain. Mixmaster dynamics in the dust time gauge. *Phys. Rev. D*, 96:044032, Aug 2017.

[71] David F. Chernoff and John D. Barrow. Chaos in the mixmaster universe. *Phys. Rev. Lett.*, 50:134–137, Jan 1983.

[72] John D. Barrow. Chaos in the Einstein equations. *Phys. Rev. Lett.*, 46:963–966, Apr 1981.

[73] D Hobill, D Bernstein, M Welge, and D Simkins. The mixmaster cosmology as a dynamical system. *Classical and Quantum Gravity*, 8(6):1155, 1991.

[74] AB Burd, N Buric, and GFR Ellis. A numerical analysis of chaotic behaviour in Bianchi IX models. *General relativity and gravitation*, 22:349–363, 1990.

[75] Claus Kiefer, Nick Kwidzinski, and Wlodzimierz Piechocki. On the dynamics of the general Bianchi IX spacetime near the singularity. *The European Physical Journal C*, 78:1–10, 2018.

[76] Donato Bini, Christian Cherubini, Andrea Geralico, and Robert T Jantzen. Electrocardiogram of the mixmaster universe. *Classical and Quantum Gravity*, 26(2):025012, 2009.

[77] K Andriopoulos and PGL Leach. The mixmaster universe: the final reckoning? *Journal of Physics A: Mathematical and Theoretical*, 41(15):155201, 2008.

[78] K. Ferraz and G. Francisco. Mixmaster numerical behavior and generalizations. *Phys. Rev. D*, 45:1158–1162, Feb 1992.

[79] Marek Szydlowski and Adam Krawiec. Average rate of separation of trajectories near the singularity in mixmaster models. *Phys. Rev. D*, 47:5323–5328, Jun 1993.

[80] Neil J. Cornish and Janna J. Levin. The mixmaster universe is chaotic. *Phys. Rev. Lett.*, 78:998–1001, Feb 1997.

[81] Neil J. Cornish and Janna J. Levin. Mixmaster universe: A chaotic farey tale. *Phys. Rev. D*, 55:7489–7510, Jun 1997.

[82] Giovanni Imponente and Giovanni Montani. Covariance of the mixmaster chaoticity. *Phys. Rev. D*, 63:103501, Mar 2001.

[83] Thibault Damour and Marc Henneaux. Chaos in superstring cosmology. *Phys. Rev. Lett.*, 85:920–923, Jul 2000.

[84] Abhay Ashtekar, Adam Henderson, and David Sloan. Hamiltonian formulation of the Belinskii-Khalatnikov-Lifshitz conjecture. *Phys. Rev. D*, 83:084024, Apr 2011.

[85] Glenn Barnich and Viqar Husain. Geometrical representation of the constraints of Euclidean general relativity. *Class. Quant. Grav.*, 14:1043–1058, 1997.

[86] Edward Wilson-Ewing. The loop quantum cosmology bounce as a Kasner transition. *Classical and Quantum Gravity*, 35(6):065005, 2018.

[87] Edward Wilson-Ewing. A quantum gravity extension to the mixmaster dynamics. *Classical and Quantum Gravity*, 36(19):195002, 2019.

[88] Timothy Blackmore and Edward Wilson-Ewing. Numerics of Bianchi type II and type IX spacetimes in effective loop quantum cosmology. *Classical and Quantum Gravity*, 40(21):215010, 2023.

[89] Edward Wilson-Ewing. Loop quantum cosmology of Bianchi type IX models. *Phys. Rev. D*, 82:043508, Aug 2010.

[90] Martin Bojowald, David Brizuela, Paula Calizaya Cabrera, and Sara F. Uria. Chaotic behavior of the Bianchi IX model under the influence of quantum effects. *Phys. Rev. D*, 109:044038, Feb 2024.

[91] Martin Bojowald, David Brizuela, Paula Calizaya Cabrera, and Sara F. Uria. Reduction of primordial chaos by generic quantum effects. *Phys. Rev. D*, 108:L061501, Sep 2023.

[92] David Brizuela and Sara F. Uria. Semiclassical study of the mixmaster model: The quantum Kasner map. *Phys. Rev. D*, 106:064051, Sep 2022.

[93] Hans Halvorson. Complementarity of representations in quantum mechanics. *Studies in History and Philosophy of Science Part B: Studies in History and Philosophy of Modern Physics*, 35(1):45–56, March 2004.

[94] Abhay Ashtekar, Stephen Fairhurst, and Joshua L Willis. Quantum gravity, shadow states and quantum mechanics. *Classical and Quantum Gravity*, 20(6):1031–1061, February 2003.

[95] Klaus Fredenhagen and Felix Reszewski. Polymer state approximation of Schrödinger wavefunctions. *Classical and Quantum Gravity*, 23(22):6577–6584, October 2006.

[96] J M Velhinho. The quantum configuration space of loop quantum cosmology. *Classical and Quantum Gravity*, 24(14):3745–3758, July 2007.

[97] Viqar Husain and Oliver Winkler. Semiclassical states for quantum cosmology. *Phys. Rev. D*, 75:024014, 2007.

[98] Victor Taveras. Corrections to the Friedmann equations from LQG for a universe with a free scalar field. *Phys. Rev. D*, 78:064072, 2008.

[99] Mustafa Saeed and Viqar Husain. Quantum cosmology as a lattice in a box. *Phys. Rev. D*, 110(10):103504, 2024.

[100] Ivan Agullo and Parampreet Singh. Loop quantum cosmology: A brief review, 2016.

[101] Norbert Bodendorfer. An elementary introduction to loop quantum gravity, 2016.

[102] Eleonora Giovannetti and Giovanni Montani. Polymer representation of the Bianchi IX cosmology in the Misner variables. *Phys. Rev. D*, 100:104058, Nov 2019.

[103] Giancarlo Benettin, Luigi Galgani, and Jean-Marie Strelcyn. Kolmogorov entropy and numerical experiments. *Physical Review A*, 14(6):2338, 1976.

[104] Steven H Strogatz. *Nonlinear dynamics and chaos: with applications to physics, biology, chemistry, and engineering*. CRC press, 2018.

[105] Riccardo Moriconi, Giovanni Montani, and Salvatore Capozziello. Chaos removal in $R+qR^2$ gravity: The mixmaster model. *Phys. Rev. D*, 90(10):101503, 2014.

[106] Gabriele Barca and Eleonora Giovannetti. Fate of mixmaster chaos in a deformed algebra framework. *Universe*, 11(2):63, 2025.

[107] U. Ellwanger. Flow equations for $N-$point functions and bound states. *Z. Phys. C*, 62:503–510, sep 1994.

[108] T. R. Morris. The exact renormalisation group and approximate solutions. *Int. J. Mod. Phys. A*, 9:2411–2450, oct 1994.

[109] T. R. Morris. Derivative expansion of the exact renormalization group. *Phys. Lett. B*, 329(2-3):241–248, jun 1994.

[110] M. Reuter and F. Saueressig. Quantum Einstein gravity. *New J. Phys.*, 14:055022, may 2012.

[111] O. Lauscher and M. Reuter. Ultraviolet fixed point and generalized flow equation of quantum gravity. *Phys. Rev. D*, 65:025013, dec 2001.

[112] M. Niedermaier and M. Reuter. The asymptotic safety scenario in quantum gravity. *Living Rev. Relativity*, 9:5, 2006.

[113] R. Percacci. *An introduction to covariant quantum gravity and asymptotic safety*. World Scientific, Singapore, 2017.

[114] A. Eichhorn. An asymptotically safe guide to quantum gravity and matter. *Front. Astron. Space Sci.*, 5:47, 2019.

[115] Karel V. Kuchař and Michael P. Ryan. Is minisuperspace quantization valid?: Taub in Mixmaster. *Phys. Rev. D*, 40(12):3982–3996, 1989.

[116] Holger Gies. Introduction to the functional rg and applications to gauge theories. In *Renormalization group and effective field theory approaches to many-body systems*, pages 287–348. Springer, 2012.

[117] Masooma Ali, Syed Moeez Hassan, and Viqar Husain. Universe as an oscillator. *Phys. Rev. D*, 98:086002, Oct 2018.

[118] Manuel Reichert. Lecture notes: Functional renormalisation group and asymptotically safe quantum gravity. *Proceedings of Science*, 384:005, 2020.

[119] Andreas Wipf. *Statistical Approach to Quantum Field Theory: An Introduction*, volume 992 of *Lecture Notes in Physics*. Springer, 2 edition, 2021.

[120] Syed Moeez Hassan and Viqar Husain. Semiclassical cosmology with polymer matter. *Classical and Quantum Gravity*, 34(8):084003, 2017.

Appendix A

Wetterich Equation in Quantum Mechanics

In this appendix, we shall now illustrate the workings of the functional renormalization group paradigm using a quantum mechanical example of a particle in an arbitrary one-dimensional potential $V(x)$ in detail. This complements the calculations in chapter 4 of the thesis. We start with the Lorentzian action for such a theory,

$$S = \int dt\, \mathcal{L}(x,\, \dot{x}) = \int dt \left(\frac{m\dot{x}^2}{2} - V(x) \right) \tag{A.1}$$

Here, the overhead dot represents a derivative with respect to t. Writing down the Euler-Lagrange equations would yield the equations of motion. Instead of writing down the canonical theory by first writing down the quantum Hamiltonian for the theory, we start with the path integral. We also add a source term $J(t)$ to our action. This yields,

$$Z(J) = \frac{1}{\mathcal{N}} \int \mathcal{D}x(t)\, e^{i(S+S_J)} = \frac{1}{\mathcal{N}} \int \mathcal{D}x(t) e^{i\left(\int dt\, \mathcal{L}(x,\dot{x}) + \int dt\, x(t) J(t) \right)} \tag{A.2}$$

Here, $\mathcal{N}$ is an appropriate normalization factor. To establish an analogy with the partition function in statistical field theory, we Wick rotate our theory at this point and consequently work with the Euclideanized version for the rest of this appendix. The Wick rotated path integral is,

$$\begin{aligned} Z_E(J) &= \frac{1}{\mathcal{N}} \int \mathcal{D}x(t)\, e^{(-S-S_J)} \\ &= \int \mathcal{D}x(t)\, e^{\left(-\int dt\, \mathcal{L}(x,\dot{x})+\int dt\, x(t)J(t)\right)} \\ &= \int \mathcal{D}x(t)\, e^{\left(-\int dt\, \left(\frac{m}{2}\dot{x}^2+V(x)\right)+\int dt\, x(t)J(t)\right)} \end{aligned} \tag{A.3}$$

In the following discussion, we will drop the subscript E. To obtain the n-point functions for the theory, we take n-derivatives of the path integral with respect to the source $J(t)$. Corresponding to these n-point functions (or n-point correlators) we have Feynman diagrams that include a 'connected' part and a 'disconnected' part. As an example, consider the 2-point function

$$
\begin{aligned}
\frac{1}{Z_0}\frac{\delta^2 Z[J]}{\delta J(t'')\,\delta J(t')}\bigg|_{J=0} &= \frac{1}{Z_0}\frac{\delta}{\delta J(t'')}\int \mathcal{D}x\,\frac{\delta}{\delta J(t')}\exp\bigg[-S[x]+\int dt\,x(t)J(t)\bigg]\bigg|_{J=0} \\
&= \frac{1}{Z_0}\frac{\delta}{\delta J(t'')}\int \mathcal{D}x\,\bigg(\int dt\,x(t)\,\frac{\delta J(t)}{\delta J(t')}\bigg) \\
&\qquad \times \exp\bigg[-S[x]+\int dt\,x(t)J(t)\bigg]\bigg|_{J=0} \\
&= \frac{1}{Z_0}\frac{\delta}{\delta J(t'')}\int \mathcal{D}x\,\bigg(\int dt\,x(t)\,\delta(t-t')\bigg) \\
&\qquad \times \exp\bigg[-S[x]+\int dt\,x(t)J(t)\bigg]\bigg|_{J=0} \\
&= \frac{1}{Z_0}\frac{\delta}{\delta J(t'')}\int \mathcal{D}x\,x(t')\,\exp\bigg[-S[x]+\int dt\,x(t)J(t)\bigg]\bigg|_{J=0} \\
&= \frac{1}{Z_0}\int \mathcal{D}x\,x(t')\,\bigg(\int dt\,x(t)\,\delta(t-t'')\bigg) \\
&\qquad \times \exp\bigg[-S[x]+\int dt\,x(t)J(t)\bigg]\bigg|_{J=0} \\
&= \frac{1}{Z_0}\int \mathcal{D}x\,x(t')x(t'')\,e^{-S[x]} \\
&= \big\langle x(t')\,x(t'')\big\rangle \\
&= \big\langle x(t')\,x(t'')\big\rangle_c + \big\langle x(t')\big\rangle\,\big\langle x(t'')\big\rangle. \qquad \text{(A.4)}
\end{aligned}
$$

Here, $Z_0 = Z[J=0]$.

In the last line, we have expanded the 2-point function to explicitly show a connected part and a disconnected part. For all practical purposes, we only need the connected part of the diagram. This is because even though the disconnected part contributes to the S-matrix for a given transition amplitude, they are not required to obtain the quantum partition function, $Z(J)$, for more details see the Linked Cluster Theorem. To circumvent this redundancy, we introduce the Schwinger function (functional, in QFT), $W(J) = \ln(Z(J))$. Taking n-derivatives of the Schwinger functional with

respect to the source gives *connected* n-point function. We can see how this is the case. Note that,

$$\frac{\partial}{\partial J(t)} W(J) = \frac{1}{Z(J)} \frac{\partial}{\partial J(t)} Z(J) \tag{A.5}$$

Then, the 2-point function would be,

$$\begin{aligned}
\frac{\partial^2 W(J)}{\partial J(t) \partial J(t')} &= \frac{\partial}{\partial J(t)} \left(\frac{1}{Z(J)} \frac{\partial Z(J)}{\partial J(t')} \right) \\
&= \frac{\partial}{\partial J(t)} \left(\frac{1}{Z(J)} \right) \frac{\partial Z(J)}{\partial J(t')} + \frac{1}{Z(J)} \frac{\partial^2 Z(J)}{\partial J(t) \partial J(t')} \\
&= -\frac{1}{Z(J)^2} \frac{\partial Z(J)}{\partial J(t)} \frac{\partial Z(J)}{\partial J(t')} + \frac{1}{Z(J)} \frac{\partial^2 Z(J)}{\partial J(t) \partial J(t')} \\
&= -\langle x(t) \rangle \langle x(t') \rangle + \langle x(t) x(t') \rangle \\
&= \langle x(t) x(t') \rangle_c \equiv G(t, t'). \qquad \text{(A.6)}
\end{aligned}$$

In the fourth line, we have used the result from equation (A.4), and defined the full quantum mechanical propagator $G(t,\, t')$ in the last line.

To summarize, from the original path integral $Z(J(t))$, we defined the quantum mechanical Schwinger function. Taking n-derivatives with respect to the source generate connected n-point functions.

A.1 Quantum Effective Action

An even more efficient method of storing the information of a theory is the quantum effective action $\Gamma(\tilde{x}(t))$. The quantum effective action is the Legendre transform of the quantum mechanical Schwinger function $W(J)$ with respect to the **mean position** $\tilde{x}(t)$ (mean field $\langle \varphi \rangle$ in QFT). More formally, we require values of the

source J over the time domain t that maximize the Legendre transformation. This entails assuming that the Schwinger function $W(J)$ is convex for which the said supremum exists and is unique. The quantum effective action (QEA) is given,

$$\begin{aligned}\Gamma(\tilde{x}(t)) &= \sup_{J(t)}\left\{\int dt\, J(t)\, x(t) - W(J)\right\} \\ &= \int dt\, J_{\sup}(t)\, x(t) - W(J_{\sup}). \end{aligned} \tag{A.7}$$

It is instructive to see how the mean position is the variable conjugate to the source $J(t)$, i.e. $\partial W(J)/\partial J(t) = \tilde{x}(t)$,

$$\begin{aligned}\frac{\partial W(J(t))}{\partial J(t')} &= \frac{\partial}{\partial J(t')} \ln\left(\int \mathcal{D}x(t)\, \exp\left[-S + \int dt\, x(t)J(t)\right]\right) \\ &= \frac{1}{\int \mathcal{D}x(t)\, \exp\left[-S + \int dt\, x(t)J(t)\right]} \\ &\qquad \times \int \mathcal{D}x(t)\, \frac{\partial}{\partial J(t')} \exp\left[-S + \int dt\, x(t)J(t)\right] \\ &= \frac{1}{Z(J(t))} \int \mathcal{D}x(t)\, \exp\left[-S + \int dt\, x(t)J(t)\right] \frac{\partial}{\partial J(t')} \left(\int dt\, x(t)J(t)\right) \\ &= \frac{1}{Z(J(t))} \int \mathcal{D}x(t)\, \exp\left[-S + \int dt\, x(t)J(t)\right] \int dt\, x(t)\, \frac{\partial J(t)}{\partial J(t')} \\ &= \frac{1}{Z(J(t))} \int \mathcal{D}x(t)\, \exp\left[-S + \int dt\, x(t)J(t)\right] \int dt\, x(t)\, \delta(t - t') \\ &= \frac{1}{Z(J(t))} \int \mathcal{D}x(t)\, x(t')\, \exp\left[-S + \int dt\, x(t)J(t)\right] \\ &= \langle x(t')\rangle \equiv \bar{x}(t'). \end{aligned} \tag{A.8}$$

Here, we have made use of the fact for the expectation of an observable $\mathcal{O}$

$$\begin{aligned}\langle\mathcal{O}\rangle &= \frac{1}{\mathcal{N}}\int \mathcal{D}\varphi\,\mathcal{O}\,e^{-S+(J,\,\varphi)} \\ &= e^{-W(J)}\int \mathcal{D}\varphi\,\mathcal{O}\,e^{-S+(J,\,\varphi)} \end{aligned} \tag{A.9}$$

$\mathcal{N}$ is a suitable normalization, $(J,\varphi) = \int J(x)\varphi(x)\,dx$, and $\mathcal{D}\varphi$ is a suitably defined measure. The second equality is the same in terms of the Schwinger function. Conversely, from the effective average action, we also have

$$\begin{aligned}\frac{\delta\Gamma[\tilde{x}(t)]}{\delta\tilde{x}(t)} &= \left[\int dx' J_{\rm sup}(x')\frac{\delta\tilde{x}(t)}{\tilde{x}(t)} + \int dx'\frac{\delta J(x')}{\delta\tilde{x}(t)}\tilde{x}(t)\right] \\ &\quad -\frac{\delta W[J]}{\delta\tilde{x}(t)} \\ &= J_{\rm sup}(\tilde{x}) + \left[\int dx'\frac{\delta J(x')}{\delta\tilde{x}(t)}\underbrace{\left(\tilde{x}(t) - \frac{\delta W[J(x')]}{\delta J(x)}\right)}_{=0}\right] \\ \frac{\delta\Gamma[\tilde{x}(t)]}{\delta\tilde{x}(t)} &= J_{\rm sup}(\tilde{x}). \end{aligned} \tag{A.10}$$

Here we have established that $W[J(\tilde{x})]$ and $\tilde{x}(t)$ (mean position) are conjugate variables. This is also the *quantum equation of motion*: the effective action $\Gamma[\tilde{x}(t)]$ encodes all dynamics of the position expectation values and their functions thereof, taking into account all quantum fluctuations.

The effective action is efficient since its derivatives with respect to the mean position generates one-particle irreducible (1PI) n-point functions. This is done by taking n derivatives of the effective action with respect to $\tilde{x}(t)$. Here, one-particle irreducible means that the corresponding Feynman diagrams cannot be cut into two diagrams

by the cut of a single internal line.

$$\begin{aligned}\Gamma^{(n)}(\tilde{x}(t)) &= \frac{\partial^{(n)}\Gamma(\tilde{x}(t))}{\partial\tilde{x}(t_1)\partial\tilde{x}(t_2)\ \ldots\ \partial\tilde{x}(t_n)} \\ &= \langle\tilde{x}(t_1)\,\tilde{x}(t_2)\ \ldots\ \tilde{x}(t_n)\rangle_{1\text{PI}} \end{aligned} \tag{A.11}$$

The last thing we wish to show using the QEA is that the 2-point 1PI function, i.e. $\Gamma^{(2)}$ is the inverse of the full quantum propagator. We do this for reasons that will become clear later. In operator notation, we want to show

$$W^{(2)}\cdot\Gamma^{(2)} = 1. \tag{A.12}$$

In more detail, we start with

$$\int dt' \frac{\partial W}{\partial J(t)\partial J(t')}\cdot\frac{\partial\Gamma}{\partial\tilde{x}(t)\partial\tilde{x}(t')} = \int dt' \frac{\partial}{\partial J(t)}\left[\frac{\partial W}{\partial J(t')}\right]\cdot\frac{\partial}{\partial\tilde{x}(t')}\left[\frac{\partial\Gamma}{\partial\tilde{x}(t)}\right];$$

using the results from eq. (A.8) and eq. (A.10), we get

$$\int dt' \frac{\partial}{\partial J(t)}\left[\tilde{x}(t')\right]\cdot\frac{\partial}{\partial\tilde{x}(t')}\left[J(t)\right] = \int dt'\,\frac{\partial J(t')}{\partial J(t')} = \delta(t-t'). \tag{A.13}$$

This proves eq. (A.12), which will allow us to write, $W^{(2)} = \left(\Gamma^{(2)}\right)^{-1}$.

A.2 Scale dependence

At this point, there has been no reference to any (probing, or reference) scale of the theory. Our bare action, eq. (A.1), encodes physics at all scales. In field theory the generating functional of the bare action is divergent— it is, thus, regularized by imposing a UV cutoff. In Wilsonian RG, the UV cutoff, often denoted Λ is the reference scale, and degrees of freedom are integrated out shell-by-shell in intervals

$(\delta\Lambda,\, \Lambda]$, hence, accessing an effective action at each integration interval. In the functional RG program, to the already regularized theory (UV cutoff), we impose an IR regulator. For our quantum mechanical example, we assume no UV divergences exist – and the IR regulator serves the purpose of damping frequencies Ω below a set reference frequency ω, and allowing all those above to contribute fully to the path integral. We start the analysis by introducing this regulator function in the path integral as a *cut-off* action $\Delta_w S[X(\Omega)]$. Before proceeding, however, it is important to introduce some new notation – $X(\Omega)$ is the Fourier space representation of the position $x(t)$. The scale-dependent path integral in the presence of a source for our quantum mechanical system is given:

$$Z_\omega(J) = \frac{1}{\mathcal{N}} \int \mathcal{D}x(t)\, \exp\{-S(x,\, \dot{x}) - \Delta_\omega S(x) + (J,\, x)\}. \tag{A.14}$$

Here, $S(x,\, \dot{x})$ represents the bare action, $\Delta_\omega S(x)$ represents the cutoff action, and lastly we introduce the shorthand notation for the source term $(J,\, x) = \int dt\, J(t)x(t)$. As expected, derivatives with respect to the source yields the n-point functions of the theory. These $n-$point functions implicitly depend on scale ω through Z_ω. Before proceeding, it is important to see how the cutoff action implements an IR cutoff and damping of frequencies below a certain reference frequency, ω. The cutoff action in the frequency domain given,

$$\Delta_\omega S(X(\Omega)) = \int \frac{d\Omega}{(2\pi)} X(\Omega)\, R_\omega(\Omega^2)\, X(\Omega), \tag{A.15}$$

the same cutoff in the time domain is,

$$\Delta_\omega S(x(t)) = x(t) R_\omega(t,\, t') x(t'). \tag{A.16}$$

Either of the two representations of the cutoff actions may be used in the following and are hence interchangeable. The fourier (frequency) representation allows to view the imposition of the cutoff scale and how frequency suppression is implemented using the regulator, R_ω, whereas, the time domain representation often provides streamlined calculations and ease. The choice of the regulator is completely arbitrary up to limiting behavior at the initial frequency at which the bare action is defined, and the final frequency for which are interested. We have the following conditions for the regulator function:

1. Suppression of frequencies smaller than cutoff ω:

$$\lim_{\Omega \to 0} R_\omega(\Omega) > 0.$$

   This can be interpreted as follows: the regulator (*suppressor of smaller frequencies*) acts on frequencies greater than zero, at least up to the cut off ω.

2. Physical limit to ensure $Z_{\omega=0} = Z$:

$$\lim_{\omega \to 0} R_\omega(\Omega) = 0.$$

   This ensures that in the limit that the cutoff is moved to zero, the action of the regulator completely disappears in conjunction with point 1. Furthermore, by the definition of the cutoff action in eq. (A.15), it is clear that when the regulator goes to zero, the cutoff action goes to zero as well, and we recover the original path integral we started with, sans any scale dependence.

3. UV limit to ensure that $\Gamma_{\omega=\Lambda} = S$:

$$\lim_{\omega \to \Lambda \to \infty} R_\omega(\Omega) \to \infty$$

This indicates damping of all frequencies, and in turn damps the partition function via the cutoff action infinitely–consequently, we are left with just the classical action.

Following the same procedure to get to a scale-dependent quantum effective average action, we pass to the scale-dependent Schwinger function – as before, this is just the logarithm of Z_ω; $W_\omega(J) = \ln(Z_\omega(J))$. Recall, that the derivatives of the Schwinger function with respect to the source gives the connected $n-$point functions of the theory. Introducing the reference frequency ω consequently introduces a scale in all such observables. From here, we can define the quantum effective average action, $\tilde{\Gamma}_\omega(\tilde{x}(t))$; this is still a Legendre transformation of the Schwinger function, with the only key difference being that the Schwinger function is scale-dependent. Note here that the $\tilde{\Gamma}$ is not the QEAA in fourier space– it serves a temporary purpose until the full $\Gamma_\omega(\tilde{x}(t))$ is defined. The said auxiliary function is scale-dependent through the scale-dependence of the Schwinger function. We have,

$$\tilde{\Gamma}_\omega(\tilde{x}(t)) = \int dt\, J(t)x(t) - W_\omega(J), \tag{A.17}$$

The full $\omega-$ dependent QEAA for the theory is defined to be,

$$\Gamma_\omega(\tilde{x}(t)) = \tilde{\Gamma}_\omega(\tilde{x}(t)) - \Delta_\omega S(\tilde{x}(t)). \tag{A.18}$$

The definition of the full QEAA in eq. (A.18) is extremely crucial. The motivation for subtracting the cutoff action will become clear as we move on to computing the flow equation for the QEAA. Moreover, it is extremely important to recall here that the QEAA is function(al) of the **mean** position, in turn, the addition of the cutoff action necessarily is a function(al) of the mean position, $\tilde{x}(t)$, **and not** $x(t)$. Lastly, note that the cutoff ω appears twice in the QEEA: once through the schwinger

function, and once through the cutoff action. All these important yet subtle details become crucial when deriving the flow equation for the QEEA.

A.3 Flow Equation

The end goal is to compute the flow equation for the couplings in the QEAA, (A.18). We define a frequency derivative– a toggle for ω in the regulator that appears in the cutoff action, and see how the couplings flow in the bare action. This frequency (or scale derivative) is given,

$$\frac{d}{d\tau} = \omega \frac{d}{d\omega}. \tag{A.19}$$

Here, τ is called the RG parameter and is defined $\tau = \ln\left(\frac{\omega}{\omega_0}\right)$, ω_0 is some reference frequency, most often taken to be the initial frequency at which the bare action is taken. We start by first computing the frequency derivative of the auxiliary QEEA (A.17),

$$\partial_\omega \tilde{\Gamma}(\tilde{x}(t)) = \partial_\omega \int dt\, J(t)x(t) - \partial_\omega W_\omega(J). \tag{A.20}$$

We compute this term by term as there are several key steps, often overlooked in the literature, that are used in computing these derivatives. We start with the scale derivative of the Schwinger function,

$$
\begin{aligned}
\partial_\omega W_\omega(J) &= \partial_\omega \ln Z_\omega(J) \\
&= \frac{1}{Z_\omega(J)} \frac{\partial}{\partial \omega} \int \mathcal{D}x(\bar{t})\, \exp\left\{-S - \Delta_\omega S + (J,x)\right\} \\
&= \frac{1}{Z_\omega(J)} \int \mathcal{D}x(\bar{t})\, \frac{\partial}{\partial \omega}\left(-\Delta_\omega S\right) \exp\left\{-S - \Delta_\omega S + (J,x)\right\} \\
&= -\frac{1}{2Z_\omega(J)} \int \mathcal{D}x(\bar{t})\, \tilde{x}(t)\, \partial_\omega R_\omega(t,t')\, \tilde{x}(t') \exp\left\{-S - \Delta_\omega S + (J,x)\right\} \\
&= -\frac{\partial_\omega R_\omega(t,t')}{2Z_\omega(J)} \int \mathcal{D}x(\bar{t})\, \tilde{x}(t)\, \tilde{x}(t')\, \exp\left\{-S - \Delta_\omega S + (J,x)\right\} \\
&= -\frac{1}{2}\partial_\omega R_\omega(t,t') G_\omega(t,t') + \partial_\omega \Delta_\omega S
\end{aligned}
\tag{A.21}
$$

where we have defined the connected quantum-mechanical propagator:

$$
G_\omega(t) = \frac{\delta^2 W_\omega[J]}{\delta J(t) \delta J(t')} \quad = \quad \langle \varphi(t)\varphi(t') \rangle - \langle \varphi(t) \rangle \langle \varphi(t') \rangle. \tag{A.22}
$$

Since we have added the frequency toggle ω in the QEAA, we get a modification in the relationship between the mean position and the derivative of the now frequency-dependent Schwinger functional. Note that, the right-hand side of (A.18) is now the Legendre transform of $\Gamma_\omega[x] + \Delta_\omega S[x]$, this follows from the definition in (A.18) (again, at the supremum of the source, J):

$$
\frac{\delta(\Gamma_\omega + \Delta_\omega S)}{\delta x(t)} = J_{\sup}(t), \qquad \frac{\delta W_\omega[J_{\sup}(t)]}{\delta J(t)} = x(t). \tag{A.23}
$$

Consequently, the connected propagator (A.22) gets the corresponding scale-dependent modification:

$$
G_\omega(t) = \frac{\delta^2 W_k[J]}{\delta J(t) \delta J(t')} = \left(\frac{\delta^2(\Gamma_\omega + \Delta_\omega S)}{\delta x(t) \delta x(t')} \right)^{-1} \tag{A.24}
$$

In the second inequality above, we have used the fact that the propagator is the inverse of the 1PI two-point function.

$$\begin{aligned} & \int dy \frac{\delta^2 W}{\delta J(x_1)\delta J(x_2)} \cdot \left(\frac{\delta^2 \Gamma}{\delta\phi(y)\delta\phi(x_2)} \right) \\ = & \int dy \frac{\partial\phi(y)}{\partial J(x_1)} \frac{\partial J(x_2)}{\partial\phi(y)} = \delta(x_1 - x_2) \end{aligned} \tag{A.25}$$

which led to conclude

$$\begin{aligned} \frac{\delta^2 W}{\delta J(t)\delta J(t')} = G(t,\, t') &= \left(\frac{\delta^2 \Gamma_k}{\delta x(t)\delta x(t')} \right)^{-1} \\ &= \frac{1}{\Gamma_\omega^{(2)}[x(t)] + R_\omega(x(t))}. \end{aligned} \tag{A.26}$$

We now use several previous results, and the definition of the scale derivative to write down the final flow equation.

$$\begin{aligned} \partial_\omega \Gamma_\omega[x(t)] &= -\partial_\omega W_\omega[J] - \partial_\omega \Delta_\omega S[x(t)] \\ &= \frac{1}{2} \int \frac{d\Omega}{(2\pi)} G_\omega(t) \partial_\omega R_\omega(t) \\ &= \frac{1}{2} \int \frac{d\Omega}{(2\pi)} \frac{\partial_\omega R_\omega(t)}{\Gamma_\omega^{(2)}[x(t)] + R_\omega(x(t))}. \end{aligned} \tag{A.27}$$

This flow equation can now be used for any choice of the postulated effective action $\Gamma[(x(t)]$, terms in the expanding polynomial using the Local Potential Approximation (LPA) can be compared to get the flow for each coupling. We shall now quickly specialize to the quantum anharmonic oscillator and compute the individual flow equations for that.

A.4 Anharmonic Oscillator

We shall now apply the machinery developed in the previous sections to the anharmonic oscillator. This section is loosely based on the notes [118, 116]. The euclidean action for the anharmonic oscillator is given by

$$S = \int dt \left(\frac{1}{2}\dot{x}^2 + \frac{1}{2}\Omega^2 x^2 + \frac{1}{24}\lambda x^4 \right) \tag{A.28}$$

We shall consider the truncation for the scale-dependent effective action where everything except for the first (kinetic) term is part of a scale (frequency)-dependent effective potential, V_ω. We take frequencies $\Omega^2 > 0$, and interaction strength $\lambda > 0$. Our starting point would thus become the effective action,

$$\Gamma_\omega[x(t)] = \int dt \left(\frac{1}{2}\dot{x}^2 + V_\omega(x(t)) \right), \tag{A.29}$$

where we define,

$$V_\omega(x(t)) = \frac{1}{2}\Omega_\omega^2 x^2 + \frac{1}{24}\lambda_\omega x^4. \tag{A.30}$$

The truncation above is not unique, in fact higher order terms can be included; below we shall employ a slightly different definition of V_ω to compute the flow equations. In this way, we have split our euclidean effective average action into a kinetic term and a scale-dependent potential truncation. We compute two functional derivatives of (A.29) with respect to $x(t)$, and then go to Fourier space

$$\begin{aligned} \frac{\delta\Gamma_\omega[x(t)]}{\delta x(t_1)\delta x(t_2)} &= \left(-\partial_{t_1}^2 + V''(x(t))\right)\delta(t_1 - t_2) \\ \Gamma_\omega^{(2)}[x(\tilde{\omega})] &= \tilde{\omega}^2 + V_\omega''(x) \end{aligned} \tag{A.31}$$

We now specialize to the optimized regulator as in chapter 4. This is,

$$R_\omega(\tilde{\omega}^2) = (\omega^2 - \tilde{\omega}^2)\Theta(\omega^2 - \tilde{\omega}^2). \tag{A.32}$$

From this we compute the frequency derivative (A.19) of the regulator,

$$\partial_\omega R_\omega = 2\omega\Theta(\omega^2 - \tilde{\omega}^2) + 2\omega(\omega^2 - \tilde{\omega}^2)\delta(\omega^2 - \tilde{\omega}^2) = 2\omega\Theta(\omega^2 - \tilde{\omega}^2). \tag{A.33}$$

Here we have used the fact that $x\delta(x) = 0$. We now have all ingredients to write down the final flow equation. We get the flow for the effective potential

$$\partial_\omega V_\omega(x) = \frac{1}{2}\int_{-\infty}^{\infty} \frac{d\tilde{\omega}}{2\pi} \frac{2\omega\,\Theta(\omega^2 - \tilde{\omega}^2)}{\omega^2 + V_\omega''(x)} = \frac{1}{\pi}\frac{\omega^2}{\omega^2 + V''(x)} \tag{A.34}$$

To get the flow for the ground state energy, it suffices to study a polynomial expansion of the potential,

$$V_\omega(x) = E_\omega + \frac{1}{2}\Omega_\omega^2 x^2 + \frac{1}{24}\lambda_\omega x^4 ... \tag{A.35}$$

The effects of the frequency dependent fluctuations are now encoded in the couplings Ω_ω and λ_ω. Their initial values are set at the values they have in the bare action in the UV. Our ground state energy E_ω is exactly the actual ground state energy, but picks up an unphysical x-independent contributions. From the flow of E_ω, we extract the flow of the true ground state energy $\tilde{E}_\omega$ by performing a subtraction to avoid the buildup of unphysical contributions – the key here being that in the limit $\lambda = \Omega = 0$, the ground state energy also has to stay zero. We go from, by comparing coefficients in the expansion on the left and right hand sides of (A.34), in terms of the frequency derivative $\frac{d}{d\tau} = \omega\frac{d}{d\omega}$,

$$\frac{d}{d\tau}E_\omega = \frac{1}{\pi}\frac{\omega^3}{\omega^2 + \Omega_\omega^2}, \tag{A.36}$$

to, the actual flow of the ground state energy

$$\frac{d}{d\tau}\tilde{E}_\omega = \frac{1}{\pi}\left(\frac{\omega^3}{\omega^2+\Omega_\omega^2} - \omega\right). \tag{A.37}$$

Equating more coefficients in powers of x, we get the flow equations for Ω_ω and λ_ω,

$$\frac{d}{d\tau}\Omega_\omega^2 = -\frac{1}{\pi}\frac{\lambda_\omega\omega^3}{(\omega^2+\Omega_\omega^2)^2}, \tag{A.38}$$

$$\frac{d}{d\tau}\lambda_\omega = \frac{6}{\pi}\frac{\lambda_\omega^2\omega^3}{(\omega^2+\Omega_\omega^2)^3}. \tag{A.39}$$

These flow equations form a set of ODEs and can be solved using any standard ODE solver. These equations can also be seen as beta functions for the flow of the couplings $\{E_\omega, \Omega_\omega, \lambda_\omega\}$ – solving for any fixed points entails setting these to zero. As it turns out, no non-trivial (non-Gaussian) fixed points exist. Furthermore, using perturbation theory, the numerical solution to the above equations can be compared with its analytic counterpart, for more details see [118]. This exercise provides a foundational playground to learn the tools of functional RG as applied to QFT using the familiar ideas of ordinary quantum mechanics. It is a controlled way to learn the method. In 0+1 dimensions, one can see, step by step, how coarse-graining works, how truncations (e.g., local potential/derivative expansions) and regulator choices affect results, and how flows reproduce spectra and correlators – then benchmark everything against results from perturbation theory. This builds intuition for fixed points, running couplings, and non-perturbative resummations before one deploys the full machinery in field theory and gravity.

Vita

Candidate's full name: Muhammad Muzammil

Universities attended:

- Aug 2020 - present, Doctorate of Philosophy *Mathematics*, University of New Brunswick, Fredericton, NB, Canada,
- Aug 2016- Jun 2020, Bachelors of Science *Physics*, Lahore University of Management Sciences, Lahore, Pakistan.

Publications:

- Mustafa Saeed, Diya Batool, Muhammad Muzammil, and Nomaan X, *Phase transitions due to Euclidean gravity*, Phys. Rev. D 112 (2025) 2, 025013, Jul. 2025.
- Muhammad Muzammil and Viqar Husain, *Semiclassical mixmaster universe*, Phys. Rev. D 111 (2025), 084071, Apr. 2025.
- Viqar Husain and Muhammad Muzammil, *Semiclassical geometrodynamics of homogeneous cosmology*, Phys. Rev. D 109 (2024), 044063, Feb. 2024.

Conference Presentations:

- Curbing cosmic chaos, Perimeter Institute of Theoretical Physics, Poster Presentation, June 2025.
- Semiclassical mixmaster universe, Atlantic General Relativity Meeting, Oral Presentation, May 2025.
- Semiclassical geometrodynamics of homogeneous cosmology, Atlantic General Relativity Meeting, Oral Presentation, June 2024.
- Semiclassical geometrodynamics of homogeneous cosmology, CAP Congress, May 2024.
- Semiclassical geometrodynamics of homogeneous cosmology, Loops 2024, April 2024.
- Inflation as a semiclassical instability, CAP Congress, June 2023.
- Inflation as a semiclassical instability, American Physical Society March Meeting, March 2023